4-21-2014 12:00 AM

Full-Scale Tests of a Wood-Frame Structure under Extreme Wind Loads

Derek A. Stedman
The University of Western Ontario

Supervisor
Dr. G. A. Kopp
The University of Western Ontario

Graduate Program in Civil and Environmental Engineering
A thesis submitted in partial fulfillment of the requirements for the degree in Master of Engineering Science

Full-Scale Tests of a Wood-Frame Structure under Extreme Wind Loads

By

Derek A Stedman

Department of Civil and Environmental Engineering
Faculty of Engineering

A thesis submitted in partial fulfillment
of the requirements for the degree of
Master of Engineering Science

Thesis Format: Monograph

School of Graduate and Postdoctoral Studies
The University of Western Ontario
London, Ontario, Canada

Abstract

Tornadoes can produce some of the strongest winds on earth; these highly localized storms can cause massive damage. Assessments of tornado wind speeds are done using post-event observations of damage via the Enhanced Fujita Scale.

A very commonly observed failure occurs at the roof-to-wall connection where the roof breaks up or flies away, typically leaving the walls in place. However, once the roof is gone the walls are more vulnerable to the wind. If a wall subsequently fails, it increases the risk of injury or death for occupants. Significant research has been done for failures of roof-to-wall connections and roof failure wind loads. In contrast, little work has been done pertaining to how the walls perform when there is no roof in place.

In the current study, experiments were performed on a full-scale, two storey residential structure with no roof. The objectives of the study were (i) to determine the wind loads and wind speeds required to cause exterior wall failure after the roof-to-wall connections had already failed, and (ii) to develop low-cost recommendations for strengthening wood-frame houses and, thereby, reducing risk to occupants during severe storms such as tornadoes.

It was found that the capacity of the walls of the test house significantly exceeded Canadian (Ontario) design loads when clad in brick veneer. The interior wall placement and connections between the exterior and interior walls are shown to have a significant effect on overall capacity. For vinyl-clad houses, increasing the stiffness of the corners of the walls will also increase capacity – which appears to be the primary structural benefit of brick cladding.
Keywords: Tornado, Full-scale, Wood-Frame, Brick Veneer, Wind Damage, Enhanced Fujita Scale, Wall Failure.

Acknowledgments

The author would like to gratefully acknowledge the contributions of his supervisor Dr. Greg Kopp and Dr. Mike Bartlett, who provided extensive support and advice throughout this entire process. As well the author would like to thank Ms. Nicole Wight, Mr. Brendan Kaus and Mr. Andrew Klazinga for their assistance with components of design, setup and running the experiment. Finally, the author is also grateful for the assistance running the experiment provided by: Mr. Jordan Kiss, Dr. Thomas Mara, Dr. Craig Miller and various other members of the Boundary Layer Wind Tunnel Laboratory staff.

Table of Contents

List of Figures

List of Tables

List of Appendices

Symbols and Abbreviations

IRLBH	Insurance Research Lab for Better Homes
3LP	Three Litle Pigs
LVDT	Linear Variable Differential Transformer
UDL	Uniformly Distributed Load
NBCC	National Building Code of Canada
ICC	International Codes Council
IRC	International Residential Code
OBC	Ontario Building Code
P-Δ	P-delta effect
ASCE	American Society of Civil Engineers
FR12	One- or Two- Family Residences
NOAA	National Oceanographic and Atmospheric Administration
EF	Enhanced Fujita Scale
DOD	Degree of Damage
F	Fujita Scale
LB	Lower Bound
UB	Upper Bound
Exp	Expected
I	Importance Factor
q	Design Wind Pressure
GCp	Combined Gust and Pressure Coefficients
Kd	Directionality factor
Kzt	Terrain Adjustment Factor
Kh	Height Adjustment Factor
ρ	Density of Air
Ce	Exposure Coefficient
Cg	Gust Coefficient
Cp	Pressure Coefficient
Cpi	Internal Pressure Coefficient
V	Velocity

Chapter 1: Introduction

Tornadoes have been responsible for an average of 84 deaths (NOAA 1948-2012) and insurance claims of US $4.9 billion (Insurance Information Institute, 2014) each year in the United States. In 2011, an unusually active year, more than 550 people died due to tornadoes (Simmons and Sutter, 2012) in the United States. Canada also experiences an average of 80 tornadoes a year (Environment Canada, 2013). While the majority of tornadoes are weak, classified as EF0 or EF1, there is still a considerable number of stronger and more damaging tornadoes (EF2 or greater) each year. It is clear that tornadoes represent a significant threat that causes severe damage and numerous injuries/deaths.

Due to the strength and localized nature of tornadoes, anemometers are rarely in the path of a tornado and, if present, are likely to be destroyed during the event. Because of this, classification of tornadoes was previously done using the Fujita Scale (Fujita, 1971) and currently is done using the Enhanced Fujita (EF) Scale (Fujita, 1971 and Texas Tech University, 2006). The scales equate levels of damage observed, after a tornado has occurred, to wind speed. The Fujita scale was originally developed by Fujita in 1971, and then the Enhanced Fujita Scale by Texas Tech University in 2006. Development of the EF scale was done by bringing together many different tornado related experts to modify of the original guidelines and provide much more detailed descriptions of damage, including different specific damage indicators.

In the EF scale, 28 different damage indicators are used (Texas Tech University, 2006). Each damage indicator corresponds to a different type of structure (e.g., one- and two- family residential, multi-family residential, etc.) and has an associated number of degrees of damage (DOD). Each degree of damage has estimated, lower- and upper-bound wind speeds. This allows a damage investigator to rate quickly the damage levels and wind speeds while increasing the

consistency of tornado ratings performed by different people in different regions. The wind speed range for each degree of damage was developed using information from different sources in different locations. This means similar damage levels will be observed for similar structures built to different building codes within the same degree of damage wind speed band. The focus of this thesis is on the damage indicator associated with one- and two-family residences, FR12. FR12 has 10 degrees of damage, shown in Table 1.1. Of particular interest for this thesis are Degrees of Damage Six and Seven, involving major damage to the roof and collapse of the exterior walls. In Table 1.1, "Exp" is the expected wind speed, while LB and UB are the lower and upper bounds for wind speed; wind speeds are presented as 3-second gust wind speeds. When the roof has failed, the horizontal restraint of the top walls is lost, leaving the walls more vulnerable. Reference pictures for Degrees of Damage Six and Seven are shown in Figures 1.1 and 1.2 respectively.

Table 1.1 - The 10 degrees of damage associated with FR12 (from Texas Tech University, 2006)

DOD*	Damage description	Exp**	LB	UB
1	Threshold of visible damage	65	53	80
2	Loss of roof covering material (<20%), gutters and/or awning; loss of vinyl or metal siding	79	63	97
3	Broken glass in doors and windows	96	79	114
4	Uplift of roof deck and loss of significant roof covering material (>20%); collapse of chimney; garage doors collapse inward or outward; failure of porch or carport	97	81	116
5	Entire house shifts off foundation	121	103	141
6	Large sections of roof structure removed; most walls remain standing	122	104	142
7	Exterior walls collapsed	132	113	153
8	Most walls collapsed in bottom floor, except small interior rooms	152	127	178
9	All walls collapsed	170	142	198
10	Destruction of engineered and/or well constructed residence: slab swept clean	200	165	220

* DOD is degree of damage **Wind Speed values are in mph

1.1 Roof Vulnerability

Roof failures are common in tornadoes; Morrison and Kopp (2012) found that due to load-sharing mechanisms in roof-to-wall connections, a total overturning failure of a roof is likely to occur. FEMA (2011) found that the roof is vulnerable to failure due to poorly constructed roof-to-wall connections and high wind loads on the roof; often houses with toe-nailed connections will fail at low wind speeds (EF1 – EF2). A commonly observed problem was use of incorrect nail sizes for roof sheathing, for example using 6d box nails instead of 8d nails. Also, common defects in construction, such as misplaced, have been shown to cause a 25 to 33% reduction in the strength of an individual toe-nailed connection (Morrison and Kopp, 2011). This shows that the roof is likely to be the first major structural failure during a tornado, leaving the walls vulnerable.

Figure 1.1 - A reference for degree of damage six (from Texas Tech University, 2006).

Figure 1.2- A reference for degree of damage seven (from Texas Tech University, 2006).

1.2 Tornado Damage Observations

1.2.1 Barrie, Ontario

A tornado struck the town of Barrie on May 31 1985, which was rated F4 (this was before the implementation of the EF scale). Figure 1.3 shows some of the damage. There is a vast range of damage, from massive destruction the front to minor roof damage near the back. The progression of damage shows the expected progression of damage as the wind speed increases. On the right side, where roofs are in place, shingles have been damaged. The building roof in right-hand foreground has failed but the exterior walls have remained intact; research has been done in this field (Morrison et al., 2012; Reardon, 1986; Xu et al. 1996; Kopp et al., 2011 and Henderson et al. 2009). Moving from the right to left of the building in the foreground, the building goes from the roof removed and no exterior wall damage to roof and exterior walls removed, an example of such damage can be seen at A. The level of damage at A is significantly higher and more likely to cause injuries or deaths. Limited research has been done on the wind speeds required to cause the walls to fail after the roof has failed (as seen in Figure 1.3), hence the need to examine this type of house failure.

Figure 1.3 - Tornado damage in Barrie, Ontario 1985 (from Davenport and Kopp, 2002).

1.2.2 Goderich Ontario

An F3 tornado struck the town of Goderich on August 21, 2011. This was not as strong as the Barrie tornado, but was still a very strong tornado which caused over $100 million dollars in damage (Environment Canada, 2013) and significant structural damage.

Figure 1.4 -A damaged structure in Goderich, Ontario. Picture courtesy of Sarah Stenabaugh

Figure 1.4 shows a multi-storey brick structure following the tornado; the top storey exhibits significant damage while the lower floors have remained intact. In particular, the roof and exterior walls have failed. The damage patterns at C and D are very similar to those seen after the Barrie Ontario tornado; the exterior wall has failed and the interior wall has not.

1.2.3 2011 Tornado Outbreak in the Southern USA

2011 saw a massive and deadly outbreak of tornadoes across the United States. General statements and observations from the damage assessment team are summarized in the FEMA report on building performance (FEMA, 2012). Most residential damage was caused by wind speeds less than 60 m/s (135 mph); these coincide with Degrees of Damage Six and Seven for a FR12 structure (Table 1.1). Failure of walls was often due to a lack of lateral support after the roof fails. In particular, FEMA writes that, for one- and two- bedroom residential structures,

"when roof and ceiling or roof truss-to-wall connections fail and leave the top of the framed wall unsupported, walls become especially vulnerable to collapse" – (FEMA 2012, p. 4-18). However, the wind speeds required to cause these wall failures have not previously been directly studied or quantified.

1.3 Research Objectives

The objectives of the research reported in this thesis are to:

1. Determine the wind speeds required to cause wall collapse after the roof fails, particularly addressing the wind speeds associated with the FR12 Degrees of Damage Six and Seven.
2. Provide recommendations on how to reduce the possibility of wall collapse after roof failure.

The approach will be to use full-scale testing of the two-storey house at the Insurance Research Lab for Better Homes as described in the Chapter 3. This thesis will discuss the results of the testing by examining different types of failure observed. The significance of these effects with respect to stronger house construction as well as the failure pressures and associated wind speeds will also be considered. In the next chapter, the results from previous experimental studies are examined.

Chapter 2: Literature Review

The literature review is divided into two sections, each discussing previous work in the different areas that pertain to this project. Several different researchers have previously performed full-house tests; their experimental setup and results have been used extensively in the design of this experiment. Wall and component test results are examined because such tests are useful to define wall performance, deflection limits and other information. The importance of examining these two fields of previous research is that they reveal the effect of the addition or removal of different components such as the roof structure or wall claddings.

2.1 Full-House Testing

Most previous research and testing performed on full-scale houses is from the Cyclone Testing Station at James Cook University in Queensland, Australia (Reardon 1986, Reardon and Henderson 1996, Xu et al. 1996, etc.). Other testing has been done at Texas Tech University and the Insurance Institute for Business & Home Safety (IBHS) in South Carolina. Reardon (1986) subjected a brick veneer house to racking[1] loads. He found under uniform racking the house withstood 120kN, six times the design load. At this load, there was no catastrophic failure but imminent signs of failure existed, such as, nails pulling out and interior wall cladding breaking away. The house was constructed with diagonal bracing in the walls designed to prevent racking deflections, however these were found to be ineffective due to the stiffness provided by the interior wall sheathing. In these tests, the internal walls prevented racking and uplift deflections. Reardon (1986) removed several interior walls to create a 9m spacing, they found the walls resisted three times the design racking and uplift pressure without significant distress. They also made observations about the strength of the brick veneer, which they found to fail in racking at a 2.95 times the design pressure. Also highlighted was the flexibility of the brick ties; the brick

[1] Walls loaded horizontally, in-plane.

veneer and wood frame racked independently of each other because the brick ties were too flexible to transmit racking forces. Based on these findings, the IRLBH house should be expected to significantly exceed design loads. Thus, the experiment requires design to apply much greater loads than the design loads and the first failures to be observed will be internal wall lining elements. As well, a progressive failure of the brick, preceded by significant cracking, is expected before the wood frame, and they are not expected to deflect, as one unit, together.

Reardon and Henderson (1996) also tested a two storey house designed to withstand 28m/s wind speeds. Testing was performed for pressure multiples of the local 33m/s design wind speed, meaning the pressure (P) associated with 33m/s was applied and then increased to 1.5*P, 2*P, etc. During the construction of the house, racking tests were performed with a ram applying lateral loads at the top plate of the house. Individual wall tests were performed on the walls as components were added. They found that the response remained linear as different components were added; however the addition of the wall lining and tiles had the most significant effect on the stiffness of the structure to horizontal loads. Figure 2.1 shows their changes in displacement of the upper wall plate (top plate) as components were added.

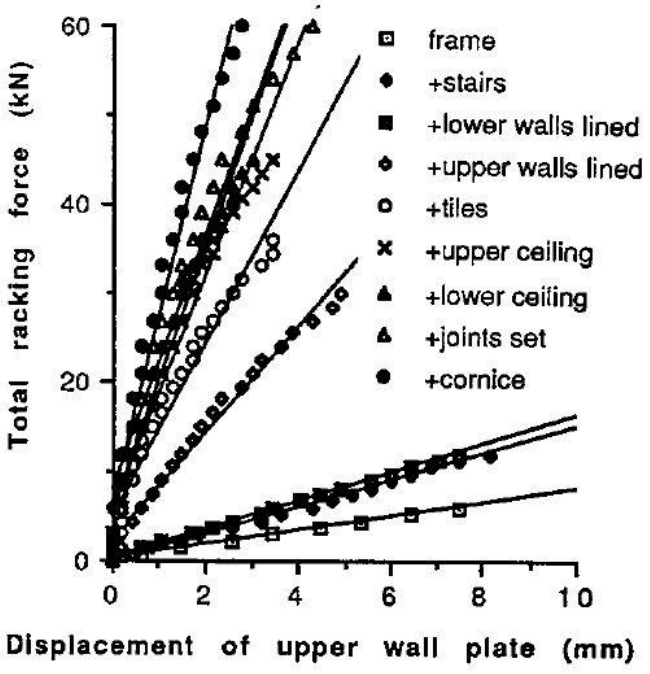

Figure 2.1 - The change in lateral response of the upper wall plate (top plate) (Reardon and Henderson, 1996).

Reardon and Henderson (1996) also found long exterior wall

sections without any transverse exterior walls to be highly flexible under lateral loading. Therefore, that area of the house should be well instrumented and photographed during the experiment. Reardon and Henderson (1996) found that while the long wall section – part of a 9x8m floor area withstood double the wind pressure due to a 33m/s wind speed and did not catastrophically fail, significant cracking of the brick veneer did occur. They concluded that if transverse walls had been built along the wall section it would have performed significantly better.

Reardon and Henderson (1996) also tested a two storey section of the house which had interior (transverse) walls installed. It withstood 2.4 times the 33m/s wind pressure with no evidence of failure. It is important to note that Reardon's test (1986) was done with the roof in place and the buildings were constructed to be "slightly better than the basic level of housing" and so would likely resist higher loads than without a roof. The increase of vulnerability of the walls after roof removal as identified by FEMA (FEMA, 2012) was discussed in chapter 1.

D'Costa and Bartlett (2003) tested a Durakit post-disaster shelter made of corrugated cardboard. While the results from this testing are not as relevant to the current full-scale house testing, the experimental setup provided useful methods which were also implemented in the current study. In particular, the loads were applied using whiffle trees and water barrels, a simple but effective solution to provide increasing loads with large deflections. Many of the loading concepts used by D'Costa and Bartlett were applied to the current full house tests.

2.2 Wall and Component Testing

Significant research on individual wall components has been conducted. Pei et al. (2012) tested wall sections, examining inter-storey drift under earthquake loads. Specifically looking at P-Δ effects on vertically loaded walls subject to large racking, where P is the vertical load applied and Δ is additional displacement caused by this load. Walls with minimal vertical loading can withstand 7-10% inter-storey drift and a load of approximately 21 kN before becoming unstable. The maximum sustainable load varied depending on differences in construction such as nail type and hold downs. Walls hold downs attach the bottom of the wall to a floor or bottom plate, walls with these in place resisted a much higher load. As the vertical load on the walls increased, the maximum drift at wall instability failure was significantly reduced. With wood frame houses, the levels of gravity loads present do not significantly limit collapse behaviour because of minimal P-Δ effects.

Pei et al. (2012) also found that the presence of wall hold downs affected the racking capacity of wood frame shear walls. At high loads and drift levels, wall hold downs provide an increase in in ductility of the wall, causing it to remain stable above 10% drift. Also, the stability of a wall is related to the connection of all the wall components. As different components of the wall (sheathing, lining, etc.) lost their connection to the framing the wall became increasingly unstable. Reardon and Henderson (1996) found that long unsupported walls are likely to see the highest transverse displacements. As these displacements occur, different components will become unattached and the wall will become increasingly unstable. Pei et al. (2012) found at 5% drift the sheathing panels began to separate from the studs and at 7% drift the corners of panels become unattached. When 10% drift is reached, just before failure Pie et al. (2012) expect all of the sheathing to become unattached.

Dolan and Heine (1997a, 1997b) found that the number, location and size of openings as well as the presence of corners significantly effects the shear capacity of wood-frame walls. They compared the racking failure loads of different shear wall specimens with different tie down conditions. A shear wall with no tie downs and no openings resisted 111.7kN; with no tie downs a shear wall with a large door and window opening only resisted 43.6kN; less than half of the wall with no tie downs. With end tie downs, the same two walls resisted 171.7kN and 53.4kN; this shows how wall tie downs and openings significantly affect the overall wall strength.

Another relevant observation from Dolan and Heine (1997a, 1997b) was that corner framing, the addition of a short wall segment to make a corner, provides a hold down effect. Providing small (2ft – 4ft) corner framing on a 40ft long wall test section provided a large change in the response of the wall sheathing; cracking and separation of sheathing was prevented. This reinforces Reardon and Henderson's (1996) findings that intact wall sheathing significantly improves wall stiffness. The length of the corner framing also effects the increase in observed stiffness; at a displacement of approximately 25mm, a wall with a 2 foot long (600mm) framed corner had a peak resistance of approximately 6800lb (30.2kN), as opposed to the wall with a 4ft framed corner, which resisted approximately 8500lb (37.8kN). The failure behaviour of a wall with a framed corner was different from straight shear walls. There was noticeable rigid body rotation until complete separation from the bottom plate.

Doudak et al. (2006) found openings to have a large influence on racking stiffness - similar to Dolan and Heine (1997a and 1997b). The shape of the load-deflection curve found by Doudak et al. (2006) is of particular interest. Shown in Figure 2.2, the shape of the curve shows a non-linear response to a peak, followed by load softening.

All of the previous research helps to allow for estimations of the failure loads, which should be significantly above pressures due to design wind loading. The lack of a roof will likely decrease the failure load of the 3LP test house, however, as the arrangement of framing and having all four walls intact will likely increase the failure load. If a portion of the house fails, it may start acting like a wall with openings but no corner framing (no resistance from the failed area) and different failures – such as component failures - may be observed.

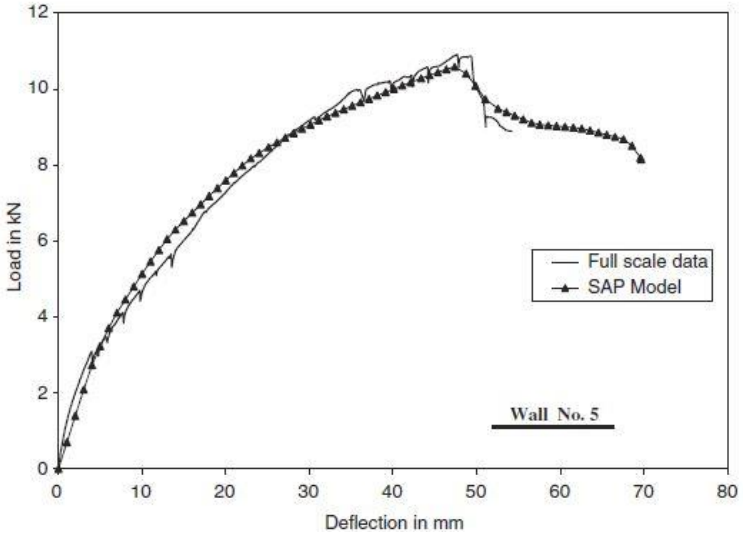

Figure 2.2 - Load displacement curve for racking of a wall section. From: Doudak et al. 2006

2.3 Summary

Significant research has been done in the areas of full house testing and wall/wall component testing. Wall/wall component testing often focuses on racking capabilities of walls; because pressures act perpendicularly to walls, the bending strength and stability of walls is something which has relatively limited previous research but is very important for the testing performed for this thesis. The full house testing has primarily focused on behaviour of the roof or behaviour of the structure as different components (eg. wall lining) are added. No research has been done in the area of full scale testing of a house after the roof has failed. The testing in this thesis is useful for examining and strengthening the weakest links in a wall system.

Chapter 3: Experimental Design

3.1 Details pertaining to the House Plan

The 3LP test house was a two storey high, wood frame construction with a brick veneer (shown in Figure 3.1). It was built following the Ontario Building Code at the time of construction (2005). During original construction, the house was inspected by more than 30 different building inspectors from Southern Ontario, to ensure typical construction. Before the current testing, the house was studied by Henderson et al. (2013) who examined the response of a hip roof subject to fluctuating wind loads and Morrison et al. (2012) who studied the same thing, but with a gable roof. This previous testing was done to the roof and roof-to-wall connections only, so they did not damage the house walls in any way that may compromise the wall testing.

Figure 3.1 - The 3LP test house with the gable roof still in place viewed from the North West looking towards the South East. With reference to Figure 3.2, the main wall with windows which can be seen is wall A1-J1.

As stated, the house was constructed with a wood frame and a brick veneer. These two main components of the house were separated by an air gap. The connection between them was made by brick ties, thin pieces of steel fastened to the wood frame structure and embedded in the mortar between bricks. These ties transmit all loads from the brick veneer to the wood frame, if these thin ties were to fail, the brick veneer and wood frame would transmit no load to each other unless one deflected to the point of bearing on the other.

Figure 3.2 shows the plan of the second storey of the house with a reference grid and labeling of key rooms. Solid lines indicate the locations of top plates while door locations are indicated by 90 degree arcs. The house is divided into a 10x10 grid, shown in Figure 3.2, which will be referenced throughout the discussion. Diagonal hatching indicates the location of the stairs, while the square hatching indicates the front hall atrium, which is open through the second floor. The majority of the displacement instrumentation (discussed in section 3.2) was installed on the second storey and all the failures occurred on the second floor. Hence, only a plan for the second storey is shown.

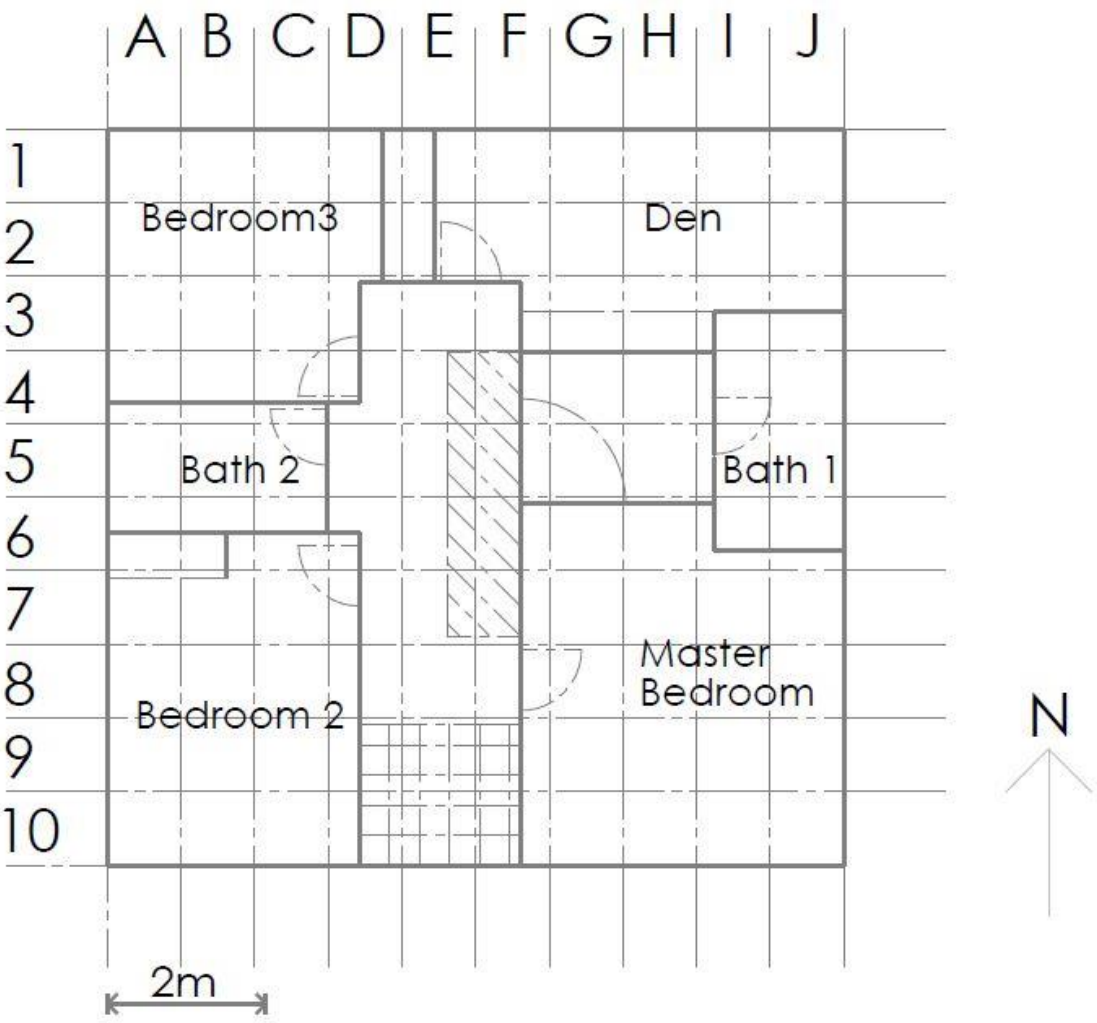

Figure 3.2 - Plan of second storey.

3.3 Load Application Design

3.3.1 Whiffle Tree Design to Simulate Negative Pressures (Suctions)

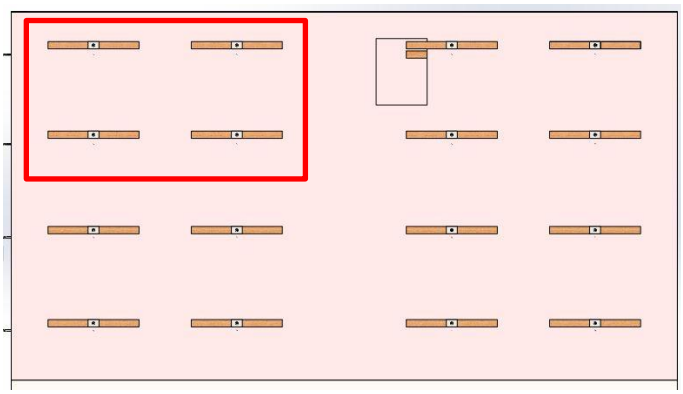

Figure 3.6 - Elevation view of the East (J1-J10) wall with load pads installed. The red box indicates the load pads acting on one whiffle tree.

The whiffle trees on the West, South and North walls applied loads simulating negative pressures (suctions, viz., outward acting loads from the walls). One whiffle tree was used to apply the loads to four load pads on any quarter of the house. The rectangle in Figure 3.6 depicts the four load pads connected in one whiffle tree. Each load pad (with one shown in Figure 3.7) was connected to 3/8" galvanized steel cables spanning from steel separation beams and attached to the reaction frame (Figure 3.8). From there the cables were joined and routed up to a 4:1 pulley array (Figure 3.10) to increase the load applied by the "come-along" (Figure 3.11), noting that a come-along is a two-way hand winch, able to incrementally increase or decrease the load (on the wall). Come-alongs were used to apply the load due to their ability to continue to apply load to the house when under large displacement as well as the high level of load control and safety resulting from using them. The same design was used for the whiffle trees simulating negative pressures on the North (A1-J1), West (A1-A10) and South (A10-J10) walls. These cables were required to withstand forces four times greater than the force being applied to each wall. Due to the size of these loads large amounts of strain energy would be carried in the cables, presenting a dangerous situation if a cable snapped. Hence the cables were designed and tested – see Appendix B, to ensure a factor of safety greater than 3.

3.3.2 Load Pads- Wood Spreader Beams

The load pads, which were wood spreader beams (Figure 3.7), were designed to provide loading across four studs in order to increase the uniformity of the load. Using the Canadian Wood Design Manual (2005), the studs were not expected to fail under the maximum loading. Designed in accordance with CAN/CSA-086-01 (2005), the spreader beams were 1200mm long, constructed of two Spruce-Pine-Fir (S-P-F) grade beams of nominal size of 38x89mm (i.e., 2x4s). They were installed to bear against the drywall inside the house, with a cable loop swaged around them which led through a drilled hole through the wall out to the whiffle tree/separation beams.

3.3.3 Design of Separation Beams

The separation beams ("A" in Figure 3.8) were attached to the steel reaction frame to keep the applied forces normal to the walls while the walls could be under large displacements in order to accurately simulate the pressure loads (which always act normal to a surface). These were steel W150x22 beams, bolted to the steel reaction frame. They were required to be constructed of steel in order to be strong enough to resist the reaction forces travelling through the pulleys.

Figure 3.7 - A wood spreader beam installed at B10, on the second floor, set up to apply negative pressure (outwards loading).

Figure 3.8 - A separation beam installed on the reaction frame. The pulleys redirect the cables from the house towards where they join.

Both load pads attached to the same separation beam were connected by one primary cable looped over a pulley attached to the secondary cable. The primary cables (black in Figure 3.9) loaded the house. At the separation beam the cables were angled up until they looped over a pulley attached to the secondary cable (blue in Figure 3.9). This design ensured that the loads on both pads were equal, as explained in Appendix C.

The secondary cable is looped over another pulley and back down to connect to the primary cable from two different load pads that were connected to another separation beam. This joined the load from four individual load pads into the tertiary cable (red in Figure 3.9) applying as well as equalizing the load at each load pad because of the pulleys connecting each cable. Figure 3.9 shows a basic two-dimensional schematic of the loading setup, where the circles represent the pulleys and the brown hatching is the house wall.

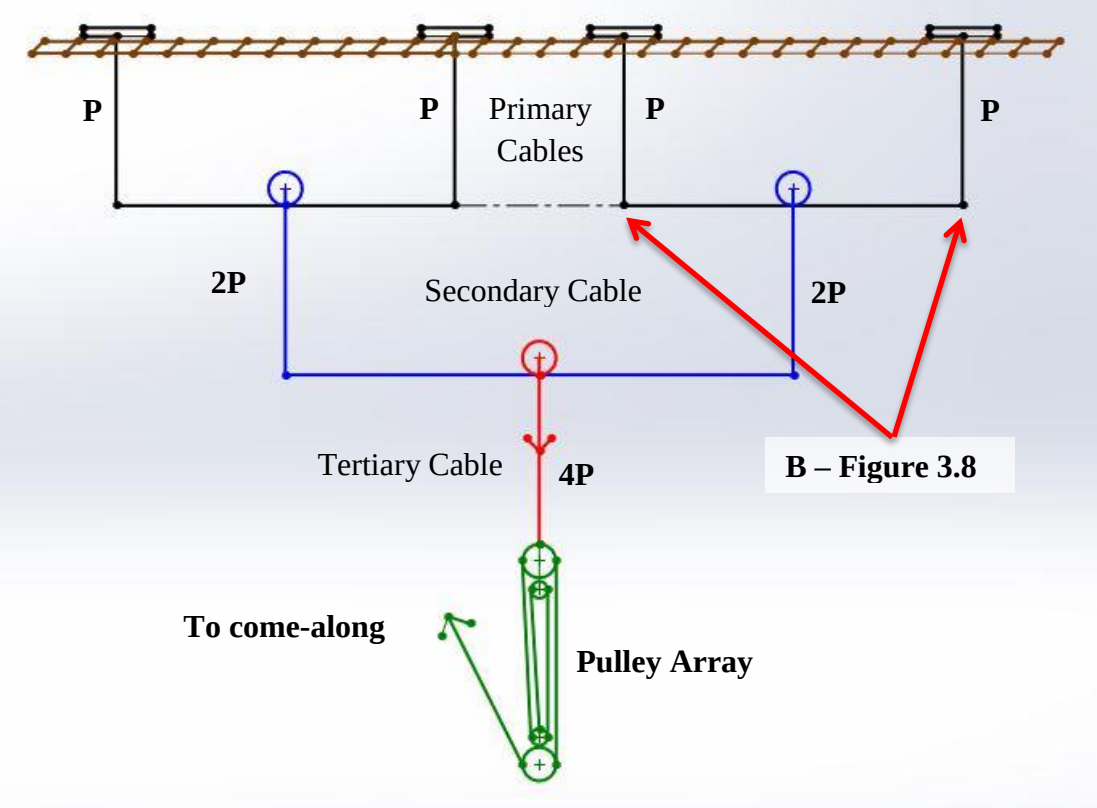

Figure 3.9 - A 2-Dimensional sketch of the whiffle tree pulley setup, P represents the pulling force.

3.3.4 Design of Pulley Array and Load Application

All four load pads were joined into the tertiary cable, which was connected into a pulley array as shown in Figure 3.9. The purpose of the pulley array was to quadruple the load applied by the come-along. The tertiary cable was attached to the yellow shackle at the top of the array (green in Figure 3.9, the shackle is visible in Figure 3.11) while the bottom of the pulley array was fixed to the reaction frame to prevent movement. A cable attached to the come-along ran down to the bottom of the pulley array, then up and down through the array twice before ending at the bottom. The pulley array causes a cable displacement of 40cm at the come-along to be reduced to 10cm at the loading point, increasing the load applied to the cable leading to the house by a factor of 4.

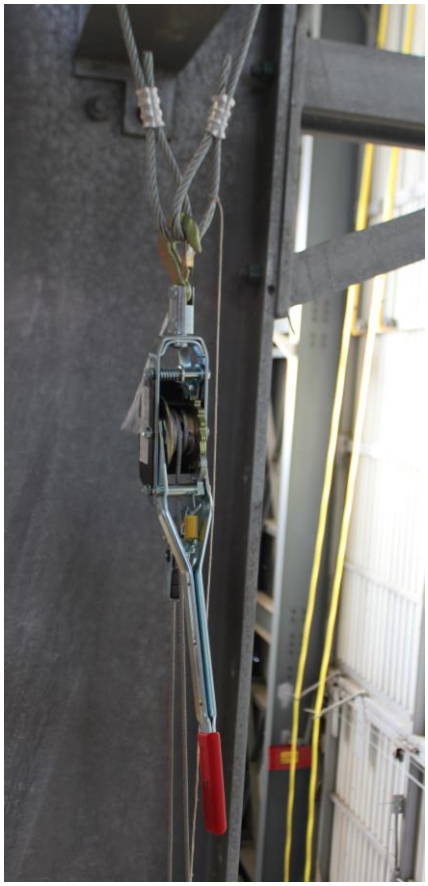

Figure 3.10 - Come-along installed on the steel reaction frame.

Figure 3.11 - Pulley Array in fully extended position.

Come-alongs were used to apply the loads to the house at a controlled rate. This method of load application was chosen due to the level of control available. A come-along allows for increasing the load by increasing the tension in the cable as the cable is winched in small increments. During the experiment, the load was increased in 0.4kN increments. One come-along was tightened at a time, starting at locations J1-J5 lower (first storey level) load and working around the house in a clockwise direction.

3.3.5 Design of Whiffle Trees to Simulate Positive Pressures

The whiffle trees connected to the East (J1-J10) wall were more of a challenge to design because, to simulate positive pressures, the loads had to be applied in the inward direction. To avoid the complex design of compression members and accommodate the continued usage of cabling, the wall had to be pulled from the inside of the house. This created the same force as if a positive force had been applied to this wall, but it removed the requirement to construct and support compression members across the entire area of the wall. The challenge this created was that the cables pulling on the wall needed to be turned from inside the house, outwards, towards the reaction frame without touching or interacting with the house. To achieve this on the top storey, steel beams dropping down from the reaction frame were connected. On the first floor, vertical steel columns were placed through small holes in the house floor and connected to the concrete strong floor, where they were anchored.

3.3.6 Load Pad Design

The "positive" load pads were designed to bear on the brick, instead of drywall. The same design was used for these load pads as was used for the "negative" load pads except that a one square-foot oriented-strand-board bearing pad was added to each side of each load pad (as seen in Figure 3.12). This was done to avoid the possibility that the load pads would punch through the brick, causing a premature failure.

Figure 3.12 - A load pad for positive loading.

3.3.7 First Storey Setup

Small holes were cut in the floor of the house in the room on the East side to allow W150x22 columns to pass through. These columns were positioned to provide reactions for two load pads in a vertical line. Therefore, a total of four columns were installed to account for all of the load pads on the first storey of the positively-loaded wall. The column in the South East (I9 area) corner is shown in Figure 3.13.

The columns were not directly fixed to the concrete strong floor, owing to the challenges involved with drilling bolts into the strong floor while also underneath the house. Instead the bottom of the column was restrained from translating by installing a horizontal truss throughout the base (see label H in Figure 3.14). This truss was anchored to steel bolts connected to the curbs supporting the house (label G in Figure 3.14) which in turn were connected to the strong floor by Hilti drilled anchors. To prevent rotation of the steel columns, cable stays were connected from the tops to the strong curb under the house (label A in Figure 3.13) as well as cross bracing between the columns (B). Bracing was also provided outwards through the window (F), in case of a loading

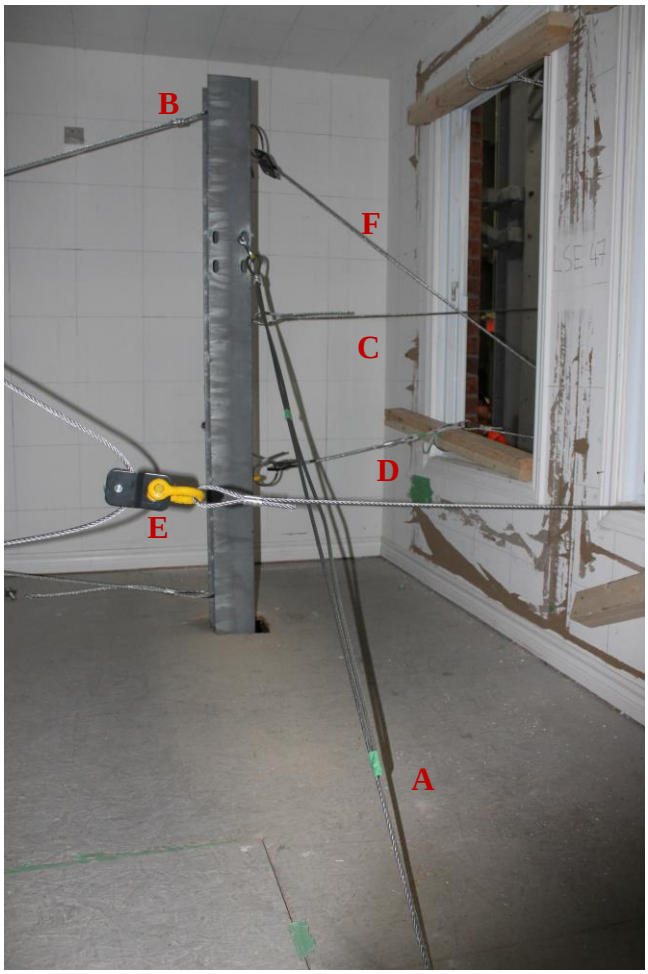

Figure 3.13 - A steel column on the first floor extending upwards to provide a reaction for the cables from two load pads.

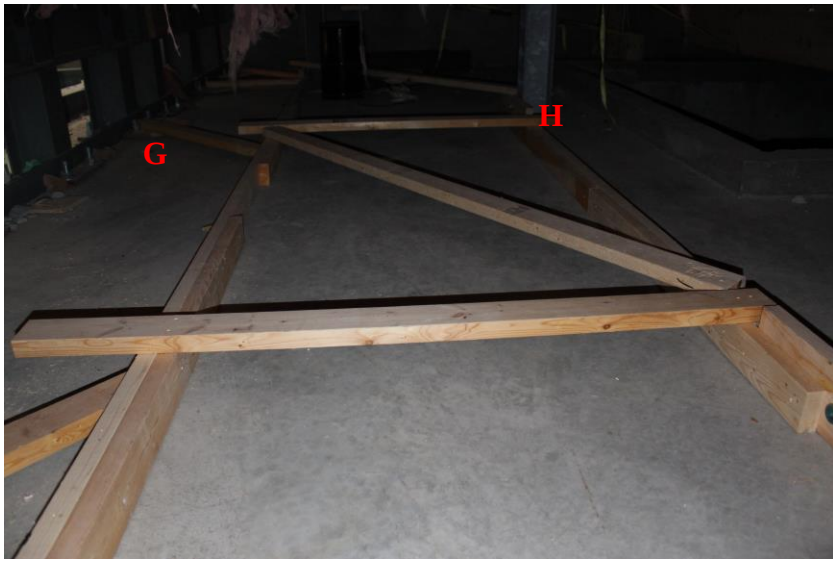

Figure 3.14 - Horizontal truss under the East side of the house, preventing translation of the base of the columns.

imbalance between the two cross braced columns. These braces were cables and so unable to act in compression, they were placed in particular orientations to directly counteract the reaction forces from the load cables (C and D).

Cables were routed out of the lower storey windows on the North and South sides of the building in order to prevent (i) any further holes being drilled in the house and (ii) unintended interactions between the house and the cables. While exiting the house, the cable leading from each of the load pads going to one column goes around a pulley (label E in Figure 3.13) – the columns essentially acting in the same way as the separation beams in the negative loading setup.

After exiting the house, the cables are connected to a separation beam and go to a pulley array and come-along. The two cables passing through the South windows were joined to create the typical four load pads to one come-along arrangement.

3.3.8 Second Storey Design

Loading of the second storey of the J1-J10 (East) wall was enabled by hanging vertical steel dropdown beams from the reaction frame. The beams hung straight down into the rooms on the second floor of the house (see Figures 3.15 and 3.16). The connection at the steel reaction frame was designed as a pin connection (label A in Figure 3.15). This meant that it was

necessary to brace the column, thus, two cable stay braces were installed (B) up to another beam on the reaction frame. When loading was applied to the wall by the primary cables (C and D) the cable stays became tensioned and prevented rotation of the dropdown beams. The dropdown beams were designed in accordance with CSA S16-09 to withstand the maximum expected forces during the experiments.

As shown in Figure 3.15, the cables coming out of the house are turned nearly 180 degrees at the dropdown beams (E), and then join together (F). There were four nearly identical setups like the one in Figure 3.15. The cable (blue cable at F) from one setup is joined to the same cable from another dropdown setup, providing four load pads to one come-along, as with the rest of the house.

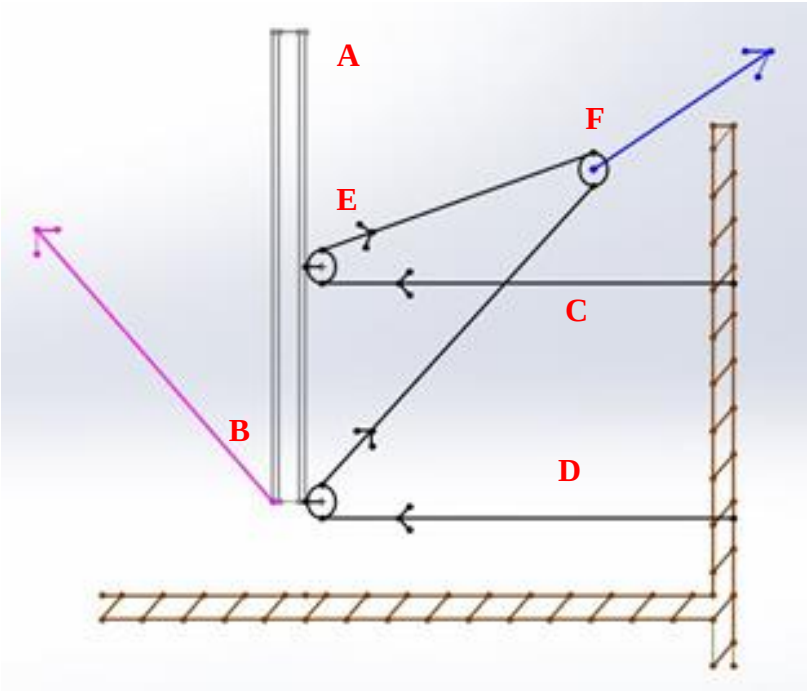

Figure 3.15 - A sketch of the positive whiffle tree setup. Primary cable in black, secondary cable in blue and cable stay in purple.

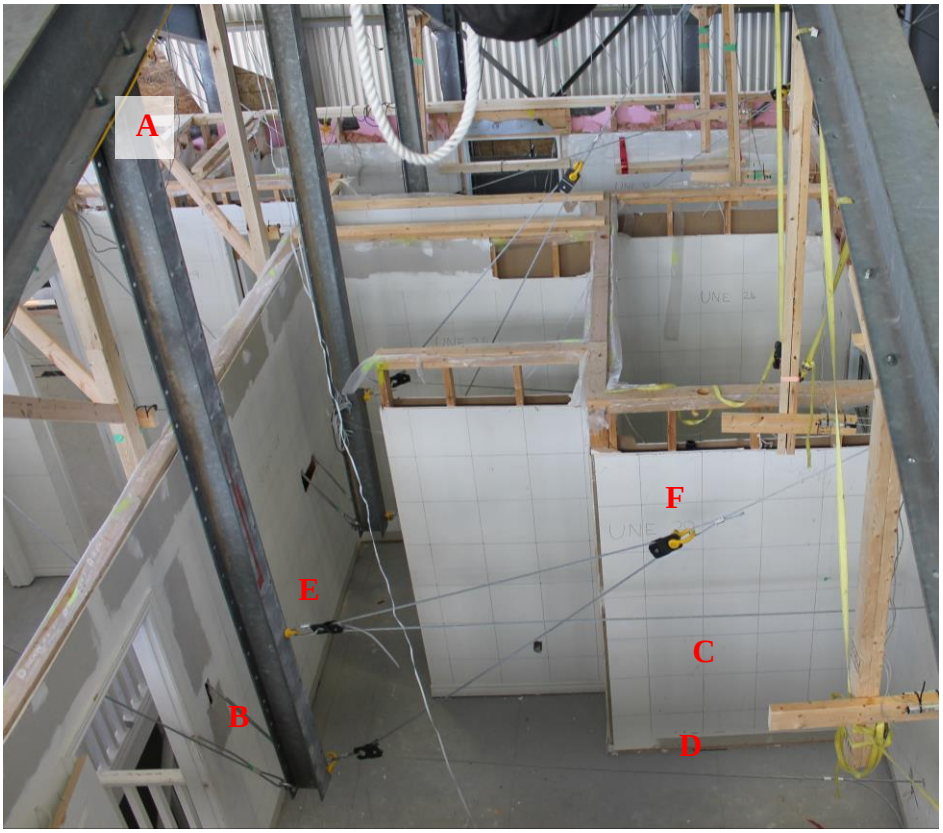

Figure 3.16 - Three drop down beams

3.4 Instrumentation Design

Two types of instrumentation were used for data acquisition: strain gauges and linear variable differential transformers (LVDTs)[2]. The strain gauges were used to read the loads applied to the house and the LVDTs were used to record displacements. Cameras and video cameras were also used in the experiments.

3.4.1 Strain Gauges

Strain gauges were attached to machined aluminum bars with waisted cross sections (see Figure 3.17), in order to make an inexpensive load cell. Each load cell was built with two strain gauges, one on each side. The readings from each strain gauge were recorded separately, to provide redundancy in the event of a strain gauge failure (since there was no bending of the load cells, which were always placed between two cables). The minimum aluminum cross section was chosen to ensure linear elastic behaviour up to a maximum load of 15kN, so the strain gauge would capture load accurately up to that limit. All strain gauges were calibrated before the tests, as is described in detail in Appendix D.

Figure 3.17 - Close up view of a strain gauge attached to an aluminum piece, forming a load cell.

One load cell was attached to each whiffle tree; on the section of cable immediately after the separation beam. A total of 16 load cells were used for the full house tests. Only one was used per whiffle tree due to the load equalization provided by the pulleys, as well as to reduce project expenses. The strain

[2] Also referred to as Displacement Transducers

gauges were attached at the same point on each cable to prevent losses due to pulleys from causing differences in load readings that do not reflect differences in the loads actually being applied.

3.4.2 Linear Variable Differential Transformers

A major challenge for this project was ensuring that the LVDTs would make measurements over the full range of displacements. To obtain measurements of the displacements at the top plate, it was necessary to suspend wood beams and/or frames down from the reaction frame towards the house (see Figure 3.18 for one example). Wood beams were used because of their high damping, low cost and ease of construction. Some LVDTs were also mounted off of the top plate to measure the relative movement between the brick and the top plate (Figure 3.19). For the test with the brick veneer in place 39 LVDTs were used, while 27 were used for the test without brick veneer. Drawings detailing the LVDT locations and names are shown in Figure 3.20, which shows the instrumentation plans for the tests with and without the brick veneer in

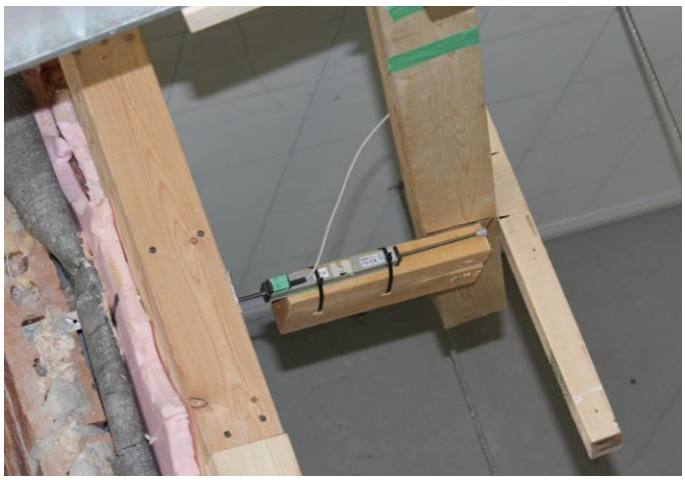

Figure 3.18 - LVDT NE1, with the wood beam from the steel reaction frame.

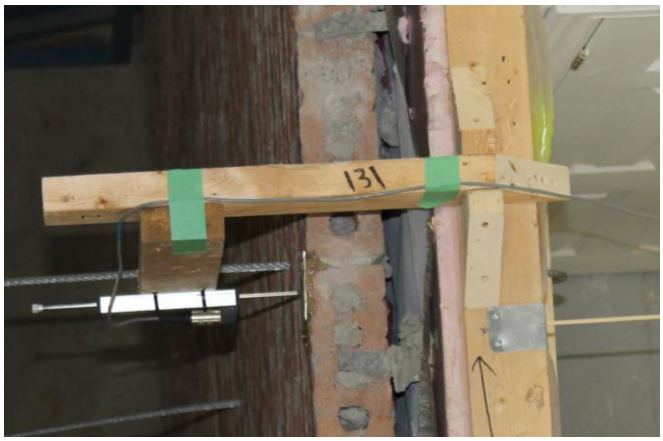

Figure 3.19 - LVDT WN5, measuring relative brick-top plate displacement

place. Only the LVDTs located along the top plate are shown. Some locations, such as the North West (A1-D1) wall in the tests without brick veneer had 2 or more LVDTs located in a vertical line where only one LVDT is indicated in the plan drawing.

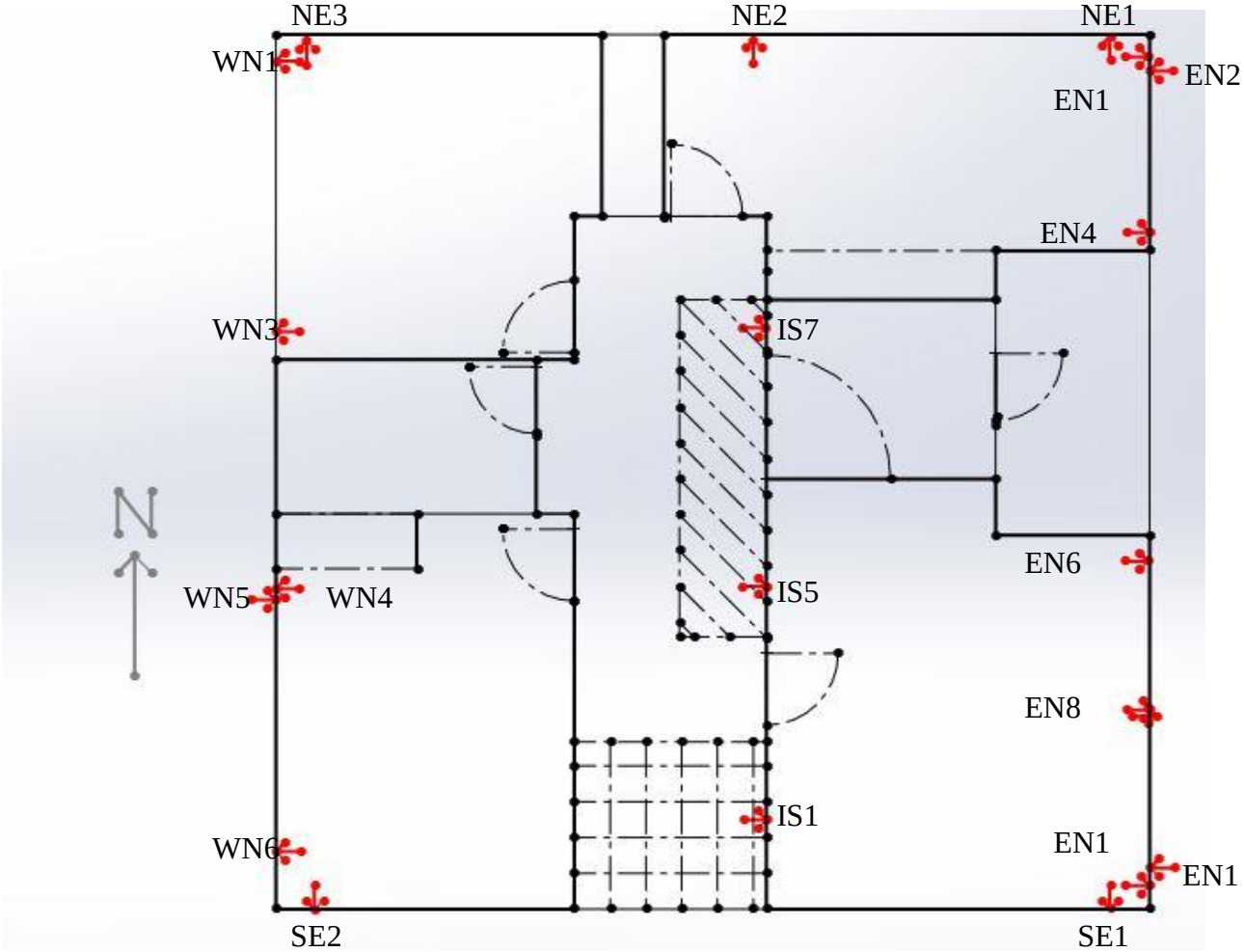

Figure 3.20a - Instrumentation plan for the test with the brick veneer in place.

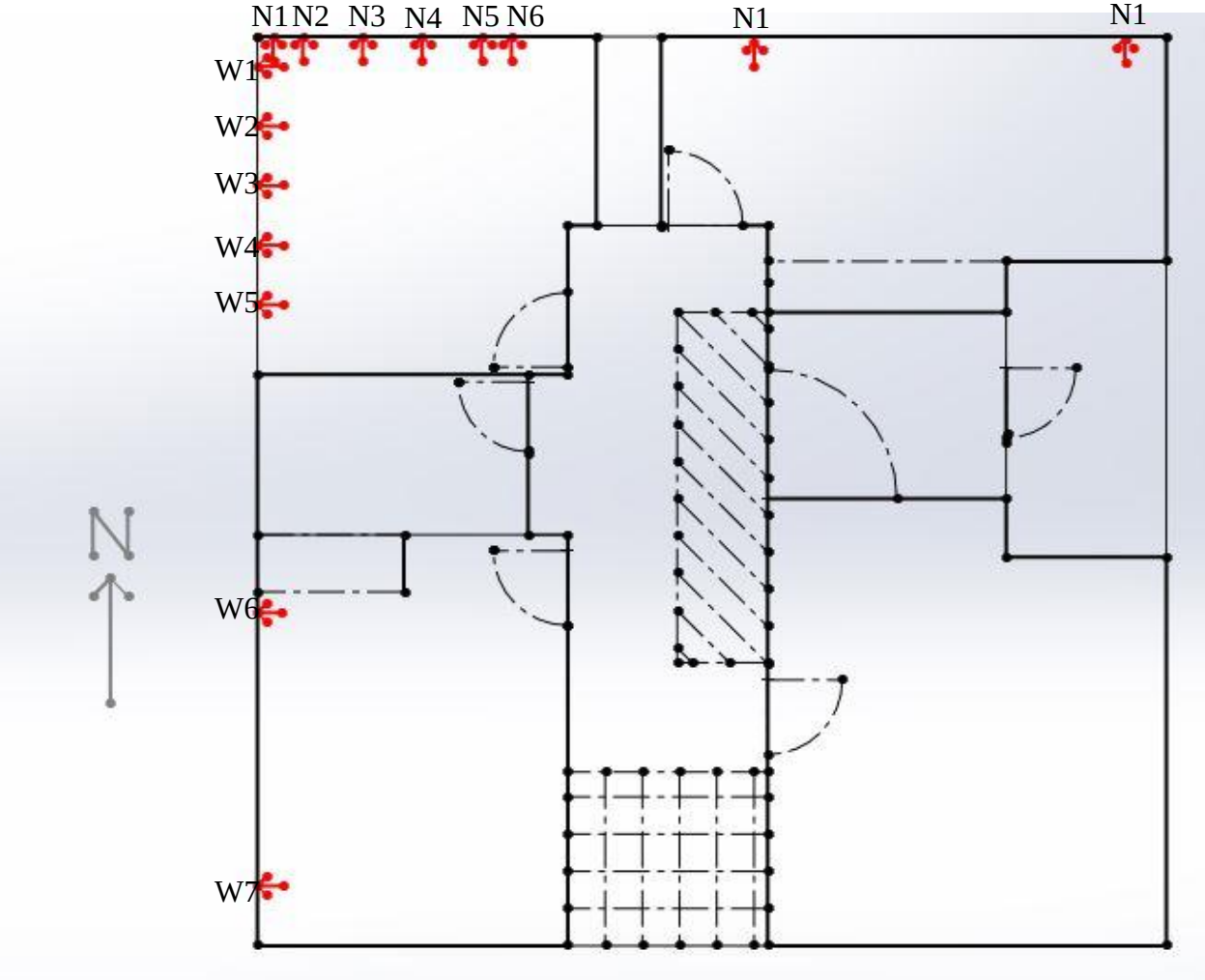

Figure 3.20b - Instrumentation plan for the test with no brick veneer in place.

Reference LVDTs were installed at many locations to ensure that measurements were accurate. Movement of the steel reaction frame was monitored by two LVDTs, one oriented North-South and the other East-West. No significant movement was recorded (see Appendix E for details). In addition, two LVDTs were installed at each corner of the base of the house, one normal to the wall on each side of the corner. These also indicated that there was no significant movement throughout the experiments (see Appendix F for details). Finally, the LVDTs reading displacements on the interior walls were mounted off of a gable beam in the reaction frame. To ensure these readings were accurate, a reference displacement transducer was also installed on the gable beam. Significant rotation of the gable beam during the tests rendered interior wall movement displacement readings unusable; this is discussed further in Appendix G.

Each individual LVDT has 100mm of travel, which in many places was sufficient for these experiments. In areas where larger displacements were expected, two LVDTs were used (see Figure 3.21a), offset from the each other by about 90mm, so that when the first LVDT ran out of travel, the other would start reading. To facilitate this, the LVDTs had thin wood skewers attached to them which would break off once the limit of travel was reached, shown at "A" in Figure 3.21a. Figure 3.21b shows one such LVDT pairing after the experiment, the skewer attached to the LVDT on the right hand side has snapped ("B" in Figure 3.21b). This was a simple solution to prevent destruction of LVDTs due to large displacements and allow for a larger overall displacement reading by matching and calibrating the displacement readings of both LVDTs to each other.

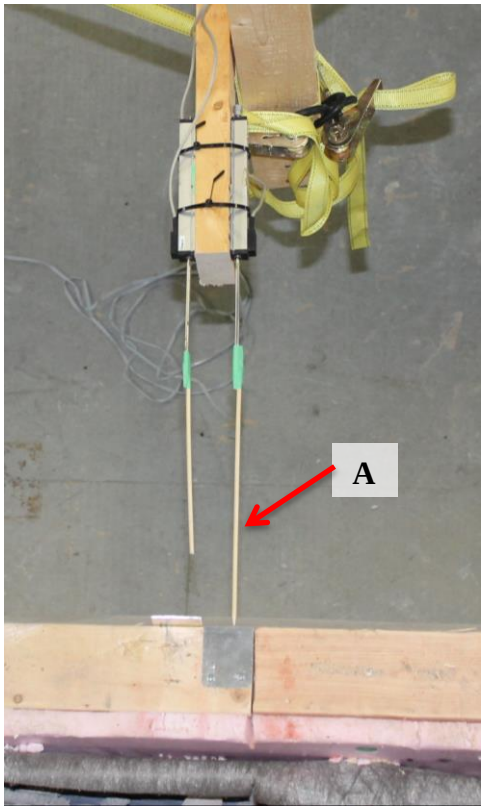

Figure 3.21a - A two LVDT setup (EN8 and EN9) before the experiment.

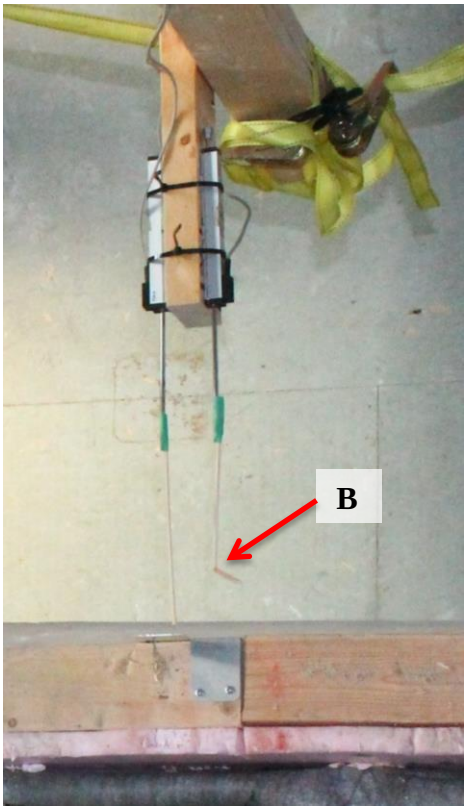

Figure 3.21b - LVDT setup EN8 and EN9 post experiment.

3.5 Experimental Control and Data Acquisition

A wood platform was built on the top of the reaction frame, to provide a location from which to control the experiments. This platform provided a bird's eye view of the entire test setup, and an unobstructed view of all of the come-alongs/load application points (Figure 3.23). The come-alongs were suspended from the top of the reaction frame at a convenient operating height for a person standing on elevated pathways (catwalks) above the top plates (Figure 3.22).

The locations for applying loads and organizing/controlling the entire experiment were selected to ensure all involved with the experiment were above the house while it was loaded. This ensured their safety from collapsing walls or falling debris Access to the catwalk and control platform was by a staircase on the North side of the house. This staircase had an oriented-

Figure 3.22 - The catwalk on the West side of the house, looking South.

strand-board shield installed along the house (South) side of the staircase, protecting anyone travelling up and down the stairs from harm. The catwalk location above the house was also ideal for observing movements of the upper floor of the house during the experiment.

National Instruments SCXI and PXI units, sampling at 200Hz throughout the experiment, were used for data acquisition. The duration of the experiment with brick veneer was approximately two hours. The sampling rate was chosen to capture the loads and displacements at the points of failure, sampling at a lower rate would have made it difficult to see any electrical noise from the strain gauges. The size and duration of the experiment reduced the feasibility or necessity of using a higher sampling rate.

An important part of the data acquisition was ensuring the zero datum was accurate for all data. This was especially important because components such as the strain

Figure 3.23 - The control platform on top of the reaction frame.

gauges were installed up to two months before the full house test. As well, the load cells to which the strain gauges were mounted were made of aluminum and were, therefore, susceptible to thermal expansion and contraction. The laboratory building was not temperature controlled, and so it underwent large temperature changes throughout the days of the tests. Data calibration and zeroing data is discussed in detail in Appendices H and I. Zero readings were taken several times over the course of the day before the experiments, during the experiments and after the experiments to capture any drift. The LVDTs showed negligible drift. However, strain gauges showed significant drift. Adjustment of the zero readings for the changes in thermal strain due to changes in the exterior temperature made the drift negligible, validating the data, as discussed in Appendices H and I.

3.6 Summary

The experimental setup was designed to be simple and inexpensive while being able to capture the required data. By applying loads with come-alongs, cables and pulleys, the experiment was easily controllable; with the ability to quickly stop or reduce applied loads in the event of a problem or safety hazard. Manual loading introduced some uncertainty and variability to the application of the loads due to the human factor. However this was easily mitigated by exercising caution and care during the experiments. The results of the experiments are discussed in the next chapter.

Chapter 4 – Catastrophic Failures

Catastrophic failures are those failures which cause permanent and significant damage to the structure, making it unsafe for use. An example of such a failure would be an entire wall collapsing. There were three catastrophic failures which occurred during the experiments. During the full house test, the complete wall at A10 – J10 (i.e., the South wall) failed. In the subsequent test without brick veneer, two catastrophic failures occurred on the North wall, the first one between A1 and D1, the second between E1 and J1. This chapter describes these three failures.

4.1 Failure of Interior-Exterior Wall Connections (on Wall A10 - J10)

The A10-J10 wall failure happened after loading had caused substantial visible bending and displacement in all four walls, but most noticeably the A10 – J10 (South) and J1 – J10 (East) walls. The top plate on the South wall (A10-J10) appeared to be acting as one long beam with the two connecting interior walls substantially limiting the overall displacements. Ultimately, it was the failure of the connections between the interior walls and the exterior wall which failed, as shown in red in Figure 4.1. The implications of the roles of the interior-exterior wall connections with respect to overall house strength are discussed in Section 5.1.

Figure 4.1 – The segment of wall C10 - E10 after

The load-displacement curve for the South wall spanning F10 – J10, shown in Figure 4.2, depicts the process leading up to failure. The load is plotted as net pressure across each wall. Pressure was calculated based on the assumption of uniform loading using the locations where the load pads were applied by dividing the load applied to each load pad by the relevant tributary area. In this Figure, the displacement is at the top plate level from displacement transducer NE1 (Figure 3.20a), part way along the way at location I1.

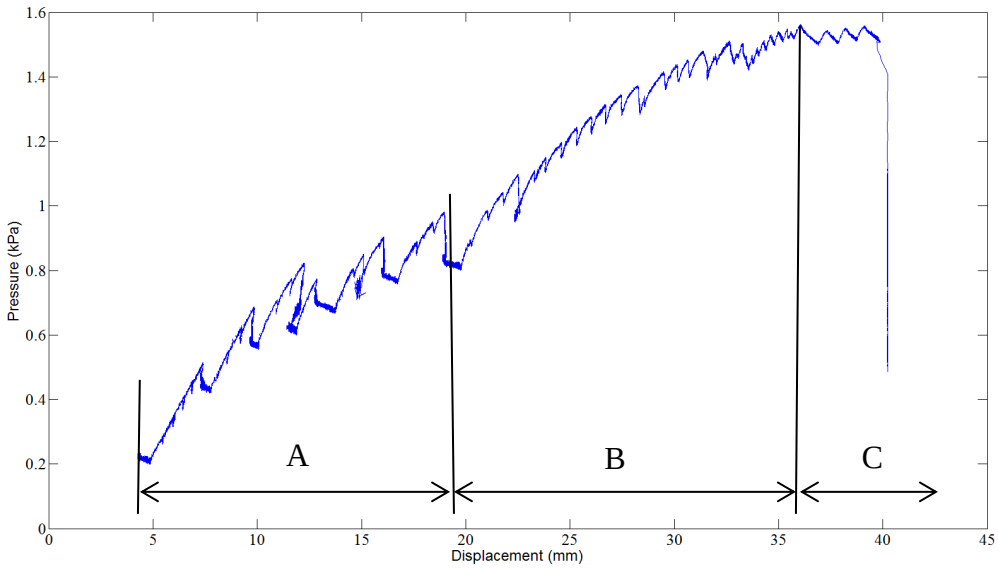

Figure 4.2 – The load deflection curve for wall F10 – J10, from a displacement transducer at I1

There are three main regions in this plot. The first region extends from a pressure of 0.2 kPa to just less than 1 kPa (and is labelled as "A"). In this area, the slopes of the curve while load is being increased are nearly identical. Between the sections of increasing load there are small load drops and a slight increase in displacement in a saw-tooth type of pattern, which are referred to as "discontinuities". The discontinuities are caused by two factors, namely, the loading method and the net loading effects, as discussed in Appendix J. In the second region (labelled as "B"), it is observed that the slope of the load-displacement curve is decreasing monotonically.

Thus, as the load is increased, the relative displacement also increases. This continued until the edge of the third region (labelled as “C”), where the load could not be further increased and the wall was simply being winched over (at a constant load).

In the region C, the wall cannot resist any higher load, corresponding to the onset of failure. The maximum resistance of a wood structure may be time dependant, decreasing as the load is applied more slowly. Morrison and Kopp (2011) found this to be an insignificant issue for failures of connections, hence, detailed examination of time effects are not considered in this thesis. The key failure was at the interior-exterior wall connections as shown in Figure 4.3. This failure occurred at a load of about 1.5 kPa. Comparing the damage shown in Figures 1.3 and 1.4 (from tornado damage surveys) to that in these Figures, there is some similarity indicating that this may be a common type of failure of wall systems following global roof failure.

Figure 4.3 - Damage to the house similar to what was observed in Barrie and Goderich.

4.2 Wall Failures Without Brick Veneer (the A1 – D1 Wall Failure)

Following the tests on the full house clad in brick veneer, the bricks were removed from the house and local testing was conducted on un-damaged portions of the walls. The first catastrophic failure for house without brick veneer is discussed here. This failure was preceded by large displacements and initiated with a split occurring in the top plate. Figures 4.4a – 4.4f show the progression of the failure as recorded by a video camera at 30 frames per second, with the image sequence spanning a duration of less than 0.2 seconds. Due to the large magnitude of the displacements which occurred with the failure, the LVDTs did not capture the dynamic movement of the wall immediately after the top plate failed. In Figure 4.4a the wall is still intact, progressing from 4.4b to 4.4d, the top plate can be seen to be splitting and a large vertical crack is forming in the Styrofoam beneath the top plate split. In Figures 4.4c and d, the initiation of a vertical crack along the edge of the corner can be seen. Finally, Figures 4.4e and f show the propagation of the cracks and continuation of the failure to the final displacement of the wall.

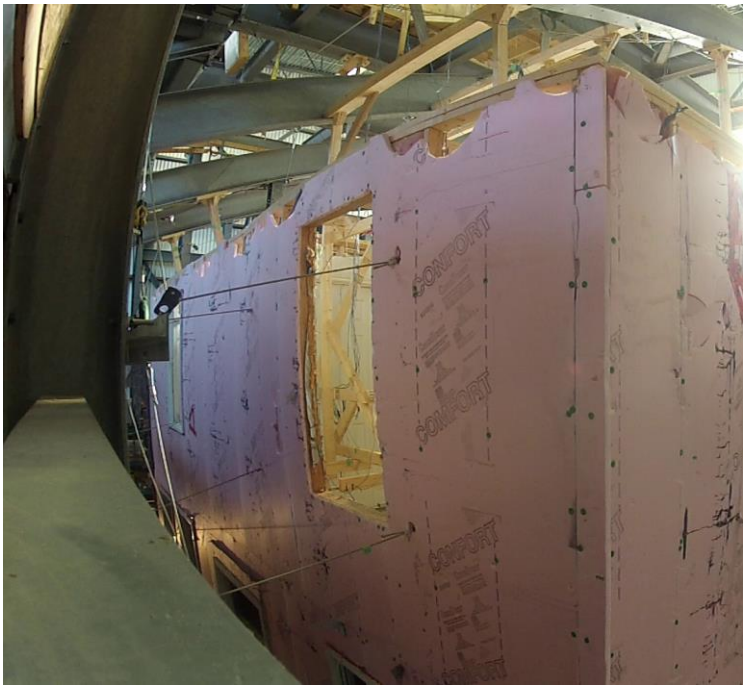

Figure 4.4a – Failure Time + 0:00.00

Figure 4.4b – Failure Time + 0:00.03

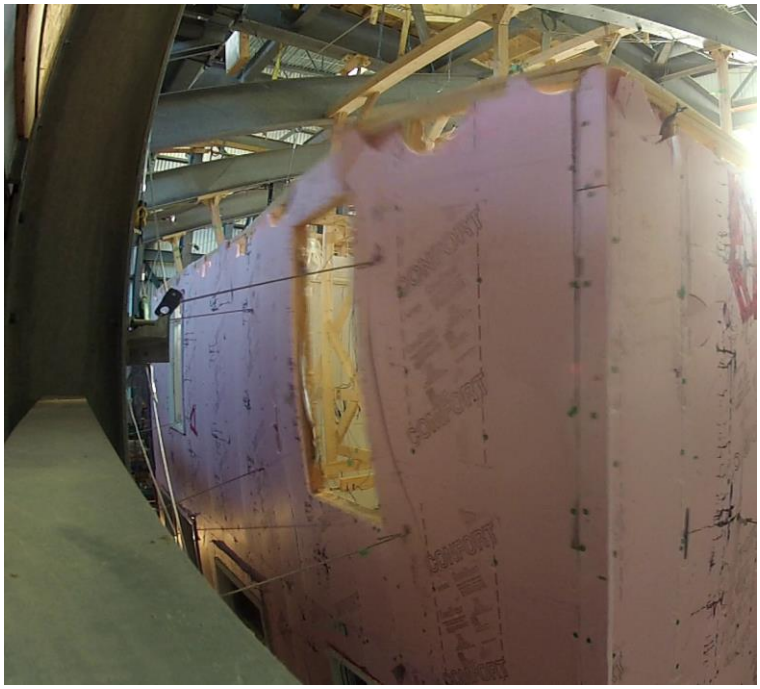

Figure 4.4c - Failure Time + 0:00.07

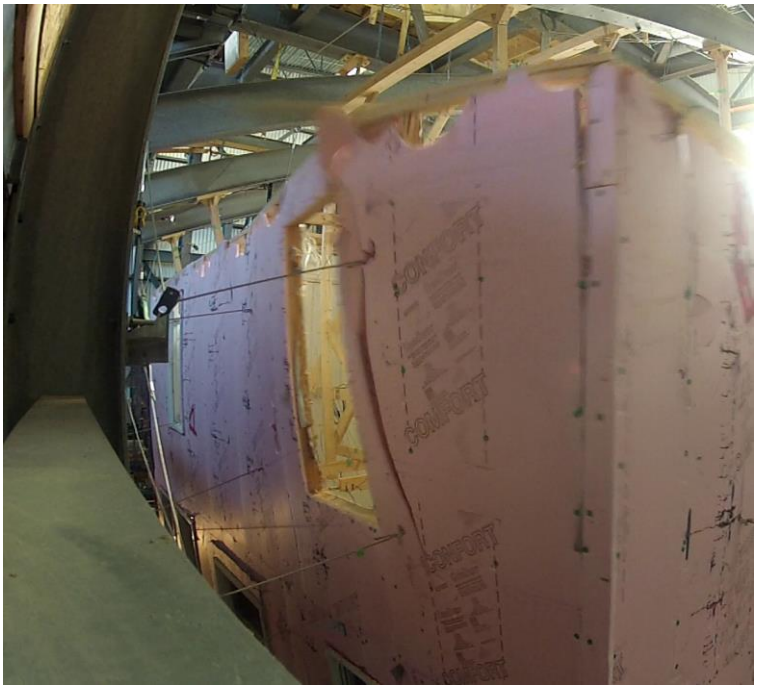

Figure 4.4 d - Failure Time + 0:00.10

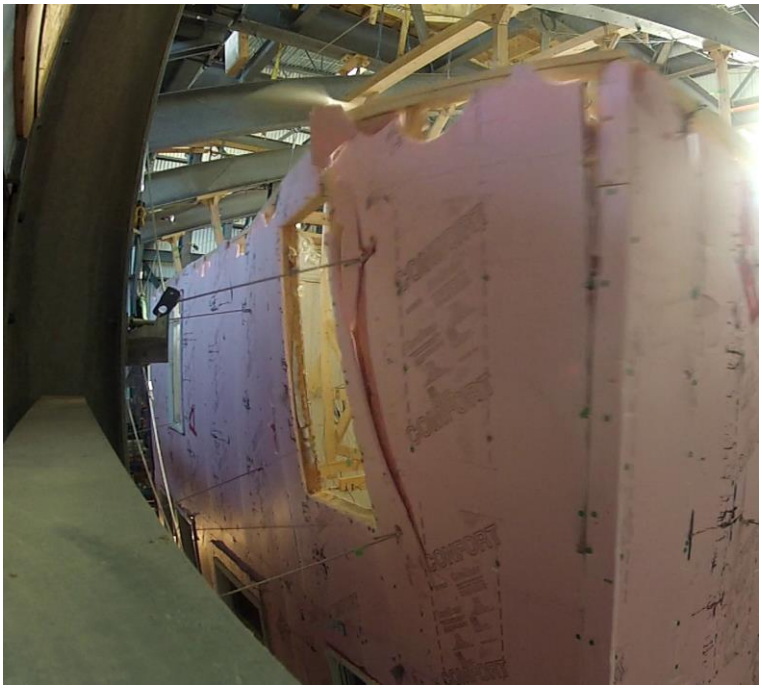

Figure 4.4e - Failure Time + 0:00.13

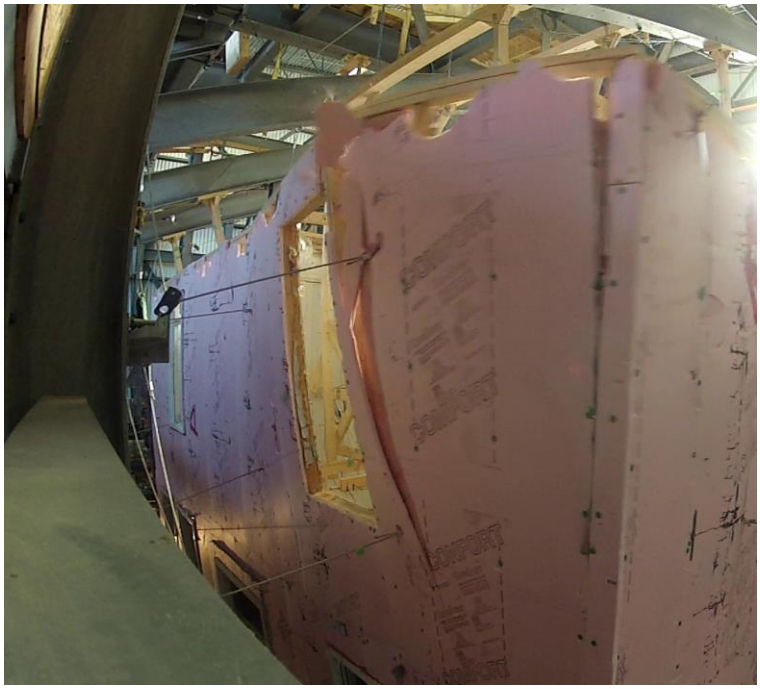

Figure 4.4f - Failure Time + 0:00.17

This failure occurred because of a relative lack of stiffness in the wall and the corner. The bending stiffness of the top plate (which had a joint at D1) was minimal due to short overlap in the two top plate members (see Figure 6.6). In addition, the presence of the window may have played a role. These issues are examined in detail in Chapter 6. The stiffness of the corner, which was reduced with the removal of the bricks, also allowed the wall to rotate outwards. The effects of brick veneer are examined in Chapter 7.

The load-displacement curve for this wall is relatively linear up to an applied pressure of about 0.8kPa. This is shown in Figure 4.5, which shows the pressure-displacement curve for an LVDT located at the top of the wall, about 160mm from the corner located at A1 towards B1. It is noted that this failure load is the same as was observed for the first failure of the full house with the brick attached (along wall A10 – J10, as discussed in the previous section). However, when wall A1-D1 failed, there was negligible damage at the current location, indicating that the brick veneer has a substantial effect and that the first failure would have occurred at a much

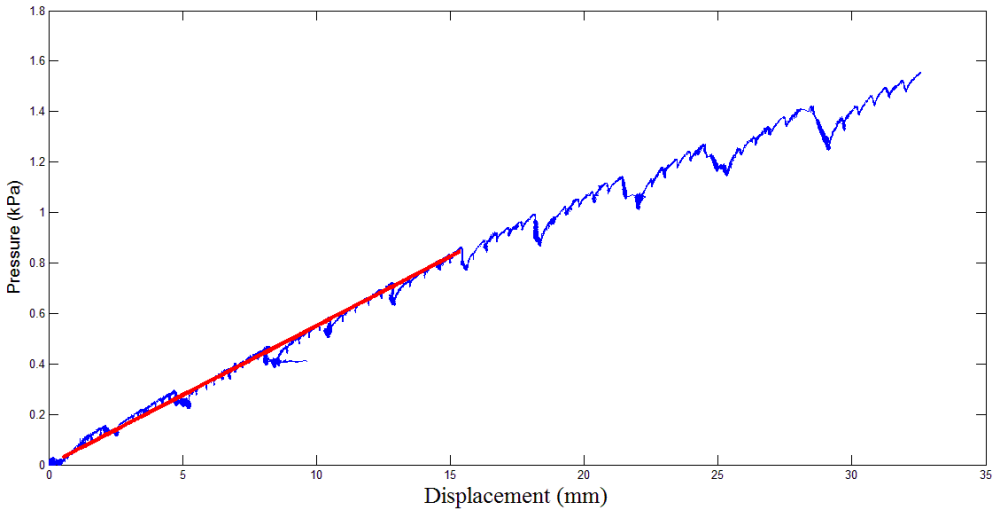

Figure 4.5 - Load Displacement curve for the wall A1-D1.

lower load had the house been without brick veneer for the first full house test. It is also emphasized that the two walls have different factors which affect the performance including the unsupported lengths, number and location of openings, and number of interior walls connecting to the external wall. Dolan and Heine (1997a, 1997b) and Doudak et al. (2006) found that these differences significantly affect wall strength.

4.3 Wall Failures Without Brick Veneer (the E1-J1 Wall Failure)

The third catastrophic failure observed during the two sets of experiments occurred following the failure described in Section 4.2. The double top plate of this wall (E1-J1) failed in shear at the location of a connection between the upper and lower members of the double top plate, as seen in Figure 4.6. Top plate failures are examined in detail in chapter 6, while the failure load and load deflection curves are examined here.

The load-displacement curve is shown in Figure 4.7, where a linear section can be seen, as shown by the red line. The Figure provides the results for the wall segment E1 – J1, with the displacement measured at the top plate at location F1. For lower loads, there is the typical increase in load and displacement, followed by a region where the load remains relatively constant while displacement increases. This is due to the loading and failure of the A1-D1 wall described in Section 4.2. When that section of the wall was on the verge of failure, load increases

Figure 4.6 - Plan view of wall E1-J1 after catastrophic failure.

on the E1-J1 segment was stopped and increased loading was continued only on the A1-D1 wall segment. These results in the observed load-displacement pattern labelled as “A” in Figure 4.7.

In this experiment, the LVDT ran out of travel because of large wall displacements. The red line is a linear representation of the load-displacement relationship. It is drawn fitting to the data corresponding to the loading leading up to failure. As discussed, there was a pause in the loading at “A”, so the most important (and the majority of the) loading occurred after this point. Hence only that area was used for the data fit.

From the data, this failure occurred at a pressure of 0.6 kPa, significantly less than the failure load of other walls. However, it sustained the highest loads in the earlier experiments. As with the first full house experiment with brick veneer in place, the wall failures appear to be similar to damage survey observations (e.g., Figures 1.3 and 1.4) which show similar final states. As previously discussed, the net loading effects allow loads applied at one location to be

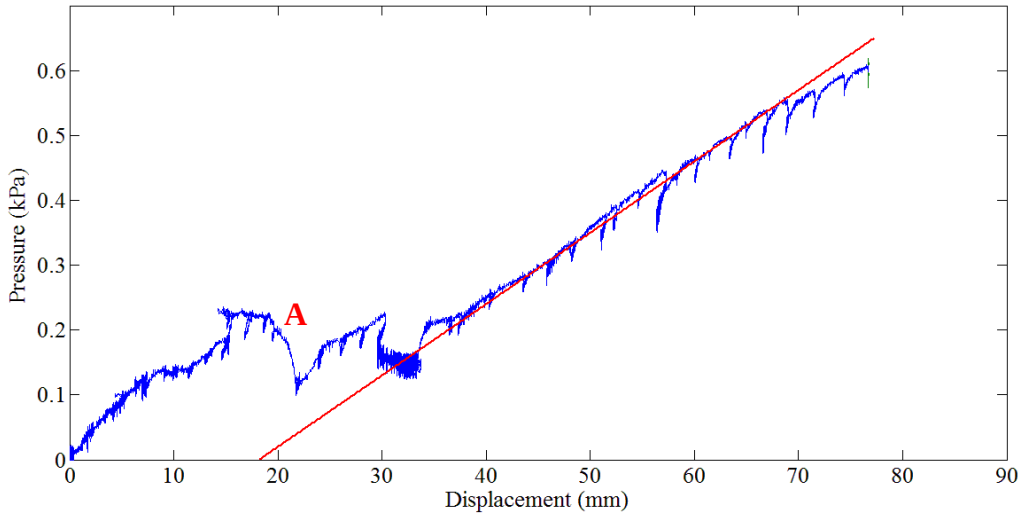

Figure 4.7 - A load displacement curve for wall E1-J1.

transferred into adjacent locations. Since the adjacent wall segment (A1-D1) had failed, little load could be transferred along this wall.

The importance of a continuous load path was discussed in FEMA (2011, section 1.2.3) as being essential for the wind resistance of houses. The ultimate loads measured during this failure emphasize the need for a continuous load path to be available. Thus, it would be expected that a lower failure load would be observed for wall segment E1-J1 following the failure of the A1-D1 wall segment.

4.4 Conclusions

After examining the three catastrophic failures which occurred during the experiments, it is clear there are several types of failure of wall systems (when there is no roof in place). Each of these failures will be examined in greater detail in the subsequent chapters. The ultimate load of Wall A10-J10 with the brick veneer still in place was found to be 1.5 kPa when the connection between an interior wall with the exterior wall failed. Without the brick veneer, wall segments A1-D1 and E1-J1 failed at 1.5 kPa and 0.6 kPa, respectively. Since the first failure without brick veneer had easily sustained a load of 1.5 kPa when the brick veneer was in place, the current results indicate that the brick veneer played a significant role in increasing the capacity of the walls compared to the case without brick veneer. In addition, the difference between the Wall A1-D1 and E1-J1 failure loads (both without brick veneer) indicate the importance of the walls remaining intact in maintaining the capacity of the system. When there was no continuous load path, the failure loads decreased significantly.

Chapter 5: Effect of Interior Wall Connections to the Exterior Walls

Catastrophic failure of Wall A10 to J10 occurred due to a failure of the interior to exterior wall connections located at D10 and F10, as discussed in Section 4.1. This chapter discusses in detail the role of the two interior walls located at D10 and F10.

5.1 Failure Progression at D10 and F10

If observed in real time, the failure of the two joints located at D10 and F10 appears to be simultaneous. However, a frame-by-frame analysis shows a different story. Failure first occurred at the joint at D10, followed by the joint at F10. Figures 5.1 to 5.4 show the progression of the failure: Figure 5.1 shows the wall in its unloaded state, Figure 5.2 shows the loaded wall immediately prior to failure, Figure 5.3 shows the wall after failure of the joint at D10 and Figure 5.4 shows the wall after failure of the joint at F10. Joint failures in each figure are identified by circles.

Figure 5.1 - Wall D10 - F10 before loading.

Figure 5.2 - Wall D10 - F10 loaded immediately prior to failure.

Figure 5.3 - Wall D10-F10 as the joint as D10 is failing.

Figure5.4 - Wall D10 - F10 after both joints have failed.

Examination of these four Figures reveals how and why this failure happened. In Figure 5.1, a small gap can be seen at the connection at D10; this connection was the first part of the wall to fail. The nails from the interior to the exterior wall at D10 pulled out of the exterior wall in tension. They can be seen after pullout in Figure 5.4.

When the connection at D10 fails, the interior wall is no longer providing a restraint at the exterior top plate. Because Wall D10 is perpendicular to the loaded wall it transferred the out-of-plane (shear) forces in the exterior wall into racking forces in the interior wall, which is strong in this aspect. A result of the joint failing is loss of this load path. Following the failure at D10, the loads being applied to the exterior wall between A10 and F10 must be restrained at joint F10 and the corners. This immediately increases the net loads at joint F10, causing this joint to fail and catastrophic failure of the entire wall. A schematic of the change in load path is shown in Figure 5.5, which shows the approximate load path before the failure at D10 (top) and then after the failure at D10 (bottom). The Figure shows a basic approximation of how the reaction forces at the interior-exterior wall connections change when the connection at D10 fails. Thus, the connection strengths at the interior-exterior wall interfaces are extremely important for the strength of the entire exterior wall.

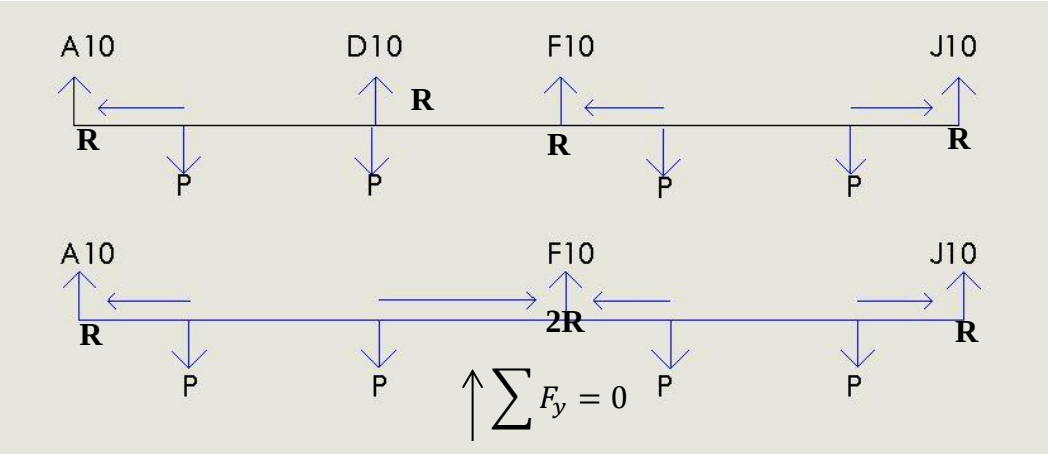

Figure 5.5 – External wall top plate load paths along the wall spanning from A10 to J10 with and without the connection at

5.2 Interior Wall Placement Effects on Wall Displacements

Although no catastrophic failure occurred on the East wall (J1 – J10), displacements of up to 120 mm occurred along J6 – J10 (in the Master Bedroom). The scale of these displacements and the lack of failure was largely affected by the placement of the interior walls. LVDTs were placed at J1, J3, J6, J8/9 and J10 in order to measure the movement of the top plate. The displacement readings at lower load levels – up to 1.0kPa are shown in Figure 5.6, higher load levels are not shown to allow for better illustration of the two different behaviors observed. The zero displacement at the corners is assumed, based on the comparison between the effects of loading the East side on West side deflections, and vice-versa, since there were no noticeable racking effects across the house. In the Figure, the thick vertical black lines represent the locations of interior walls. The thin vertical red lines represent the points where the loads were applied. There were three LVDTs in the master bedroom, and two in the den. No LVDTs were placed in the bathroom due to quantities of available instrumentation.

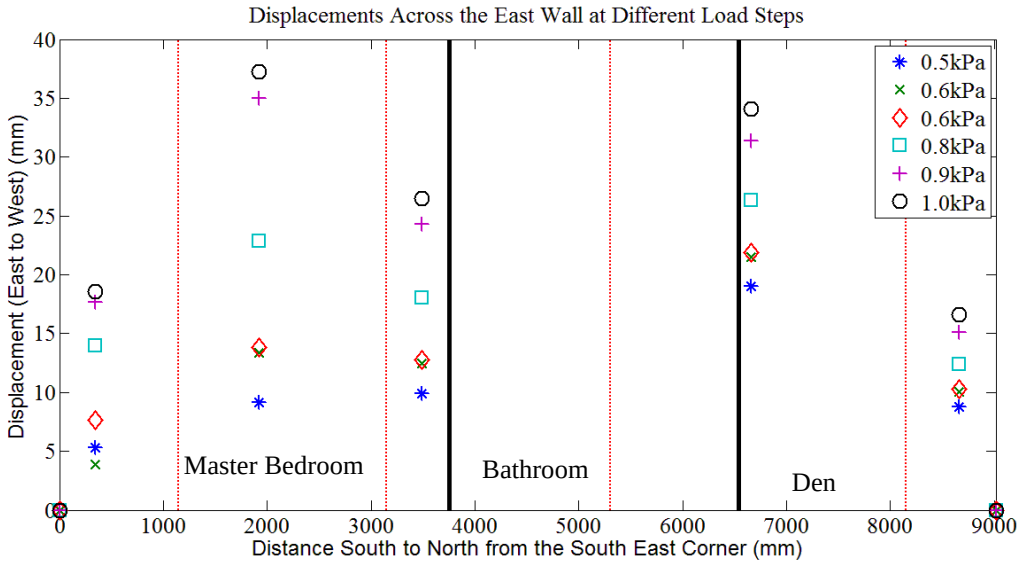

Figure 5.6- Wall J1 - J10 LVDT readings at increasing loads.

Two patterns can be observed in the data. First, during the early stages of loading (0.5kPa, 0.6kPa and 0.6kPa[3]), more movements of the whole wall are seen. As the load increases, the behaviour changes, showing more local deflections with a maximum occurring near the middle of the Master Bedroom wall segment.

In the bathroom, there were no LVDTs, so no quantitative measurement could be made. Despite a vertical line of loads being applied in the middle of that room, where the maximum possible top plate bending effects would be seen, there was no bending noticed of this top plate (from observations and a qualitative analysis of photographs, such as Figure 5.7). The same loads were applied to this room as the master bedroom, which saw significant bending. This may be because the unsupported length of the bathroom wall is only 2/3 of the unsupported length of the master bedroom wall. For simplicity, if the walls are assumed to be simply supported beams subjected to a uniformly distributed load, the maximum deflection is governed by the span, *l*, to the power of four, as given by equation 5.1.

Figure 5.7 - Wall J7-J3 (left to right) under load.

[3] Due to required readjustments of the come-alongs during the experiment, the load of 0.6kPa was achieved twice, during the readjustment the load decreased.

$$\Delta_{max} = \frac{5wl^4}{384EI} \qquad (5.1)$$

Assuming uniform loading across all exterior walls (per the experimental design) and that Young's Modulus (E) and the Moment of Inertia (I) are constant, then the deflection is almost entirely controlled by the unsupported length of each wall. For the difference between the bedroom and bathroom this translates into a fivefold increase in deflections from the bathroom to the bedroom (ignoring possible differences in the displacements at the ends of the segments). Clearly, more evenly spaced interior walls would increase the overall exterior wall strength and reduce the wall deflections in large rooms. Of course, stiffening of the wall would also help by adding wall studs or an additional top plate member.

At the point of failure on the south wall, the maximum displacements on the east wall were about 120 mm. This again points to the importance of the connections under suction loads, since the interior-exterior wall connections under the positive pressures on the east (windward) wall would not fail; rather the structural members would have to fail. Since the capacity of the connections under pull-out are the weak link, the south wall failed first. This suggests that increasing fastener strengths between the interior and exterior walls, say by using hurricane straps or screws, would increase the resilience of the walls should the roof fail first.

5.3 Conclusions

Two main conclusions can be drawn from the observations of the effects of wind loading on the interior-exterior wall connections. The first is that, when acted upon by negative pressure, the strength of interior-to-exterior wall connections directly affects the overall capacity of the exterior wall. Increasing the capacity of these connections, say by using hurricane straps or screws, would allow larger displacements of the wall and lead to failures of structural members

(instead of connections) at higher wind loads (i.e., higher wind speeds). The second conclusion is that the placement of interior walls affects the local bending, specifically in larger rooms. Obviously, smaller rooms and more interior walls would create a stronger house once the roof has failed. This is contrary to current house plans which typically feature large master bedrooms and “open concept” plans, which is contrary to known flexural beam theory and deflection as well as this research. Longer unsupported spans require additional wall stiffness to resist the same loads.

Chapter 6: Top Plate Failures

Failures of the top plate were observed in these tests, as discussed in Chapter 4. These failures are examined in this chapter. A top plate is a beam on top of the wall studs which extends on the top of all walls in a house/structure. The top plate in the 3LP house was constructed as a double top plate, with two 2”x4” members stacked on top of each other to form a 4”x4” member. Double top plates are very common for construction as they are required by section 9.23.11.3 of the Ontario Building Code 2010 unless a loadbearing wall contains a lintel beam provided the lintel forms a tie across the lintel; or if concentrated loads from ceilings, floors and roofs are not more than 50mm to one side of the supporting studs. Non-loadbearing walls are also permitted to have single top plates, however all exterior walls are loadbearing. Failures of the top plate are represented by three dominant failure modes: cracking of the top plate through nailed sections; and separation of the two top plate members due to a small overlap between member ends and splitting of the top plate due to high displacement.

6.1 Cracking of the Top Plate

Cracking of the top plate occurred in several locations; Figure 6.1 shows a span of the East wall, the segment from J7 to J3. With closer examination (Figure 6.2), it can be seen that the top plate has cracked along the line of the nails (point A in Figure 6.1). This is a failure of the member due to overall deflection of the wall and the nails being placed too close to the edge of the top plate member. In addition, the bottom member of the top plate failed further along (B, or Figure 6.3) and moved out of alignment with the top member, as shown in Figure 6.3.

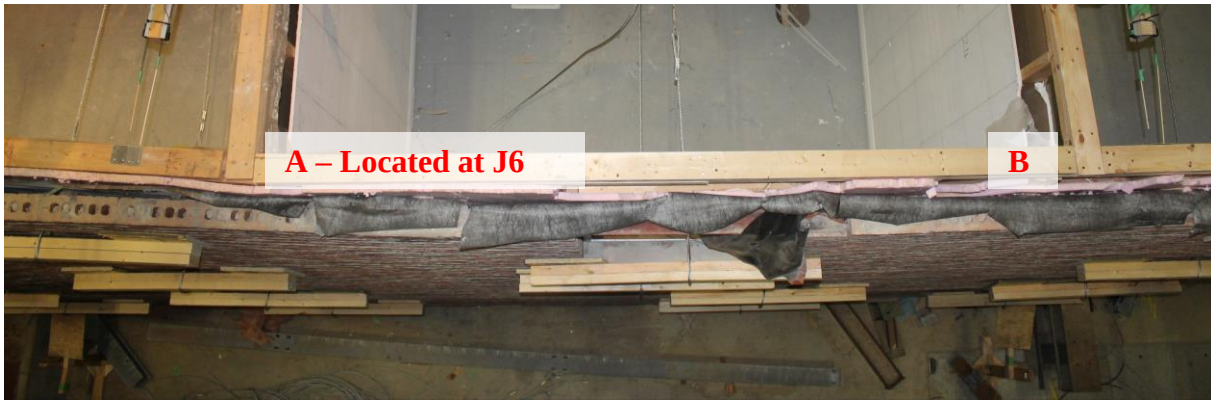

Figure 6.1 - Looking along the East wall from J7 – J3.

The failure of these members reduces the ability of these members to transfer load through the basic load path across the top plate, transferring the out-of-plane (shear) force into racking forces in the interior walls. Therefore, it can be stated that placement of a few additional (or better placed) shear connectors (nails) between the two top plate members would increase the strength of the wall. As well, better control over the distance between top plate edge and the nails would reduce cracking and this type of failure.

Cracking and failure of the top plate also occurred in the North wall spanning from E1 to J1 in the tests without brick veneer. This was the second catastrophic failure which occurred during the tests without brick veneer, occurring after the failure of the adjacent wall segment (A1 – D1), as discussed in Section 4.3. Failure of the top plate occurred at an area with

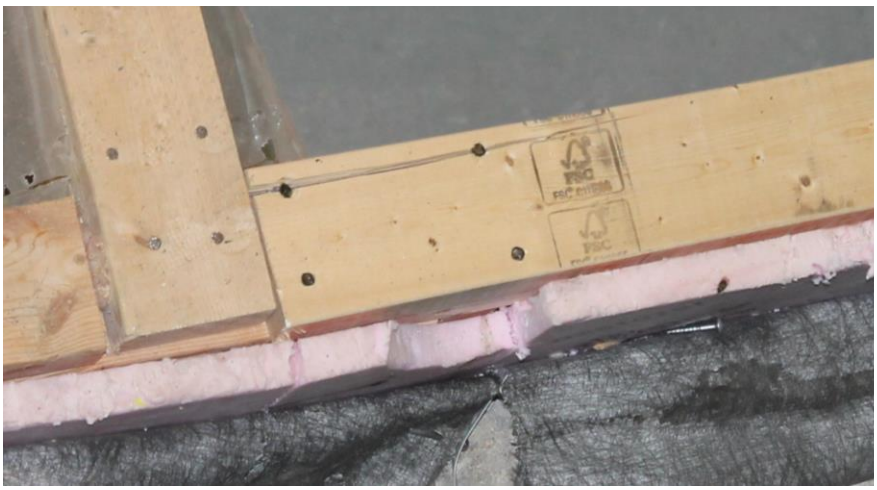

Figure 6.2 - Close up of top plate crack (A in figure 6.1) J6.

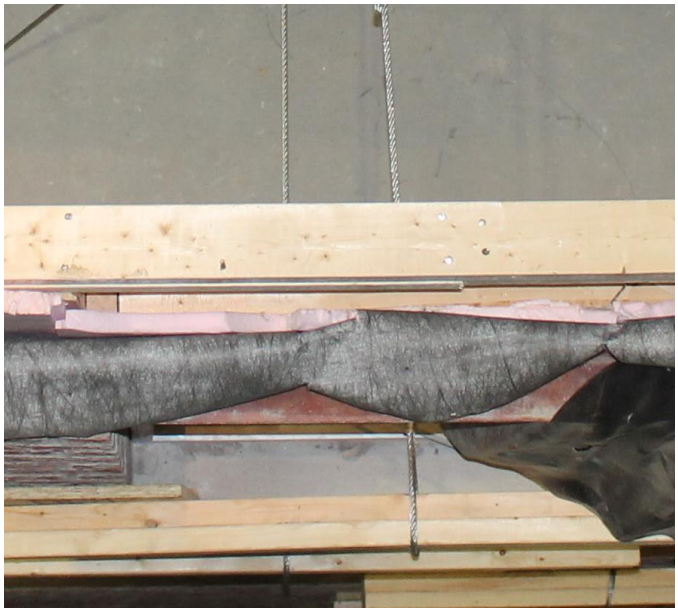

Figure 6.3 - Close up view of top plate slip (B in figure 6.2) J4-J5.

a relatively small overlap between connections on the upper and lower top plates. Figure 6.4 shows the wall under load prior to failure, with the location of the point of failure labeled "C". Figure 6.5 shows this location after failure.

Before the failure occurred, there was a visible slipping at the joint in the upper top plate at the location of the nails. The wood in the connection failed, causing the top plate to become two members pinned at D (instead of one long member subject to bending). As with the previous failure, more nails placed closer to the center of the member would have created a stronger connection and given a higher failure load.

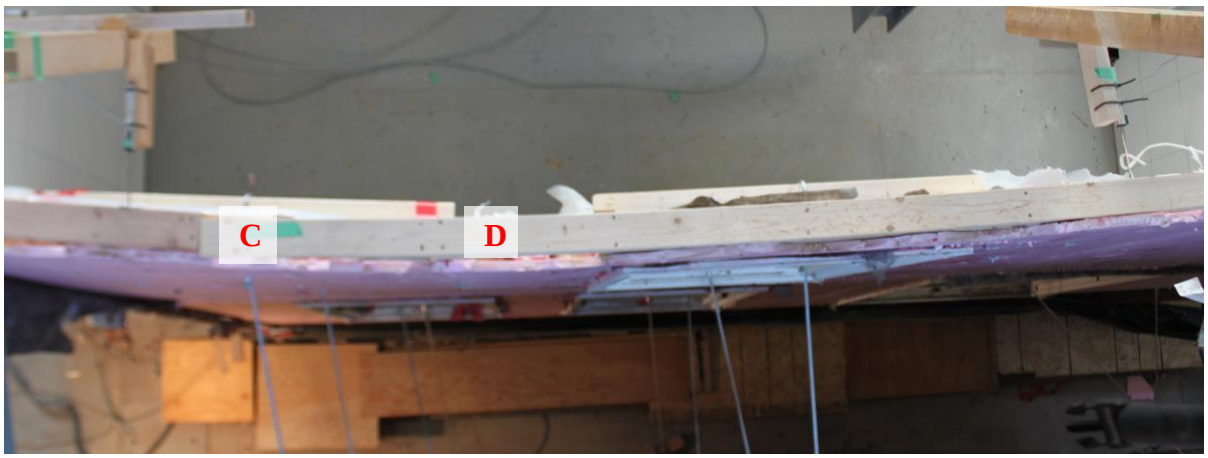

Figure 6.4 - The North East wall prior to failure E1 – J1.

.A conclusion which can be gained from this is that the overlap of the top plate and the strength of the shear connection between the two top plate members effects the strength of the wall. If there had been more nails spaced with a longer overlap, it is likely the wall would have withstood a higher load before failing.

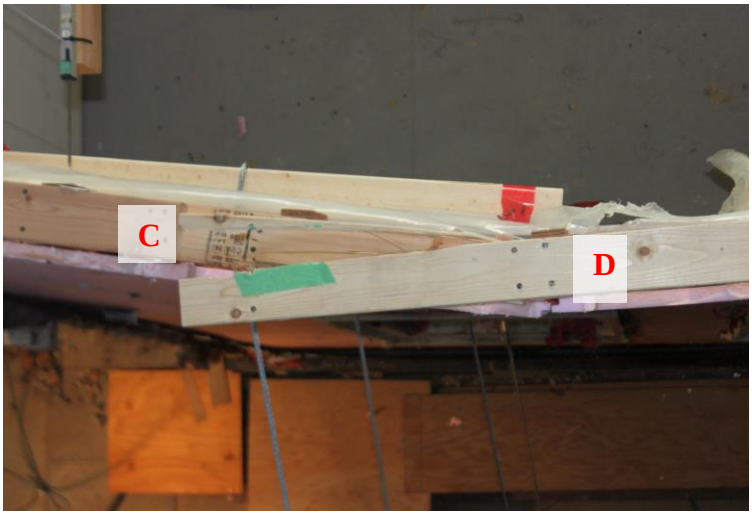

Figure 6.5 - The failure location on the North East wall H1-I1.

6.2 Top Plate Overlap Failures

There were two instances of top-plate-overlap related failure, the first occurring at location D1 during the tests without brick veneer. In this case, a lack of overlap between the two top plate members allowed for significantly increased rotation and deflection of the top plate members in the adjacent room (A1-D1). The second instance was during the full house test (with brick veneer), at location F10, after the failure of the interior-exterior wall connections the top plate failed, causing increased deflections. This latter failure will not be discussed further.

Figure 6.6 shows the result of minimal overlap of the top plate members from the first instance discussed above. This joint has allowed almost free rotation of the top plate in the adjacent room (A1 – D1) this pin-like behavior and resulting room A1-D1 deflections is further examined in Appendix K. Because of the connection to the interior wall, the upper member of the top plate ends to allow space for the interior wall top plate to be connected. The lower member of the exterior wall top plate does not extend very far beyond this connection (towards

the left in Figure 6.6). The type of connection in Figure 6.6, when observed in a plan view appears to behave like a simple pin support, providing minimal rotational resistance, as if the top of the wall was acting like a flexural beam.

The wall below would have influenced the rotational behaviour, but a full 3-dimesional analysis was outside the scope of this thesis. Rotation of the lower member of the top plate relative to the upper member of the top plate is easily visible in Figure 6.7, just to the left of the point where the interior wall enters from the top of the image. In the background (D1) of Figure 6.7, it can be seen how the rotation of the top plate is effecting the overall displacement of the wall, by allowing a much higher maximum displacement. The difference in deflection which could be affected by more rotational resistance depends on how much fixity is added. If one end of a wall span is built to resist rotation, the maximum deflection under the same load will be

Figure 6.6 – Minimal top plate overlap located at D1.

Figure 6.7 – Exterior wall looking from A1 – foreground and D1 – background.

approximately 40% of the maximum deflection if neither end of the wall span resists rotation. If both ends are fixed, it would be 20% of the deflection if neither end resisted rotation. These differences are based on standard flexural beam deflections as shown in equation 6.1, using the same E, I, w and L for all calculations.

$$No\ Rotational\ Resistance\ at\ Either\ End\ (Pin - Pin)\ \Delta_{max} = \frac{5wL^3}{384EI} \qquad (6.1a)$$

$$Rotational\ Resistance\ at\ One\ End\ (Fix - Pin)\ \Delta_{max} = \frac{wL^4}{185EI} \qquad (6.1b)$$

$$Rotational\ Resistance\ at\ Both\ Ends\ (Fix - Fix)\ \Delta_{max} = \frac{wL}{384EL} \qquad (6.1c)$$

The differences presented do not account for the 3-dimensionality of the wall, they consider two dimensional bending of the wall which is visible looking in plan. Inclusion of the effect of the wall below the top plate would add very significant and difficult to quantify properties to the wall. The wall would be reducing the overall top plate deflections, but how much would depend on the construction of the wall and level of fixity with the floor. To accurately capture the full wall displacement a finite element model would likely have to be used and this is outside the scope of this thesis; hence only a 2-dimensional beam model is considered here.

6.3 Splitting Due to Large Displacements

There was one failure of top plate splitting due to large displacements, which occurred during the tests without brick veneer on the exterior wall spanning A1 to D1, first discussed in Section 4.2. This wall is shown in Figure 6.8 immediately prior to failure; the location of failure is labeled point F. The top plate is subjected to deflection of approximately 70mm in this picture, representing a significant amount of strain energy in the top plate.

This failure shows the importance of the overlap between the members of the top plate. Point “A” in Figure 6.9 shows how the top plate has acted as a joint in the wall allowing

Figure 6.8 - The top plate of exterior wall A1-D1, immediately before failure.

Figure 6.9 - Wall section B1 immediately after failure.

significant rotation. This is the joint is also shown in Figure 6.6; and as previously discussed, if the overlap between the top plate members had been larger there would have been significant resistance to the large deflection observed because of added rotational resistance (equation 6.1). A reduction in the deflection would have reduced the strain on the top plate and a failure by splitting would not have been observed and the wall would have withstood a higher load. In the tests with the brick veneer in place, the resistance was provided by the bricks (as discussed in the next chapter) and the wall withstood the same net loads with much lower displacements. For vinyl clad walls, increased wall stiffness is required to achieve the same performance. An important note about this type of failure is that it is unlikely to be observed in post event damage surveys. Generally, damage surveys find connection failures, and there are relatively few material failures of this type (FEMA 2011)

6.4 Conclusions

Based on the three different failure types observed for top plates, two main conclusions can be drawn. First, additional shear connectors and shear connectors placed farther from the edges of the beam would reduce cracking and failure. The Ontario Building Code 2010 (OBC 2010) section 9.23.11.4 requires joints in top plates to be staggered at least one stud spacing. Based on the failures observed, all the top plates were built in accordance with this code. The

joint at D1 where the wall rotated would appear to not be in compliance, except that the code contains additional sentences pertaining to corners and intersections, which only have a minimum fastening requirement[4]. After observing the experimental results, it is apparent that more control of the overlap of the joints of the two top plate, especially at wall intersections, would increase the flexural strength of the walls. This is a specification in the International Residential Code 2012 (IRC 2012), section R602.3.2 states: "[…] a double top plate installed to provide overlapping at corners and intersections with bearing partitions. End joints in top plates shall be offset at least 24 inches." Changing of the OBC 2010 to more closely reflect the IRC 2012 would result in an increase in the required overlap of top plate members. This would decrease rotations and deflections along the top plate, specifically near the joints, increasing the overall wall capacity.

[4] 9.23.11.4 (4) Ties referenced to in Sentences (2) and (3) shall be the equivalent of not less than 75mm by 159mm by 0.91mm thick galvanized steel nailed into each wall with at least three 63mm nails.

Chapter 7: Effects of Brick Veneer on Exterior Wall Corners

A popular method of construction in Southern Ontario has a brick veneer on the front of the house and vinyl siding on the sides and back of the house. This is done because brick construction is more expensive than vinyl construction, but the brick is more aesthetically appealing. The IRLBH house was built with a brick veneer on all four walls. The first tests performed on the house had the brick veneer in place on all four walls; two of the walls were not significantly damaged and so the brick veneer was removed and the house tested again. This allowed for a direct comparison of wall behaviour with and without a brick veneer. This chapter examines the effects of brick veneer on wall performance.

7.1 Corner Rigidity with No Brick Veneer

In the tests without brick veneer, the corner was visibly opening (shown in Figure 7.1), which was not observed in the full house tests with brick veneer. Figure 7.2 shows a sketch of how the opening angle was obtained from the wall displacement data. The applied torque on opening angle were calculated using equations 7.1 and 7.2 The total opening angle at the corner was calculated for the test with no brick veneer, as shown in Figure 7.3.

Figure 7.1a - The corner located at A1 with no brick before loading.

Figure 7.1b and 7.1 c – From left to right, the corner located at A1, progressively throughout the test with no brick veneer. The far right picture is after failure.

$$Torque = P * L \qquad (7.1)$$

$$\theta = tan^{-1}\left(\frac{\Delta}{L}\right) \qquad (7.2)$$

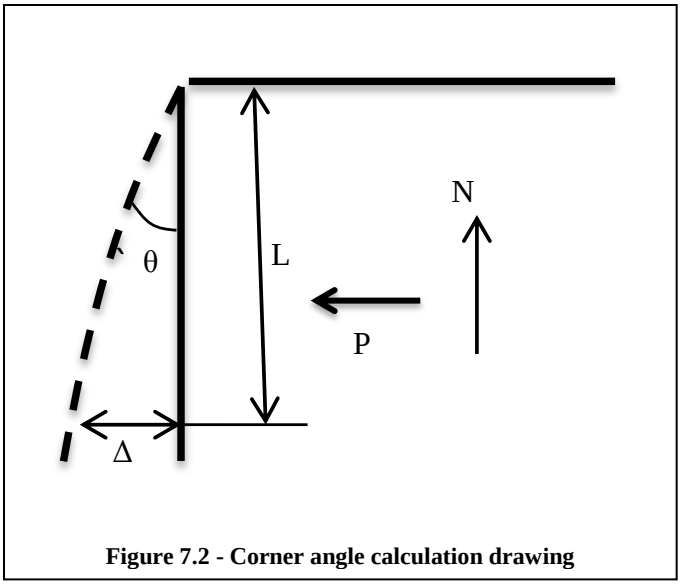

Figure 7.2 - Corner angle calculation drawing

The total angle is the change increase in corner angle from 90 degrees. Failure occurred at a load of 17.7 kNm, and an angle of 15 degrees. Most of the total angle was on one side of the corner, namely, on the wall spanning A1-D1 where the failure occurred (discussed in Section 4.2). The angle of the other wall (A1-A4) at the point of failure was 3.7 degrees, while the angle along wall segment A1-D1 was 11.6 degrees. (The two different angles were calculated using the deflection from each wall based on the assumption that the entire corner did not twist. This observation is supported by the photographs in Figure 7.1.)

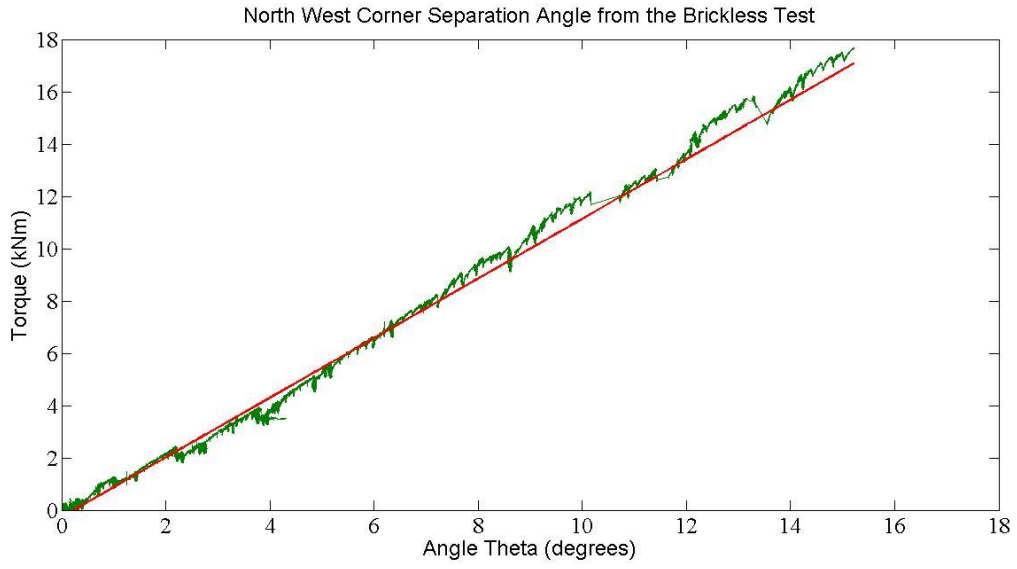

Figure 7.3 - The full angle of opening of the North West corner during the test with no brick veneer.

7.2 Corner Rigidity with the Brick Veneer Present

No catastrophic failure of wall A1-A4 occurred during the tests with brick veneer in place; meaning no breaking of the top plate, falling brick or detachment from interior walls. However, the wall failed by the definition of being unable to resist more load. At an applied torque of 16.0 kNm, the load carried by the wall dropped significantly while the angle increased, suggesting the maximum capacity of the wall had been reached - as can be seen in Figure 7.4 Figure 7.4 only shows half of the total angle, the opening of wall A1-A4, the total angle was not calculated due to a malfunctioning strain gauge which rendered accurate total angle calculation impossible. The strain gauge on the North side of the corner (wall A1-D1) malfunctioned and did not produce any useable data, thus the opening angle of that corner could not be calculated.

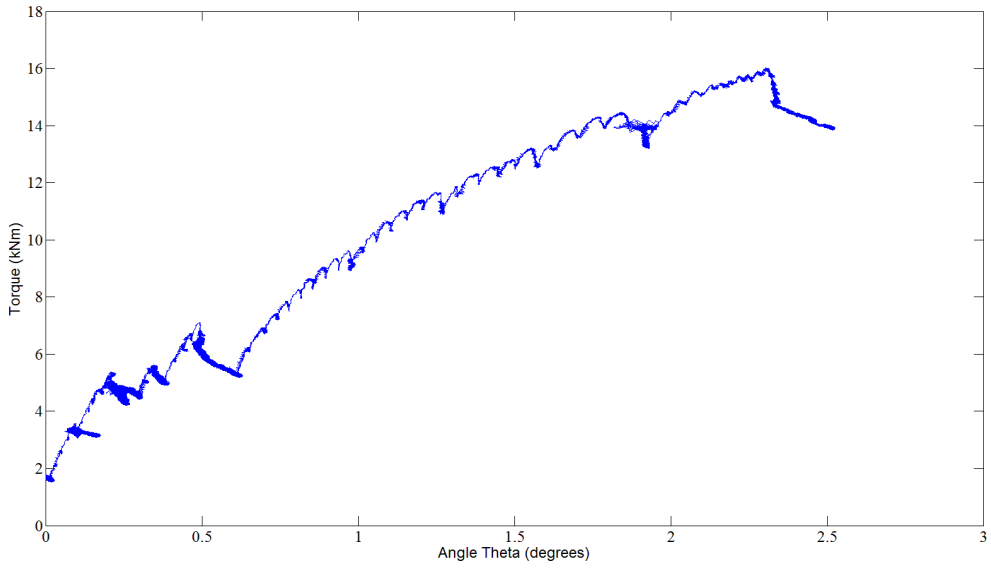

Figure 7.4 - Applied torque - opening angle curve for the corner on wall A1-A4 during the full house test.

7.3 Comparison of Corner Stiffness with and without brick veneer

Comparison between the two tests was only performed for the corner at A1 with respect to the wall spanning from A1 – A4 (North end of the West wall). This comparison is shown in Figure 7.5. At the failure load from the tests without brick veneer (7.5 kNm), the angle θ was 3.7 degrees. The angle theta for the corner with brick veneer at a load of 7.5 kNm was 1.0 degrees. Thus, the deflection without the brick at that point is 3.8 times greater than the deflection with the brick. It can also be seen that the maximum load resisted by the corner effectively doubled from 7.5 kNm to 16.0 kNm from with no brick veneer to with brick veneer respectively. Thus, the brick veneer adds considerable stiffness to the corner by reducing deflections at equivalent loads. This increase is due to the stiffness of the brick corner, which behaves similar to a fixed corner, allowing little rotation and opening and preventing the wood frame from being able to open.

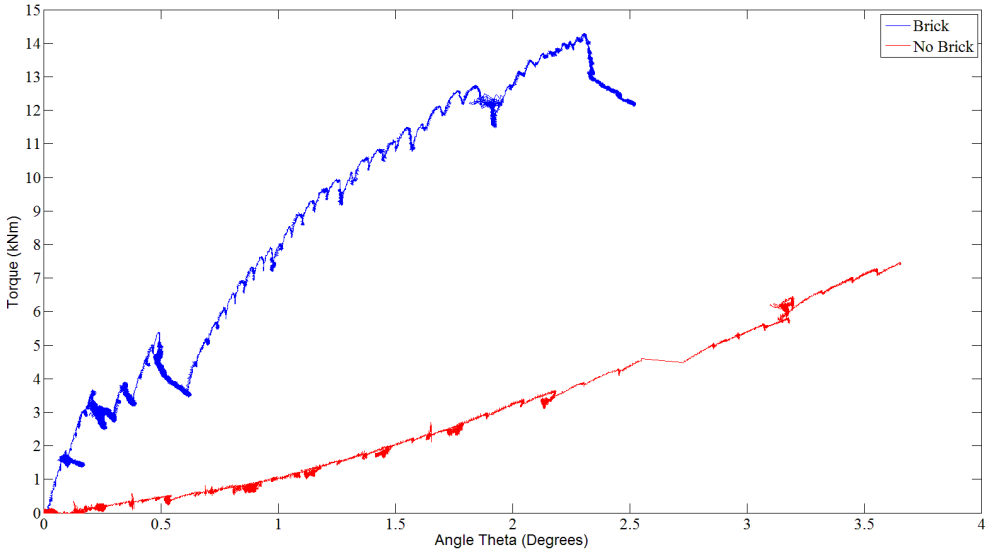

Figure 7.5 - West side of the North corner response comparison with and without the brick veneer.

7.4 Conclusions

It was observed that the presence of brick veneer around the circumference of the house significantly increased the capacity by reducing the wall deflections. In particular, the experimental results show that the presence of brick veneer provided a significant increase in the strength and stiffness at the corners. The brick veneer increased the rotational resistance of the corner. The effect of this increase was shown in equation 6.1; basically decreasing maximum displacements by up to 60%. At the load causing wall failure, the included angle at the corner without a brick veneer was observed to be almost a factor of 4 higher than when the brick veneer was present.

Chapter 8: Second Floor Diaphragm Effects

8.1 Wall Deflections at Location B1

A vertical line of LVDTs was installed at B1 spanning from the second floor to the top plate as indicated by the markers in Figure 8.1; spaced approximately every 600mm up to a height of 2400mm. This line of LVDTs happened to be placed directly in line with the location at which the top plate failed catastrophically in the tests without brick veneer. Analysis of this line of displacement transducers showed the wall to be rotating about the connection between the wall base and the second floor, as shown in Figure 8.1. The responses for 3.8kN and 4.55kN do not show the reading from the displacement transducer at the top of the wall because it ran out of travel and so provides no more useful data past this point. In all cases, 0mm of displacement is assumed at 0mm of height because of the linear response over the bottom half of the wall as well as from experimental observations. The bottom two LVDT readings have an average ratio of 1.98 for the displacement quotient from the LVDT 600mm and 1200mm off the floor. There is very little variation in that ratio, with a standard deviation of 0.03.

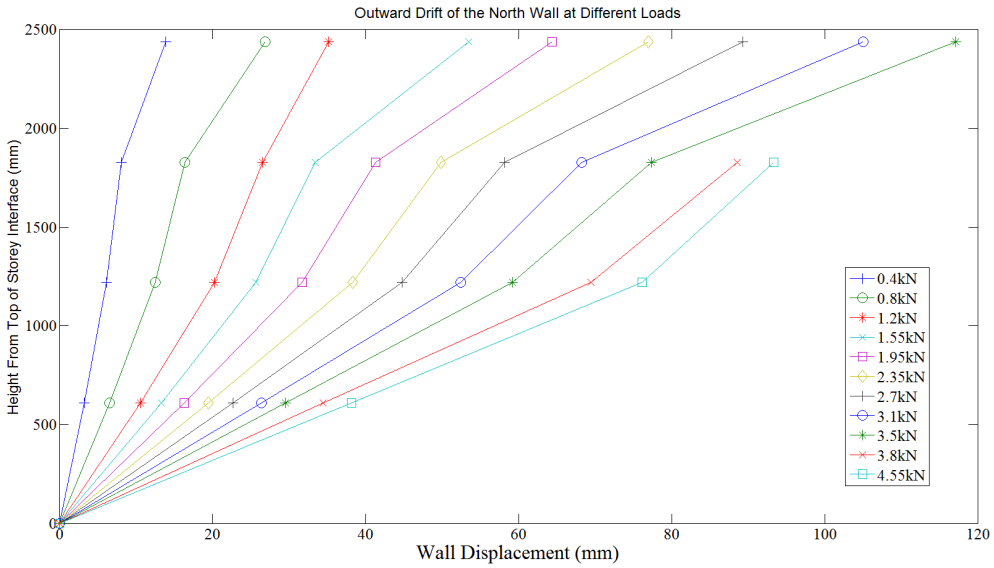

Figure 8.1 - Profiles of the North Wall deflection at different loads

The data shows a significant increase in the displacement from the LVDT located at 1800mm to the LVDT on the top plate (2400mm). Because the wall is rotating outwards about the bottom and not bowing outwards with a local maximum in the middle – as it would if the top plate was attached to a firm diaphragm.

8.2 Removal of Wall at F10 – J10

Another argument for separate treatment of the first and second stories is the attachment of the base of the second storey wall to the second storey floor. The base was nailed into the top of the floor, creating a pin-like connection. Figure 8.2 shows a close up of the floor – wall connection after from the exterior wall between F10 and J10, after the catastrophic failure of this wall occurred. A gap can be seen under the wall ("A") in the area where it has rotated away from the floor. When the wall was removed, no damage to the second floor was observed. It was found that the floor-wall connections were nailed between the wall framing and the wood floor, and would primarily resist horizontal movements of the wall base. This meant that deflections and rotations of the wall pulled the nails straight out of the floor with limited resistance.

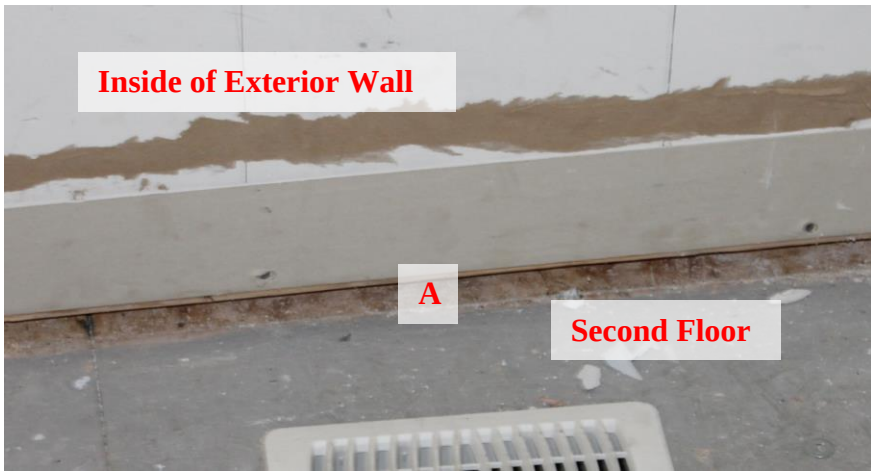

Figure 8.2 - Second storey floor-wall connection post failure

If rotational resistance was installed, it would decrease the top plate displacements, in a way shown in Figure 8.3, where F represents the deflected shape of a vertical member with a fixed connection, and P represents the deflected shape with a pinned connection. Even partial fixity, which could be provided by something as simple as a Simpson Strong-Tie, would increase the rotational resistance.

Figure 8.3 - Deflection difference due to fixity.

8.3 Conclusions

There was no visible damage or deflections on the first floor after the tests were completed. This shows how the second floor was effectively resisting deflection as well as allowing the load to distribute across the house and facilitating a load path down to the ground which was free of load concentrations which may cause damage. Meaning a better wall-to-floor connection on the second floor would have resulted in a higher overall resistance. This result is unique because most other full scale testing of houses was not able to continue applying load in a controlled manner under such significant displacements. Most often testing would stop after the peak load was sustained because this is the most interesting point for failure loads, as is used for the failure wind speeds during the next chapter. The testing in this thesis allowed a unique perspective on the later stages of the failure and the mechanics of the failure – such as the second storey wall rotating off of the first storey. Results from this testing concerning what happens during failure and specific failures provide an interesting insight which allows for more specific recommendations on increasing the strength of residential construction.

Chapter 9: Analysis of Failure Wind Speeds

Using the wind load coefficients from the ASCE 7-10 (2010) and NBCC (2010) and the failure pressure from the tests, the wind speeds associated with the observed failures will be calculated. Then, these wind speeds will be compared with the expected wind speeds from the Enhanced Fujita and Fujita scales for one- and two- family residences for degrees of damage six and seven.

It is important to note that the wind speeds calculated are straight line wind speeds and not tornado winds. Tornado winds have increased temporal and directional variation; they also tend to have a significantly shorter duration than other high wind events. However, design codes to not have specific tornado wind design requirements and use wind loads as calculated in sections 9.1 and 9.2. Limited knowledge is available about exactly what winds are occurring inside a tornado due to a lack of actual measurements and that each tornado is not the same size, shape and intensity, so it is impossible to truly know exact failure wind speeds in a tornado. However, using the design wind speeds from recognized standards will give an appropriate and applicable range of wind speeds.

9.1 ASCE7-10 Wind Speeds

Using the (GC_p) values for wind pressures on a building in the area that failed (side walls), a wind speed was calculated. The structure was considered normal importance, while all of the other adjustment factors were calculated as per ASCE7-10 as if the structure was in open terrain[5], noting the a directionality factor, K_d of 1.0 was used, to correspond with the worst possible wind direction. Wind speeds were considered with the structure in both open and in suburban terrains. Equation 9.3 shows how the calculation was performed when including

[5] Open terrain: "level terrain with only scattered buildings, trees or other obstructions, open water or shorelines." Ontario Building Code 2010 4.1.7.1 (5)(a)

internal pressures, with the results summarized in Table 9.1. The calculated failure wind speed based on the measured failure pressure in open terrain was 62.2m/s neglecting the internal pressure coefficient and 46.6 m/s including the internal pressure coefficient, GCp_i = +/-0.55. In suburban terrain the failure wind speeds were 70.6m/s and 52.8m/s, not including and including internal pressures these results are included in Table 9.1.

$$\hat{V}_{10m,3\ second\ gust} = \sqrt{\frac{2 * p_{failure}}{(GC_p - GC_{pi})\rho k_{zt} k_d k_h I}} \qquad (9.3)$$

9.3 NBCC 2010 Wind Speeds

Using a similar procedure that was adopted for ASCE7-10, the wind speed corresponding with the failure pressure observed was calculated. Equation (9.4) shows the procedure used to calculate the NBCC design wind pressure (q), and Equation (9.5) to change from wind pressure to wind speed. NBCC wind speeds are 10m, mean hourly wind speeds, and so are translated into 10m, 3 second gust speeds using Equation (9.6). The ratio for changing from mean hourly to 3 second gust speeds comes from the Durst curve (ASCE 7-10, 2010). The wind speeds were calculated considering internal pressures and not considering internal pressures. When considered, the internal pressure coefficient was +/-0.7, as if the house was partially enclosed. Partial enclosure of the house was chosen to generate the largest range of wind speeds and simulate the worst case scenario, as if several windows or doors were open or broken which is quite possible to occur. The house was considered in both open and suburban terrain. The calculated 3 second gust failure wind speed using NBCC 2010 with the house in open terrain was 64.6m/s when not considering internal pressures and 46.5m/s when internal pressures are considered; in suburban terrain the wind speeds were 73.3m/s and 52.7m/s. These results are included in Table 9.1.

$$q = \frac{p_{failure}}{IC_eC_gC_p + IC_eC_{gi}C_{pi}} \qquad (9.4)$$

$$\bar{V}_{10m,1\ hour} = \sqrt{\frac{2 * q}{\rho}} \qquad (9.5)$$

$$\hat{V}_{10m,3\ second\ gust} = \left(\frac{\hat{V}_{3second}}{\bar{V}_{1\ hour}}\right) * \bar{V}_{10m,1\ hour} = 1.52 * \bar{V}_{10m,1\ hour} \qquad (9.6)$$

Table 9.1 - Comparison of Failure Wind Speeds

Wind Speed Calculation Method			Failure Wind Speed (m/s)
ASCE 7-10	Open Terrain	Cpi=0.55	46.6
		Cpi=0	62.2
	Suburban Terrain	Cpi=0.55	52.8
		Cpi=0	70.6
NBCC 2010	Open Terrain	Cpi=0.7	46.5
		Cpi=0	64.6
	Suburban Terrain	Cpi=0.7	52.7
		Cpi=0	73.3

The two codes produce highly similar but not identical results for each situation. Differences between the two codes come from underlying methodology in the calculations such as the incorporation of 3 second gusts in ASCE 7-10 and requiring a post calculation translation to 3 second gusts in NBCC 2010. The open terrain situations have lower design wind speeds because there is less turbulence and less disturbance of wind flow along the ground, so higher wind speeds closer to the ground. This changes the overall wind speed profile to create higher loads lower down on the structure. To account for the increased roughness along the ground in suburban terrain, the 10m wind speed required to produce the same forces are therefore higher.

9.4 Fujita Scale Comparison

The failure wind speed was found to be in the range between 46.5 m/s and 73.3 m/s. This relates to a tornado which would be rated from upper end of EF1 to the top of EF3 to cause failure of the exterior walls. For the Fujita scale, the building would be expected to fail in the range from the upper end of an F1 tornado up to the lower end of an F3 tornado. In relation to degree of damage six and seven for FR12, the expected wind speeds are 46.5-63m/s and 50.5-68.4m/s respectively. These wind speed ranges are completely encompassed by the wind speed required for failure of the IRLBH test house, suggesting the test house performed as would be expected. If the IRLBH test house is a good representation of typical Canadian house construction, it is a good indicator the EF scale is a reasonably accurate regarding wind speeds required to cause wall collapse of brick-clad houses. For vinyl-clad walls, the failure wind speeds would be lower.

Chapter 10: Building Code Loads and Tornado Design Recommendations

This chapter presents the design wind loads from the National Building Code (NBCC, 2010) and compares these to house performance. Potential changes which could be applied in order to prevent these failures from occurring are also discussed.

10.1 NBCC 2010 Design Wind Pressure

Design of houses is based on Part 9 of NBCC, which is a prescriptive standard. The NBCC design wind pressure was calculated for this type of structure using Equation 10.1, which corresponds to the wind load calculation procedure presented.

$$p = I_w q C_e C_p C_g + I_w q C_e C_{gi} C_{pi} \qquad (10.1)$$

To perform this calculation, the following assumptions are made: where I_w is the importance factor, q is the reference pressure, C_e is the exposure coefficient and C_p and C_g are the pressure and gust coefficients respectively, found in the building code commentaries

- Normal importance (I_w=1.0)
- Roof in place, because this is consistent with the design of the structure.
- Suburban terrain (C_e)
- Structure located in London, where the reference pressure is 0.79kPa
- The structure is category 1 for internal pressures, with few openings (windows sealed).
- The pressure (p) is multiplied by the ultimate limit states factor of 1.4.

The design pressures for the different walls are shown in Table 10.1. It is important to note that each wall requires designing for the worst positive and negative pressures. Because the structure is small, the edge zones of the walls encompass the entire wall, so the edge zone values apply across the full wall width.

Table 10.1 - Factored design pressures

	Factored Design Pressure (kPa)
Windward Wall	0.63
Side Wall	-0.59
Leeward Wall	-0.59

Given these design pressures, the tests indicate clearly that the walls without roof met or exceeded the design requirements when the catastrophic failure occurred, the first at a pressure of -1.5 kPa. Thus, the walls of a brick veneer, double-top-plate wood-frame house will most likely not fail at the ultimate code wind pressures specified by the NBCC. This implies houses constructed to code in Ontario are significantly stronger than what is specified by the minimum wind load requirements.

10.2 Tornado Resilience Design Recommendations

The recommendations presented herein are intended to be easily implemented and inexpensive to apply in order to improve the resilience of wood-frame houses to tornadoes:

1) Ensure adequate double top plate member overlap to increase the strength of top plate connections: this can be accomplished by either of the following methods.
    a. Regulation of the overlap of the two members in a double top plate. Specifically requiring a minimum distance between an interior to exterior wall connection and the end of the lower top plate member. This will prevent large wall rotations and increase shear force transfer between the two top plate members. As a result the walls will be stronger. This change requires no additional construction materials and thus would be inexpensive to implement.

b. Required placement of metal connection plate (such as a Simpson Strong Tie mending plate) on top of top plate connections. This would increase the transfer of forces between the joints in the top plate.

2) Stiffening of long unsupported walls: Large local deflections were observed in the longest unsupported wall spans. The length of wall at which this becomes critical is unknown, however, and requires further research. The following two alternatives can achieve this goal:
    a. Placement of additional studs and a third top plate member. This will increase the overall stiffness of the wall and create a stronger load path.
    b. Mid-span lateral bracing of the top plate. Installation of a tie running through the ceiling which provides lateral bracing and stability to the top plate member, creating a load path midway through the wall reducing maximum moments and shear forces.
3) Increase the strength of interior to exterior wall connections: This inexpensive change would increase the overall strength of an exterior wall. Interior walls provide a load path for wind-induced shear forces travelling through the exterior wall. Installation of Simpson Strong Ties at each connection; this would require very little effort or expense complete.
4) Extension of brick veneer around front corners: Change the relatively common practice of installing a brick veneer on the front of a house only. As has been clearly shown, brick extended around the corners would significantly increase the strength and stiffness of the corners and the adjacent walls. If it is impractical to extend brick

around the corners, specifically for the back corners where both sides of the corner are vinyl clad, stiffening of the corner framing would also provide a strength increase.

5) Increase the Stiffness of the Back Corners: Because many houses are constructed with vinyl siding on the back and sides, it is fairly impractical to suggest brick veneer be installed around the back two corners and not the remainder of the house (which would be expensive and time consuming). Instead, the addition of metal angles, wood beams or other ways to increase the stiffness and opening resistance of the back corners would positively effect the overall house strength.

Chapter 11: Summary of Conclusions and Recommendations for Future Work

11.1 Conclusions

In the research reported in this thesis, two tests have been performed on a two storey house: the first with the brick veneer in place, the second without. The house was loaded to simulate uniform wind pressure with positive pressure on the windward wall, and negative pressures on the side and leeward walls. Three catastrophic failures were observed and the mechanisms involved were analyzed. Based on these observations and analyses, the following conclusions can be made:

1. Small, inexpensive changes to the construction of residential structures would cause a significant increase to the ultimate strength of individual walls and the structure as a whole. These changes are all intended to maintain a continuous load path and prevent local failures that disrupt the load path. The changes include: controlling double top plate member overlap, increasing interior to exterior wall connection strength and extending brick veneer around corners or significantly increasing the rigidity of corners.
2. The observed loads causing failure of the test specimen correspond to wind speeds that considerably exceeded the NBCC 2010 design wind speeds. Although the structure is more vulnerable to collapse after failure of the roof, the walls of the two-storey test specimen were able to resist larger wind forces than is required by these design codes.
3. Exterior wall failure after roof loss appears to require an EF-3 tornado with the wind speeds reasonably consistent with DOD-7 in the EF-Scale.
4. If no basement or safe room is available, small windowless rooms on lower floors will provide the safest refuge during a tornado. While the walls on the upper floor were

experiencing significant deflection and catastrophic failures, the lower floor walls did not noticeably deflect and were not significantly damaged. As loads increased, local deflections of unsupported walls occurred because the unsupported wall did not have sufficient stiffness. Hence, smaller and lower floor rooms are much safer in a tornado because local deflections of the walls are less likely and so the lower floors are safer.

11.2 Recommendations for Future Testing

There are several projects, which if undertaken would allow for refining of the building code recommendations as well as increasing the accuracy of the failure wind speed estimates.

1. Finite element modeling of the house and exterior walls. Because the failure mechanisms are now better known, the model can easily be verified for accuracy. A finite element model would allow for variation of the construction practices – changing the strength of connections due to poor or perfect construction for example. Allowing for generation of a more accurate range and distribution of wind speeds expected for this level of damage. This would increase the accuracy of damage surveys and wind speed estimates.
2. Examine the effectiveness of top plate overlap changes. Test top plates in flexure to simulate the bending observed in the full house tests. By changing the overlap of the two top plate members, an optimum overlap for strength could be determined. As well, the effect of changing the number and/or placement of shear connectors could be examined.
3. Examination of the extension of brick veneer. Test wood and brick corners to determine the distance around a corner a brick veneer needs to be extended to get the optimum resistance to opening and deflection resistance. As well, the examination of alternative methods to stiffen the corner without the application of brick veneer, this is especially relevant to the corners at the rear of the house.

4. Examination of potential methods to stiffen long unsupported walls to reduce local deflections. To determine if an additional top plate member or additional wall studs could significantly increase out of plane wall stiffness.

References

2006, “A Recommendation for an Enhanced Fujita Scale (EF-Scale)”, Revision 2, Wind Science and Engineering Center, Texas Tech University.

2010, “Ontario Code and Construction Guide for Housing”, Ontario Building Officials Association, Toronto, Ontario.

2011, “The Enhanced Fujita Scale (EF Scale)” NOAA/National Weather Service. Website. http://www.spc.noaa.gov/faq/tornado/ef-scale.html, accessed November 2013.

2012, “2012 International Residential Code”, International Code Council, USA.

2014, “Tornadoes and Thunderstorms”, Insurance Information Institute, Website, www.iii.org /facts_statistics/tornadoes-and-thunderstorms.html, accessed January 2014

Allen, D.E., 1984 “Tornado Damage at Blue Sea Lake and Nicabong, Quebec, July 1984”, National Research Council of Canada, Division of Building Research.

Allen, D.E., 1986, “Tornado Damage in the Barrie/Orangeville Area, Ontario, May 1985”, Institute for Research in Construction, National Research Council of Canada.

American Society of Civil Engineers, 2010 “ASCE/SEI 7 Minimum Design Loads For Buildings and Other Structures”.

Canadian Institute of Steel Construction, 2010, “Handbook of Steel Construction”, Tenth Edition.

Canadian Wood Council, 2005, “Wood Design Manual 2005”. Fresens, Altona, MB.

Davenport, A.G. & Kopp, G.A., 2002, “Natural Disasters,” *Encyclopedia of Environmetrics* (eds. El-Shaarawi, S. and Piegorsch, W.W.), vol. 3, pp. 1356-1362, John Wiley and Sons, Chichester

D’Costa, M.J. and Bartlett, F.M., 2000, “Design of Static-Equivalent Wind Load Test for a Full Scale Corrugated Fibreboard Shelter”, CEE department, University of Western Ontario. 3rd Structural Specialty Conference for the CSCE, London, Ontario, June 7-10.

D’Costa, M.J. and Bartlett, F.M., 2003, “Full Scale Testing of Corrugated Fibre Board Shelter Subject to Static-Equivalent Wind Loads”, CEE department, University of Western Ontario, Journal of Wind Engineering and Industrial Aerodynamics 91, pp 1671-1688.

Dolan, J.D. and Heine, C.P., 1997, “Sequential Phased Displacement Cyclic Tests of Wood-Framed Shear Walls with Openings”, Virginia Polytechnic Institute and State University.

Dolan, J.D. and Heine, C.P., 1997, "Sequential Phased Displacement Tests of Wood-Framed Shear Walls with Corners", Virginia Polytechnic Institute and State University.

Fujita, T 1971. "Fujita Scale Rating the Severity of Tornadoes". Environment Canada Information Release.

Ginger, J.D., Reardon, G.F. and Whitbread, B.J., 1998, "Wind Loads on a Typical Low-Rise House", James Cook Structural Testing Station, Technical Report #46.

Henderson, D.J., Ginger, J. Morrison, M.J. and Kopp, G.A., 2009, "Simulates cyclonic wind loads for low cycle fatigue loading of roofing", Wind and Structures 12, pp363-400.

Henderson, D.J., Morrison, M.J. and Kopp, G.A., 2013, "Response of toe-nailed, roof-to-wall connections to extreme wind loads in a full scale, timber-framed, hip roof", Engineering Structures, 56 (November 2013), Pp 1474-1483.

Kopp, G.A., Galsworthy, J.K. and Oh, J.H., 2010, "Horizontal Wind Loads on Open-Frame, Low-Rise Buildings", Journal of Structural Engineering 136(1), pp 98-105.

Kopp, G.A., Morrison, M.J. and Henderson, D.J., 2011, "Full scale testing of low-rise buildings using realistically-simulated wind loads", keynote paper, 13th International Conference on Wind Engineering, Amsterdam, Netherlands.

Mans, C., Kopp, G.A., and Surry, D., 2005, "Wind effects of parapets on low buildings: Part 3. Parapet loads", Journal of Wind Engineering and Industrial Aerodynamics 93, pp 857-872.

Morrison, M.J., Henderson, D.J. and Kopp, G.A., 2012, "The reponse of a wood-frame, gable roof to fluctuating wind loads", Engineering Structures, 41 (August 2012). pp 498-509.

National Research Council of Canada, 2010, "National Building Code of Canada", Ottawa: Associate Committee on the National Building Code, National Research Council.

Pei, S., van de Lindt, J.W., Wehbe, N. and Liu, H., 2012, "Experimental Study of Collapse Limits for Wood Frame Shear Walls", Journal of Structural Engineering 139, issue 9 pp1489-1497.

Reardon, G. and Henderson D., 1996, "Simulated Wind Loading of a Two Storey Test House", James Cook Cyclone Testing Station, International Wood Engineering Conference, New Orleans, Louisiana, USA.

Robertson, A.P. and Hoxey, R.P., 2007 "Full-Scale Study of Wind Loads on Roof Tiles and Felt Underlay and Comparisons with Design Data", Winds and Structures, vol 10, No 6.

Reardon, G., 1986, "Simulated Cyclone Wind Loading of a Brick Veneer House", James Cook Cyclone Testing Station, Technical Report #28.

Salenikovich, A. and Dolan, J.D., 2000, "The Racking Performance of Light-frame Shear Walls with Various Tie-down Restraints", World Conference on Timber Engineering, Whistler Resort, British Columbia, Canada.

Simmons, K and Sutter, D., 2012 "Deadly Season: Analysis of the 2011 Tornado Outbreaks". American Meteorological Society, Boston.

"Spring 2012 Tornadoes: April 25-28 and May 22 Building Performance Observations, Recommendations and Technical Guidance" Mitigation and Assessment Team Report, FEMA P-908, May 2012. pp 4-18

St. Pierre, L.M., Kopp, G.A., Surry, D. and Ho, T.C.E., 2004, "The UWO contribution to the NIST aerodynamic database for wind loads on low buildings: Part 2 Comparison of data with wind load provisions", Journal of Wind Engineering and Industrial Aerodynamics 93, pp31-59.

Xu, Y.L., Reardon, G.F., Mahlberg, J.A. and Henderson, D.A., 1996, "Comparison of Wind Pressure and Fatigue Damage to Hip and Gable Roof Claddings", James Cook Cyclone Structural Testing Station, Technical Report #43.

Appendices

Appendix A: New South Wall Top Plate for the House Test with No Brick Veneer

For the house test with no brick veneer, it was required to install new members to simulate the stiffness of a top plate along wall A10-J10. Because the wall was destroyed in the full house test, the exterior wall A1-A10 had very little stiffness. In order to be able to perform an accurate test (specifically on the A1 corner) new stiffness was needed. A long wood beam was installed where wall A10-J10 used to run. This provided the required stiffness, it is shown in Figure J1.

Figure J1 - The false top plate installed at A10-E10 to increase the stiffness of wall A1-J1.

Appendix B: Cable Tension Strength Test

June 25 2013 11h00

A 3/8” Galvanized steel wire rope with two swaged loops (Figure G1) was tested in tension until failure. The purpose of this test was to determine the ultimate tensile strength as well as the strength of the swaged connections relative to the expected ultimate strength of the cable. The listed breaking strength of the wire rope is 14 400lbs and the swages are recommended to be considered to have 80% of the ultimate strength of the cable. The wire rope construction is 7x19 and was shipped from WebRiggingSupply.com in the USA. The experiment was run in the structures lab at the University of Western Ontario (UWO). The load was increased until failure of the cable occurred. The setup is shown in Figure G2.

Figure G1 - The tested cable post failure

Figure G2 (LEFT) - The experimental setup. Figure G3 (RIGHT) - Bottom of experimental setup, showing how the loop was held in place

Results and Discussion

Failure Load: 56.4 kN (12 600lbs)

Loading Rate: 6 MPa/min

Failure occurred by slippage of the upper wire through the swage (as shown in Figures G4a and G4b), this failure mode was sudden and caused an instant relief of the applied load. At this point no further loading was applied. While sudden, this failure did not cause total failure of the cable, which is good for safety of the experiment. However, it is likely that total failure of the cable would occur very shortly after this initial failure.

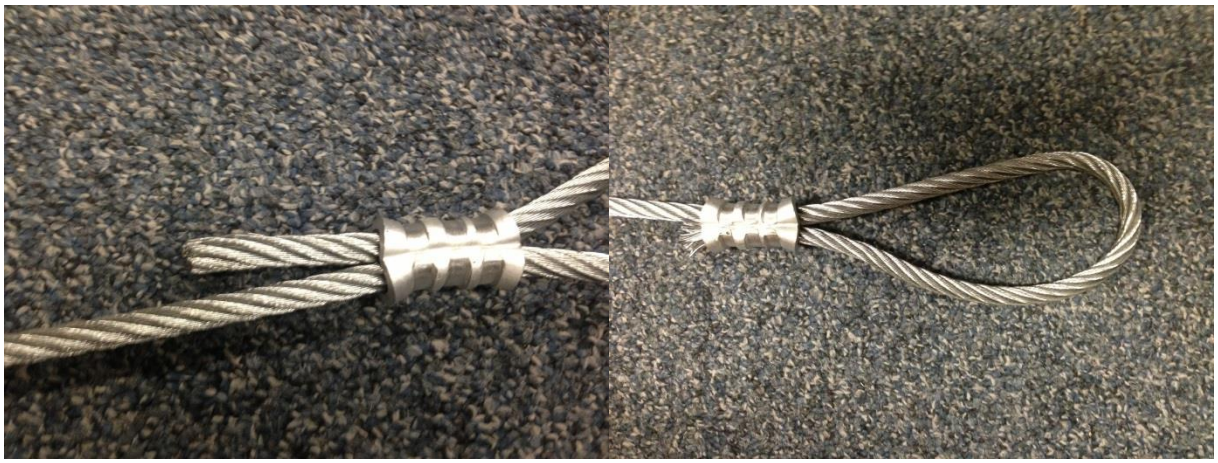

Figure G4a (LEFT) - An unfailed swaged cable connection . Figure G4b (RIGHT) - The swaged cable connection post failure

Conclusion

The failure load is 87.5% of the breaking strength of the cable, which is a higher result than expected based on information provided by the swag company. The maximum tensile load expected in any individual cable is 15kN (3350lb), thus meaning the connections have a factor of safety of 3.64.

Appendix C – Load Equalization Setup

The load which was applied by one come-along was ensured to be equally divided among the four load pads by the usage of pulleys at the separation points, as shown in Figure H1. One cable, called the primary loading cable which goes from one load pad, out to the separation beam, through a pulley and back to another load pad on the house. Pulleys were used at each of the cable splits instead of just loops because the tension in the cables coming out of each sides of the cables is always equal, so when the geometry changed during the experiment the loads applied to the walls remains uniform. Figure H1 shows a sketch of the setup from where the tertiary cable comes down from the come-along and pulley array to where the four different cables go to their respective locations in the house.

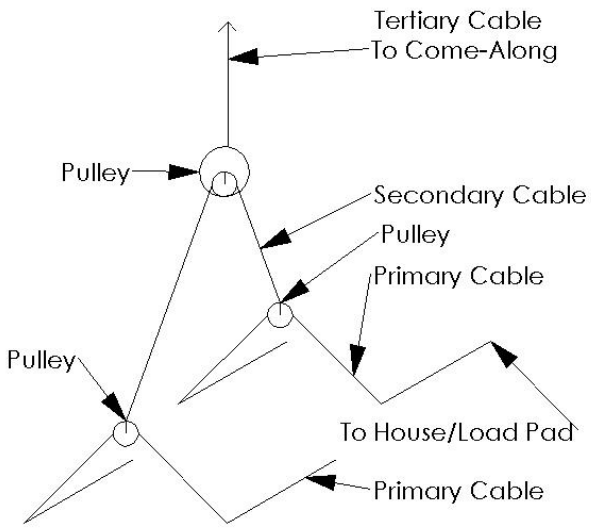

Figure H1 - Sketch showing the general pulley and cable arrangement to equally split the load across four load pads

Figure 2 - Cable Separation point from primary loading cable to secondary cable.

Appendix D– Strain Gauge Calibration Test

The strain gauges required calibration in order to determine the loads corresponding with various strain readings. A test was set up as shown in Figure F1, up to four load cells (with strain gauges attached) were put in series with a come-along and a digital load cell. The load was increased by tensioning the come-along. The strain readings were recorded over a period of 10 seconds at 200Hz at four different loads. 10 seconds was used to capture enough data points to see any changing load, while avoiding any possible drift or small plastic deformation of the load cells due to loading before the real test. The load shown by the digital load cell was recorded for each time strain readings were recorded.

Figure F1 - Strain gauge calibration test setup. From left to right, come-along to apply load, three load cells and digital load cell.

Using the four points, average strain readings were plotted against the load and the data fit to a straight line. The data was fit to a straight line because the loads applied were within the linear-elastic range of the load cells. As expected, the data from each gauge fit almost perfectly to a straight line, with r^2 values in the area of 0.999 helping to confirm correct setup and good testing procedures. Two strain gauges were attached to each load cell, one on each side. This provided a backup if one of the gauges failed during the experiment as well as could record any bending of the load cell during loading.

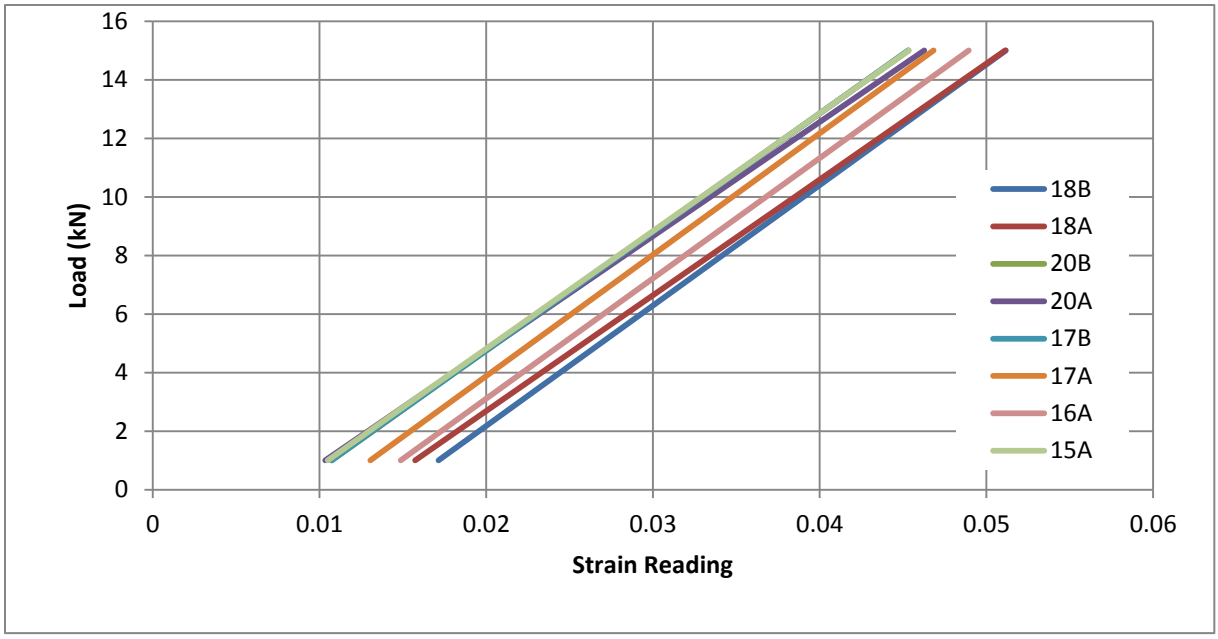

Figure F1 - Load-strain plot for 8 strain gauges

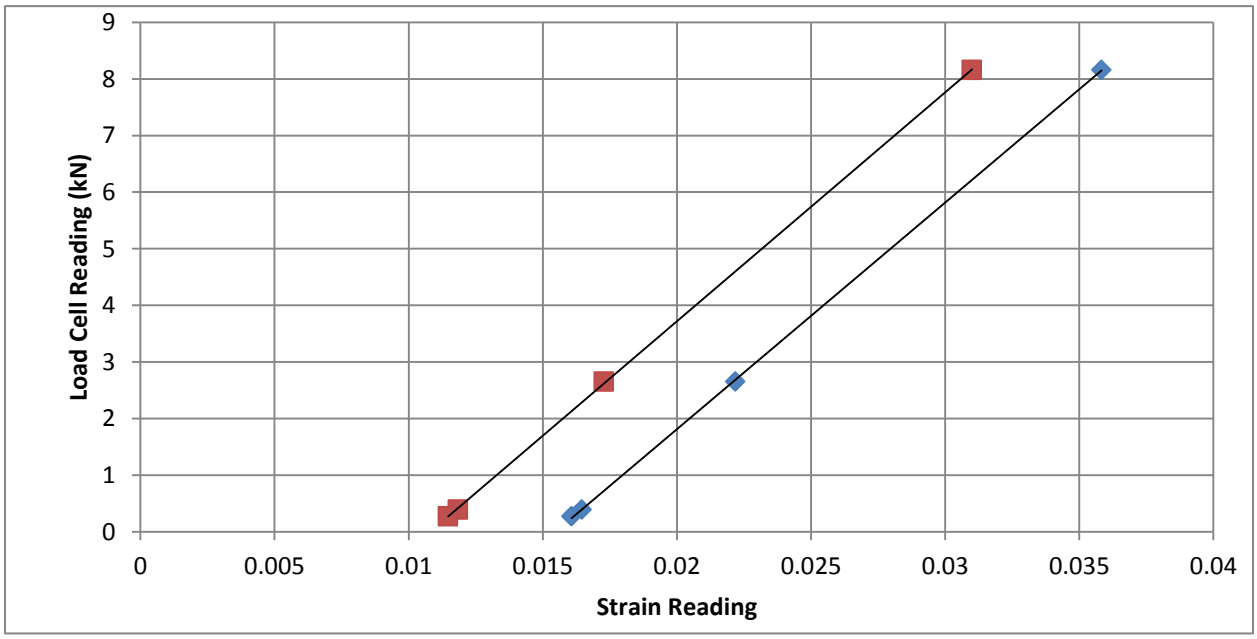

Figure F3 - Strain readings and line fit for strain gauge "1", to show the accuracy of the line fit.

Analysis of the data showed great consistency in the slope of the load-strain lines, but differences in the intercepts. This difference is due to differences in the wiring, soldering, etc. Plots from eight of the strain gauges are shown in Figure F1, only eight of the strain gauges plots are shown to keep the Figure from becoming too convoluted. The data shows that if the strain readings at zero load are removed from the strain reading, all the load cells give consistent and accurate data. When full house experiment was conducted, the loads around the house were able to be accurately controlled and the data properly analysed because of the know zeros and calibration data for the load cells/strain gauges.

Appendix E– Reaction Frame Movements

An important consideration for the validation of the displacement measurements taken was the movement of the reaction frame, which most of the LVDTs were mounted on. LVDTs were mounted on a wood frame built outwards from a different steel frame (not attached to any other parts of the experiments, see Figure D1) to read any movements in the reaction frame during the experiment. The results showed insignificant movement of the reaction frame in both the North-South and East-West directions. Figures D2 and D3 show time histories of the reaction frame movements over the course of the full house test.

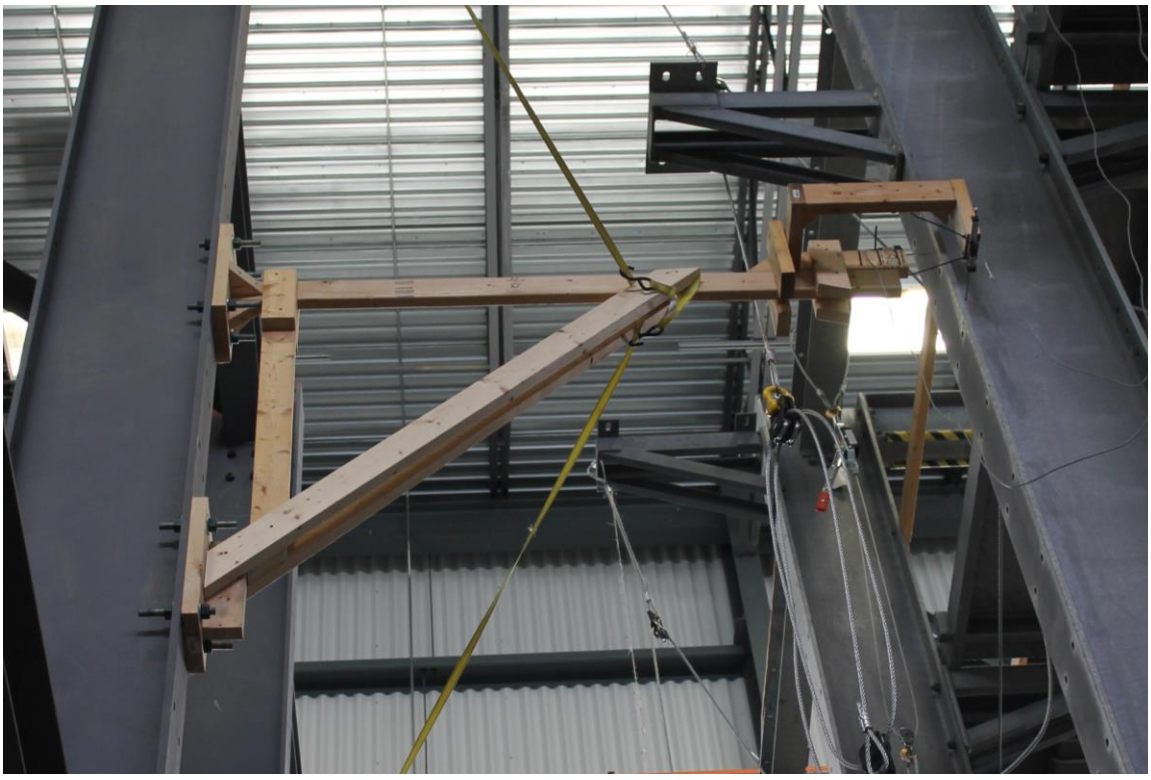

Figure D1- Built frame for recording reaction frame movements

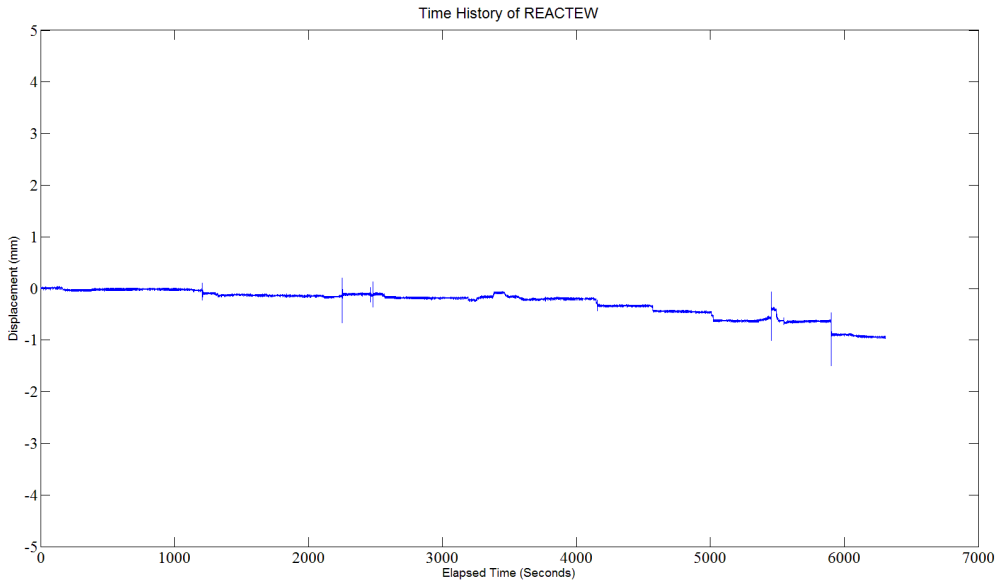

Figure D2 – East – West movements of the reaction frame.

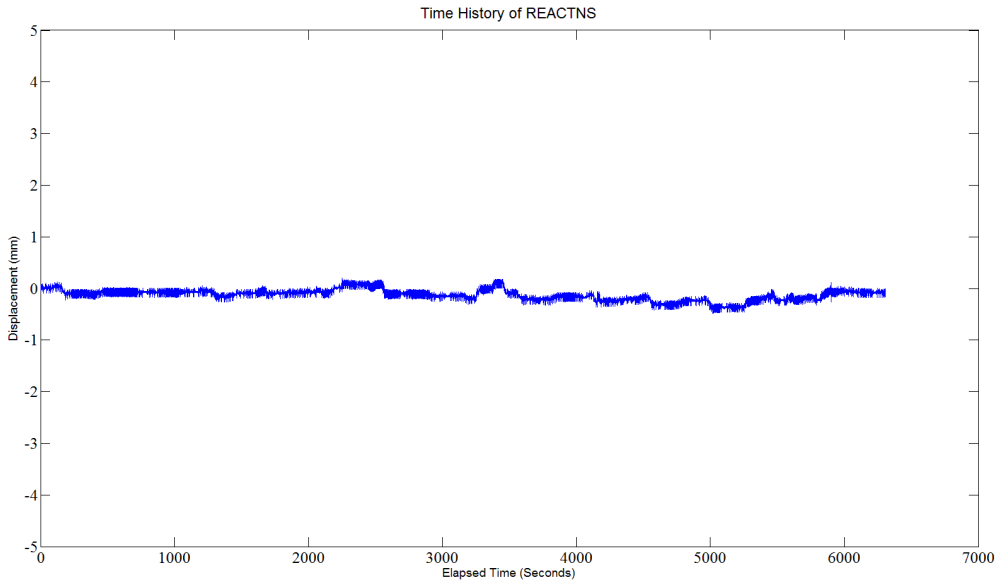

Figure D3 – North-South movements of the reaction frame.

Appendix F: Movements of the Base of the House

The base of the house was connected to concrete curbs by either load cells or wood blocks. Before the test, it was thought that the net load on during the full house test may cause lateral movement of the entire house. Any lateral movement of the base of the house would cause erroneous displacement readings at the top plate. To check for movements, LVDTs were placed at each corner at the base level of the house, as shown in Figure C1. There were no significant movements of the base of the house during the experiment; this is shown in Figures C2-C10, which show the time history plots for the house base LVDTs. Some of the plots appear to drift, which may be indicative of house movement. However, the maximum of any of these movements is 0.3mm, which is insignificantly small, between 0.2 and 1% of maximum displacements in the experiment.

Figure C1 - A base LVDT located facing North at the South West Corner.

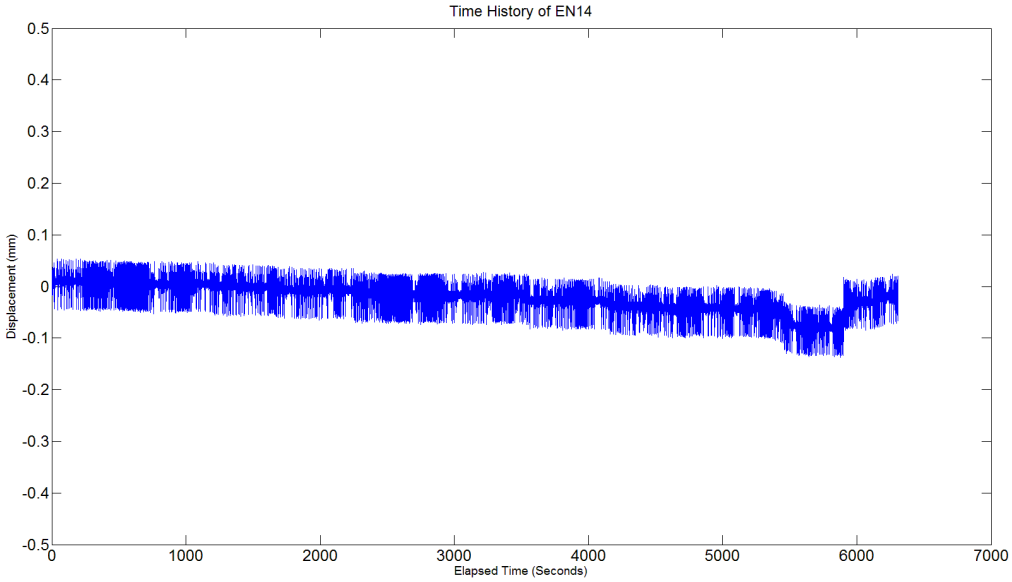
Time History of EN14
Displacement (mm)
Elapsed Time (Seconds)
0.5
0.4
0.3
0.2
0.1
0
-0.1
-0.2
-0.3
-0.4
-0.5
0
1000
2000
3000
4000
5000
6000
7000

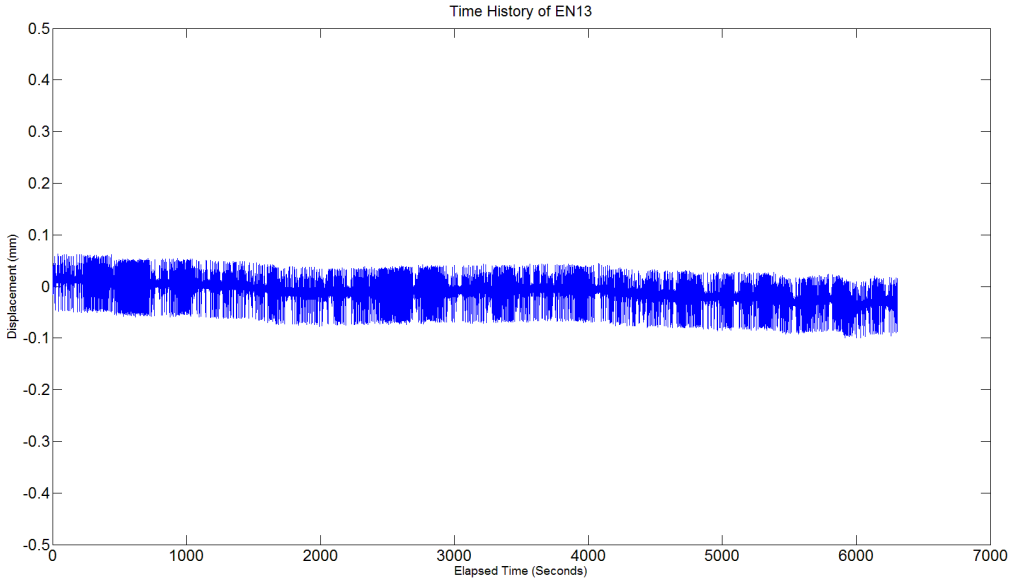
Time History of EN13
Displacement (mm)
Elapsed Time (Seconds)
0.5
0.4
0.3
0.2
0.1
0
-0.1
-0.2
-0.3
-0.4
-0.5
0
1000
2000
3000
4000
5000
6000
7000

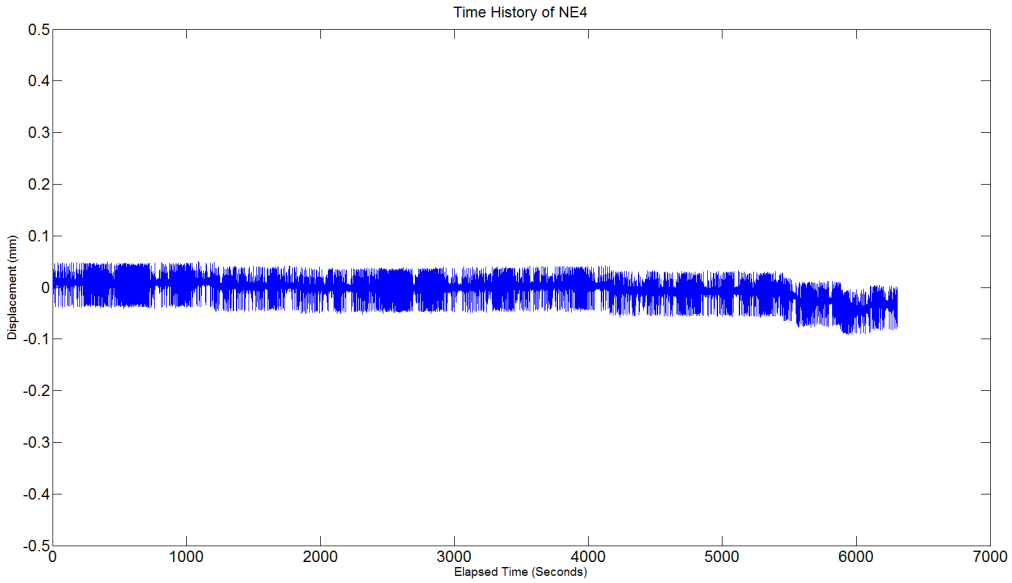
Time History of NE4
Displacement (mm)
Elapsed Time (Seconds)
0.5
0.4
0.3
0.2
0.1
0
-0.1
-0.2
-0.3
-0.4
-0.5
0
1000
2000
3000
4000
5000
6000
7000

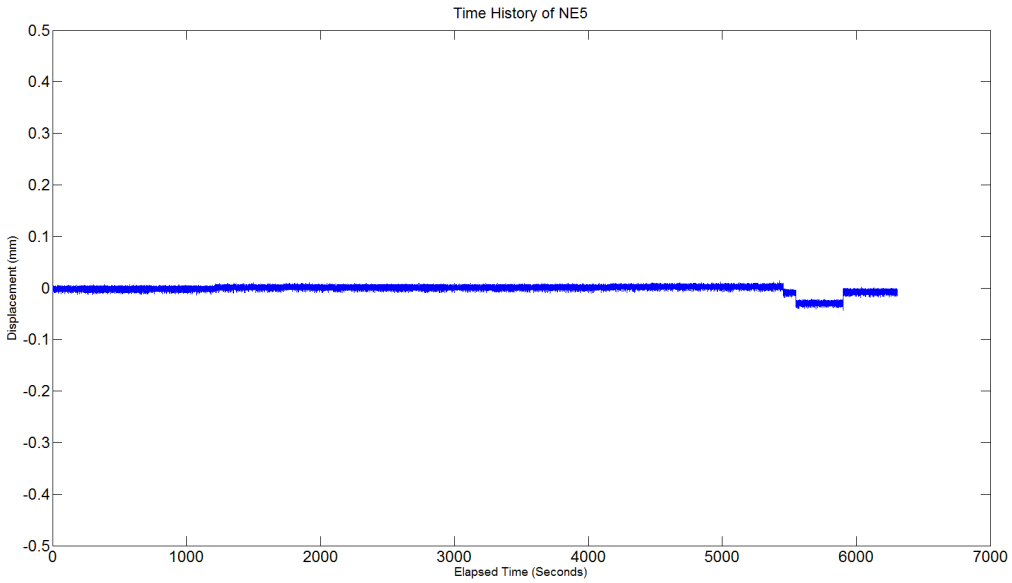
Time History of NE5
Displacement (mm)
Elapsed Time (Seconds)
0.5
0.4
0.3
0.2
0.1
0
-0.1
-0.2
-0.3
-0.4
-0.5
0
1000
2000
3000
4000
5000
6000
7000

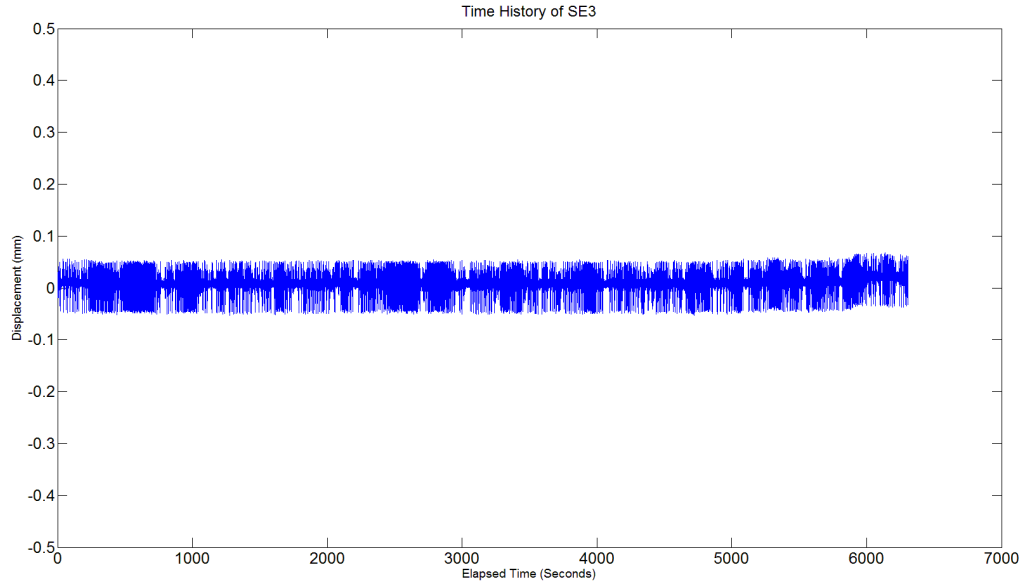
Time History of SE3
Displacement (mm)
Elapsed Time (Seconds)
0.5
0.4
0.3
0.2
0.1
0
-0.1
-0.2
-0.3
-0.4
-0.5
0
1000
2000
3000
4000
5000
6000
7000

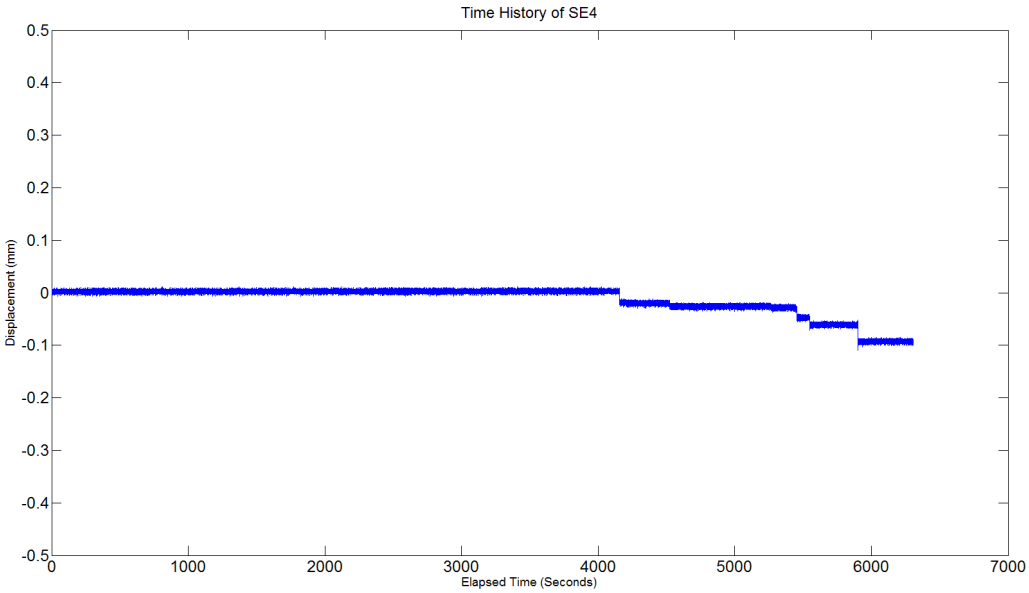
Time History of SE4
Displacement (mm)
Elapsed Time (Seconds)
0.5
0.4
0.3
0.2
0.1
0
-0.1
-0.2
-0.3
-0.4
-0.5
0
1000
2000
3000
4000
5000
6000
7000

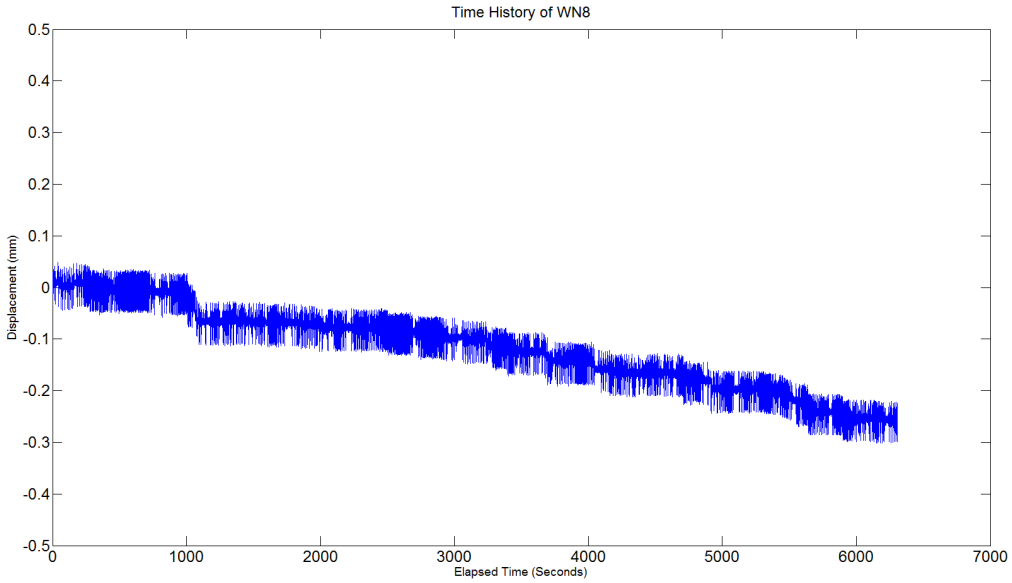
Time History of WN8
Displacement (mm)
0.5
0.4
0.3
0.2
0.1
0
-0.1
-0.2
-0.3
-0.4
-0.5
0
1000
2000
3000
4000
5000
6000
7000
Elapsed Time (Seconds)

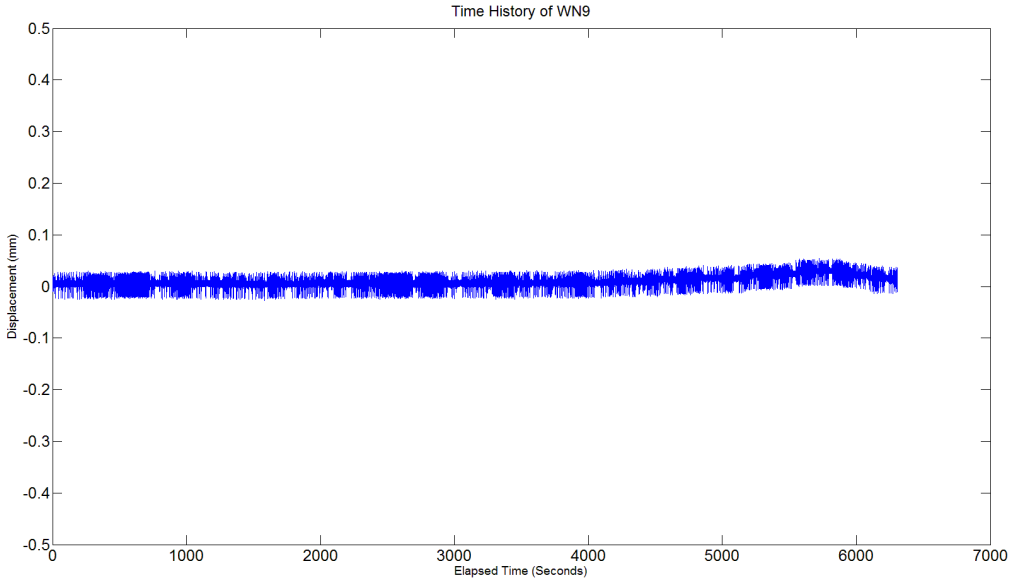
Time History of WN9
Displacement (mm)
0.5
0.4
0.3
0.2
0.1
0
-0.1
-0.2
-0.3
-0.4
-0.5
0
1000
2000
3000
4000
5000
6000
7000
Elapsed Time (Seconds)

Appendix G: Gable Beam Rotation

During the experimental setup, it was noted that if the drop down steel beams for the second storey positive whiffle trees moved at all, there was noticeable twisting in the gable beam they were attached to on the reaction frame. This was a potential problem because some of the LVDTs measuring interior wall movements were mounted off of this gable beam and if the beam rotated, it would cause a change in the displacement reading of these LVDTs. To compensate for this, an LVDT was placed at the midspan of the gable beam, measuring any rotation of the beam – Figure E1. Some rotation was measured throughout the experiment (see Figure E2). This rotation requires great care to be taken when observing the displacements from any LVDTs mounted off of this gable beam. The entire interior wall LVDTS were mounted off of wood frames mounted between the rotating gable and the next gable along (not rotating). Based on the rotation and the lever arm for the drop down wood frame, an estimate of the rotation induced displacement can be made, which makes the interior wall LVDT data usable for analysis. In Figure E3, the gable rotation (in mm) is compared with the interior wall LVDT IS8 reading. This LVDT was located at the top of the

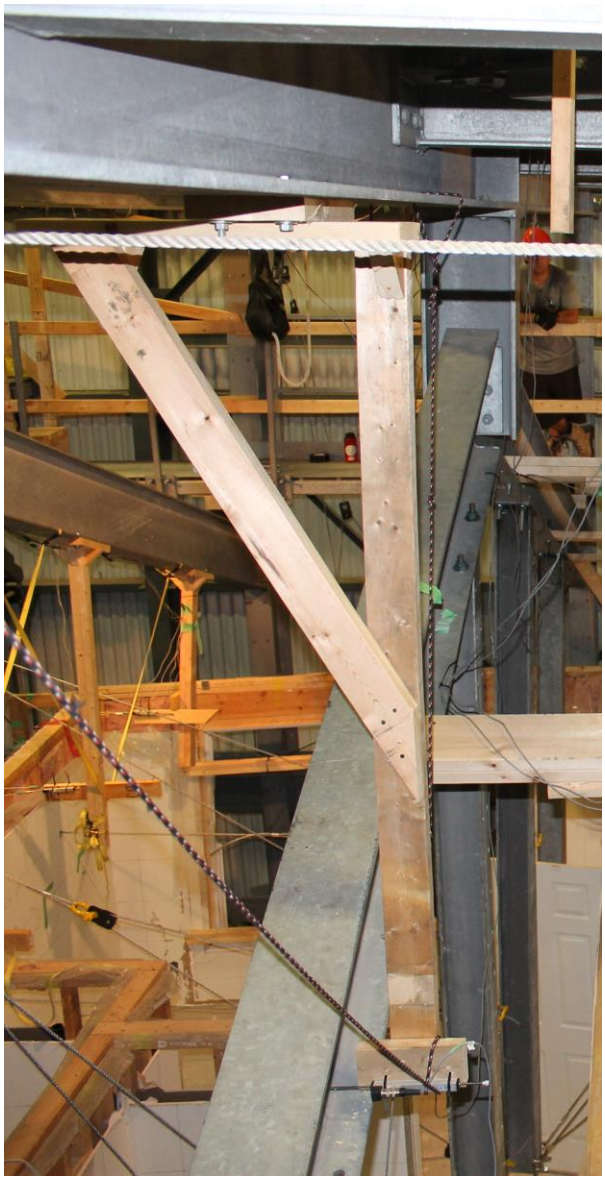

Figure E1 - LVDT dropping down from higher up on the reaction frame to record gable beam rotations.

stairs on the inside of the house, mounted off of the gable beam very close to where the rotation was measured. It is apparent from the Figure that the displacement reading of IS8 is directly correlated to the rotation of the gable beam. Because IS8 is mounted on a longer lever arm which would cause a larger displacement under the same rotation, the reading or IS8 was divided in half and the plotted against the rotation of the gable beam, this is shown in Figure E4. The IS8 reading was chosen to be divided in half as opposed to a fraction with a closer correlation to the different in lever arms because the wood beam dropping down from the gable beam is not perfectly stiff and is braced, so when the gable beam rotated, some of that rotation was absorbed by the beam itself. There were no measurements on the curvature of the wooden beam, so an accurate factor cannot be determined. From observing Figure E4 as well as what occurred during the experiment, it would appear that the interior walls at that point did not move at all.

Figure E2 - Time history of Gable Beam rotation.

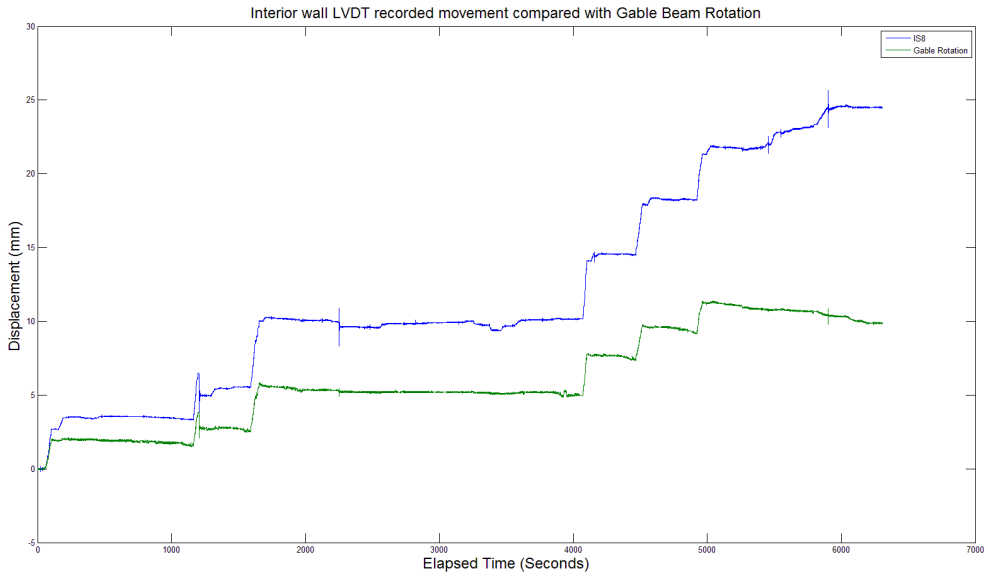

Figure E3 - Time history of IS8 and Gable Beam rotation.

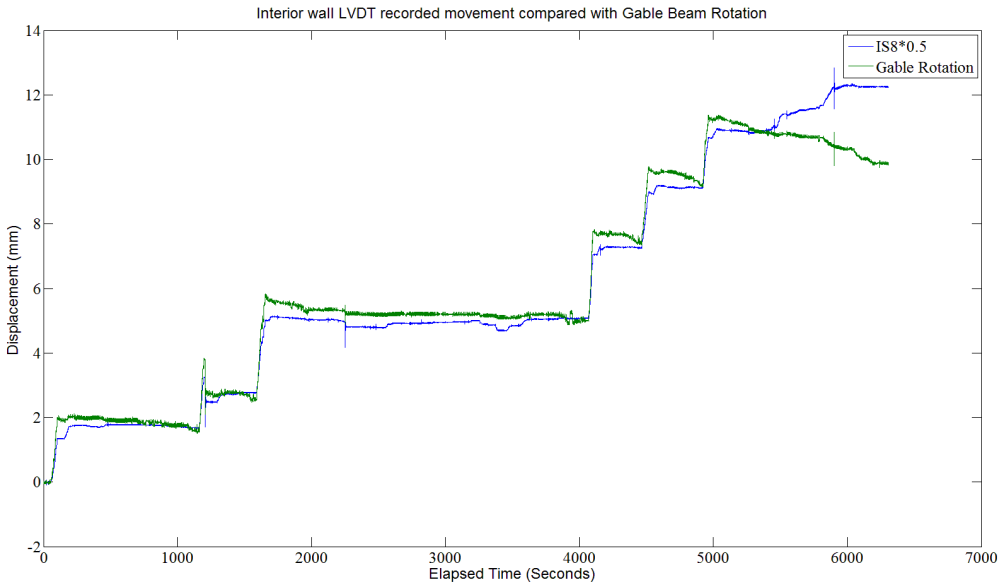

Figure E4 - Half of the IS8 displacement reading compared with the Gable Beam displacement reading.

Appendix H: Justifying Accuracy of Data – Full House Test

Several steps were taken to ensure that the data used for analysis was accurate as well as consistent. Specifically, ensuring that the data set used to zero the loads and displacements were correct and did not drift during the experiment. The equipment used for data acquisition was turned on the day before the experiment and left running overnight and through the day until the experiment was completed in order to reduce electronic drift.

Zero readings were acquired at 09h30, 11h40 and 14h30 on the day of the experiment to allow for the observation of any long term drift of the equipment due to temperature changes, electronic drift, or any other factors. The experiment took place between 18h30 and 20h20. There were no usable zero readings between 14h30 and 18h30 due to adjustments and fixes being applied to the rigging during this time; so at no one time was the entire house completely unloaded. Temperature changes appeared to cause a significant difference in the data for the load cells, this overall trend is shown in Figure A1 which shows the normalized hourly temperature compared with the average normalized zero strain gauge readings.

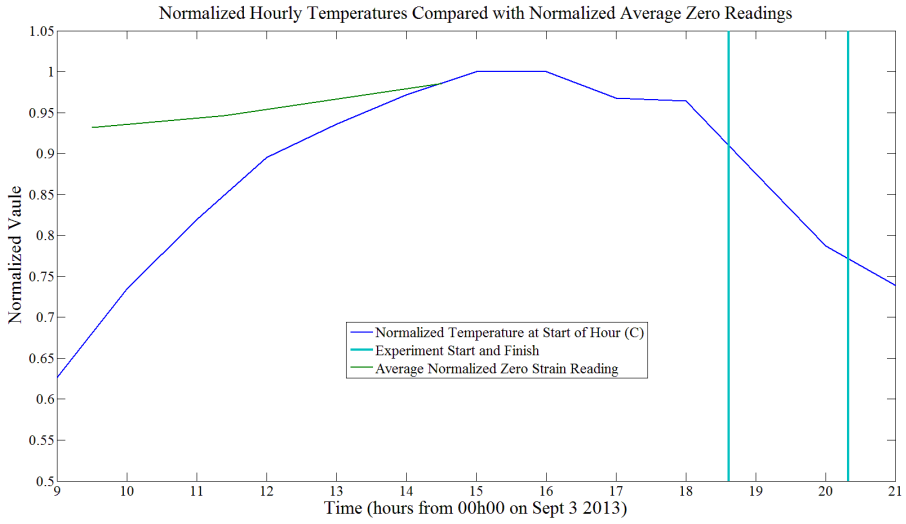

Figure A1 - Normalized Hourly Temperatures and Normalized Average Zero Readings

Load Cells/Strain Gauges

The load cells were made of aluminum and had one strain gauge attached to each side (see Figure A2). Each gage was wired separately (named A and B sides) so that in the event of the failure of one strain gauge, there would still be usable load readings from that load cell.

The aluminum is subject to thermal expansion and contraction; this would cause a difference in the strain reading of the DAQ. Equation A1shows the strain caused by a temperature difference. Each of the strain gages was connected to the DAQ in a quarter Wheatstone bridge setup. The voltage reading change expected with this setup is shown in

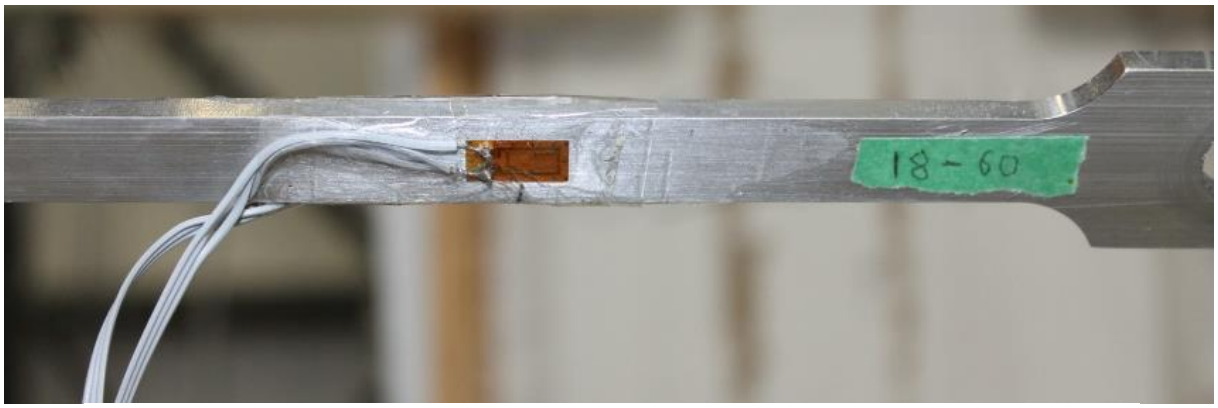

Figure A2 - Aluminum load cell with strain gage attached.

equation A2. Hourly temperature data for the experiment day (Environment Canada) was used to determine the temperature at each time when a zero reading was taken. By application of the equations, the strain and voltage change for the DAQ could be calculated (table A1).

$$\delta_T = \alpha * \Delta T \qquad (A1-a)$$

$$\alpha = 22.2 * 10^{-6} \ [{}^{m}/_{m}\ K]$$

$$\varepsilon = \frac{\delta_T}{l_o} \qquad (A1-b)$$

$$\frac{V_o}{V_{EX}} = \frac{GF * \varepsilon}{4}\left[\frac{1}{1 + GF * \frac{\varepsilon}{2}}\right] \qquad (A2)$$

Here V_o is voltage reading, V_{EX} is excitation voltage (6.25V) and GF is the gauge factor (2.1). In the table, the initial strain is set to zero because that is the initial zero reading. The change in temperature occurs between each of the zero points. Temperature readings were linearly interpolated from data taken at the start of every hour.

Table A1 - Change in temperature and corresponding expected voltage changes for the three zero readings

Time	Temperature (°C)	Ɛ	Vo
09h30	19.35	0	0
11h40	22.80	0.0121	0.0392
14h30	24.90	0.0194	0.0623

The temperature effects of strain readings would cause an increase in the zero strain readings as the day progressed. This trend is visible in Figure A3, which shows the normalized A side strain gauge reading for all the load cells. All but one strain gauge (East South Lower) show a similar trend and similar normalized values, this strain gauge is discussed in detail later. To account for the thermal strain in the zero readings, the expected change in voltage was scaled according to the scale used for the output data from the DAQ (100, for readability purposes) and then subtracted from the output strain data. The results show significantly less drift upward drift, and instead show much less change in the zero strain values as time progresses (Figure A4). There is one exception; the strain gauge on the North West Upper B side, which shows significant downwards drift across the zeros, this strain gauge is discussed in detail later. The average normalized drift at each time in 0.98, 0.96 and 0.97 for 09h30, 11h40 and 14h30 respectively, strain values were normalized due to the differences in zero values. The zero values for the different strain gauges varied very significantly. This variance is not a problem as it is due to wire length variation and other similar factors. Normalization allows for a direct comparison

between all the different strain readings. These are very small drift values and represent an insignificantly small difference in the load being applied to the house; the average of the maximum difference[6] at each gauge being 0.16kN, representing approximately 2% of the average maximum applied loads.

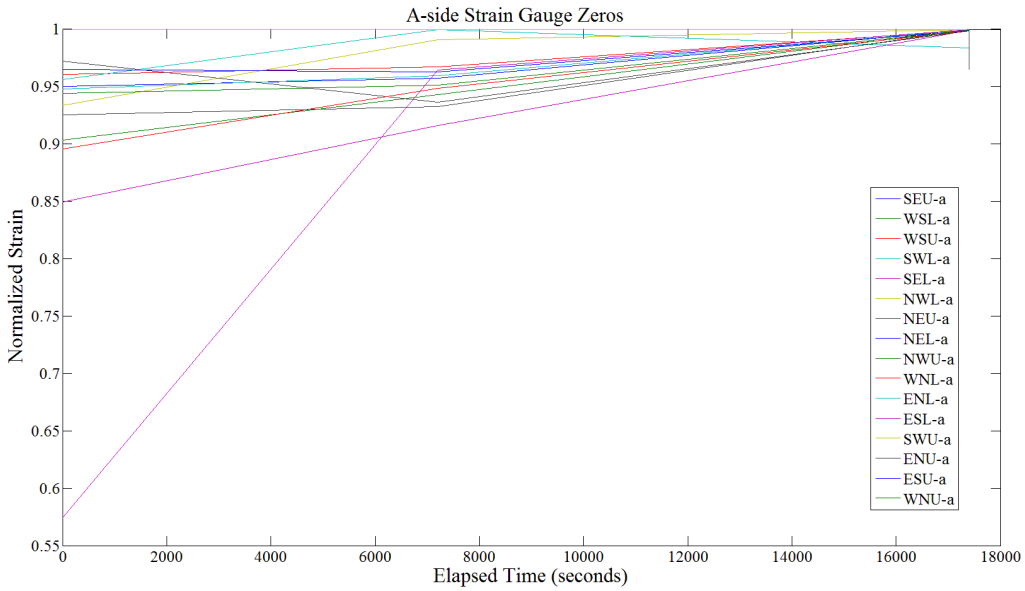

Figure A3 - Normalized strain gauge readings for all zero points.

[6] Maximum difference between zeros: the maximum zero value minus the minimum zero value observed by that strain gauge.

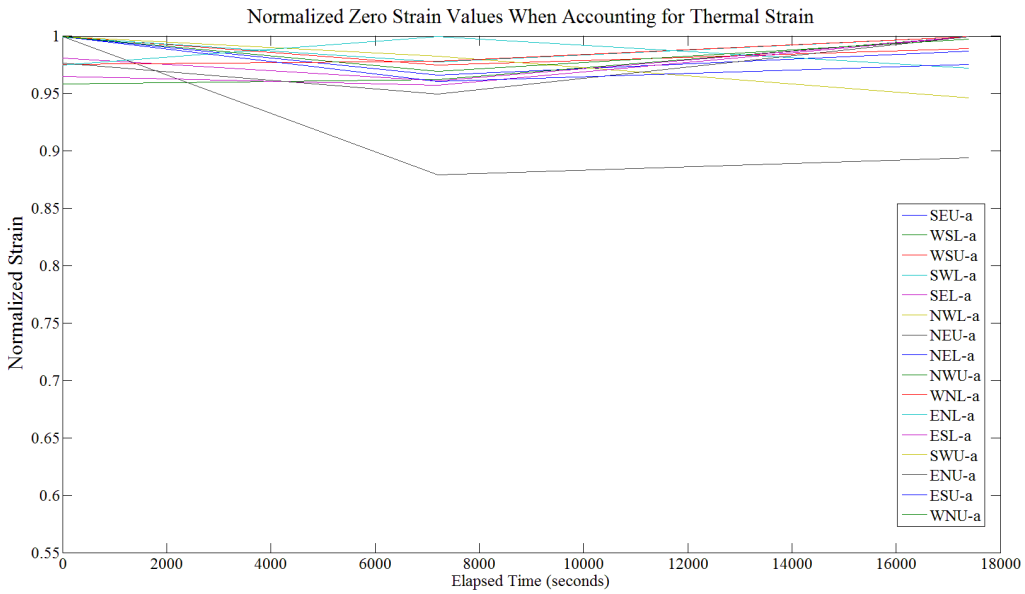

Figure A4 - Zero strain readings when thermal strain is accounted for

East South Lower Strain Gauge

The strain gauge located on the East South lower A side had an initial normalized zero reading of 0.574, while the zero readings on the B side of the same load cell had normalized zero readings for the second and third data sets of 0.626 and 0.670. This change is shown in Figure A5 caused suspicion that something had occurred between the 09h30 zeroing and the 11h30 zeroing to cause a significant change in the strain on this load cell.

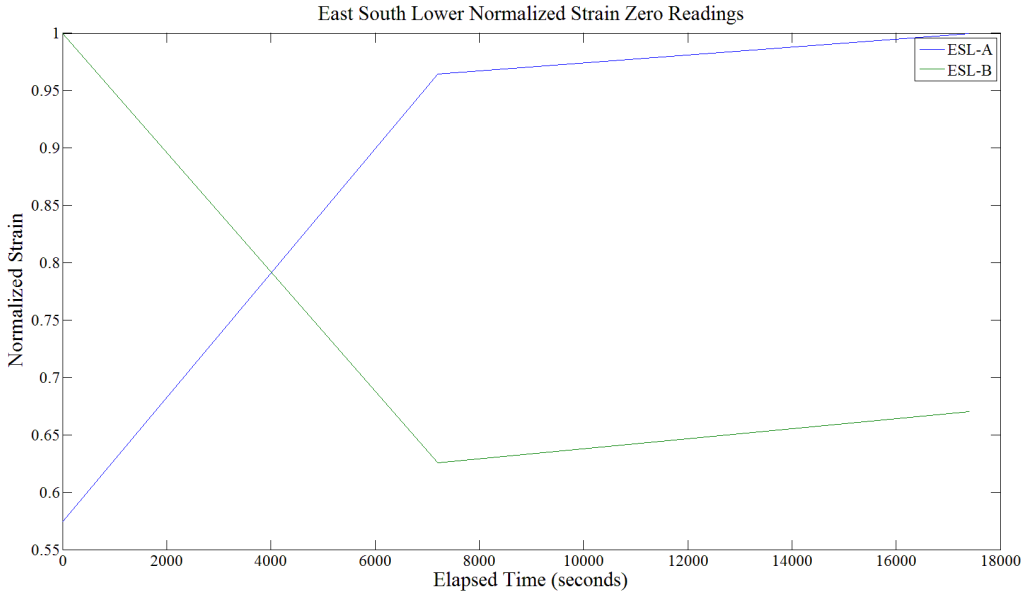

Figure A5 - Original normalized zero strain readings for the East South Lower load cell.

Figure A6 - East South Lower setup before the morning zeroing

From the data it would appear that the data from the A side started recording to the B side channel and vice versa. There is no evidence to support this hypothesis. However, notes from the day of the experiment suggest a potential source of the problem. Figure A6 shows

the lower East South strain gauge in its setup before the 09h30 data zeroing. As part of the final setup between the morning zeroing and the next zeroing, the wooden load pad had its location adjusted to remove a geometric problem with the cable rigging. Instead of the load cell passing overtop – as shown in the photo, it was moved to pass underneath the load pad instead. This switch did not change the loading being applied to the walls of the house (0kN). However, it did change the bending stress on the load cell, from one side to the other. When the first zeroing data point is swapped from each side the resulting normalized data is highly sensible compared to the remainder of the strain gauges (see Figure A7). The first zeroing data point is switched to simulate the same bending stress on each side for the 09h30 zeroing as is observed for the 11h40 and 14h30 zeroings. The data shown in Figure A7 has not had thermal strain accounted for, when accounting for thermal strain, the readings have even less variance from the first – last zeroing.

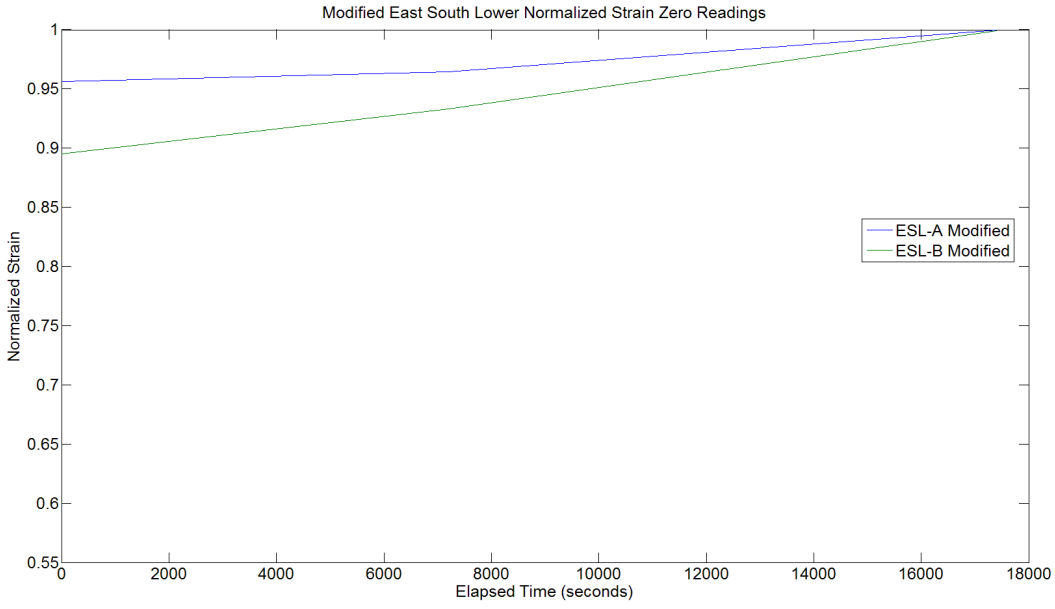

Figure A7 - Zero strain readings for Ease South lower load cell when the first zero point is switched.

North West Upper Strain Gauge

When the strain gauge zeros on the North West Upper load cell are adjusted for temperature, the normalized value from the B side drops from 1.00 at the 09h30 zeroing to 0.81

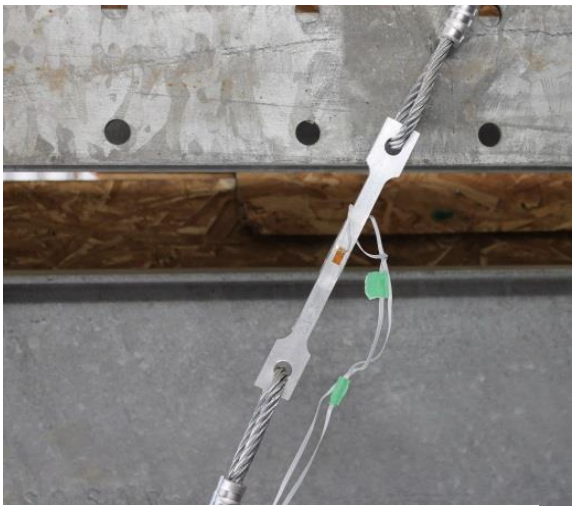

Figure A8 - North West Upper Load Cell After Adjustment, before PVC fix

Figure A9 - North West Upper Load Cell After PVC fix

and 0.80 at the 11h40 and 14h30 zeroings respectively. The strain gauge on the A side of the North West Upper load cell did not function correctly and so provides no usable readings. A potential explanation for why the zero strain readings trended downwards instead of upwards is a fix which was applied to the load cell at 13h20. This load cell had pulled tight up against a horizontal beam on the react frame (see Figure A8), and it was expected to cause problems during the running of the test. A quick fix solution was performed by encasing the load cell in a ‘PVC tube, which was allowed to slide along the beam while preventing bending of the load cell (Figure A9). This does not explain why the zero changed between 09h30 and 11h40, as the fix

was applied after. It was noted in the experimental log that the North West Upper load cell was giving odd readings at 12h11, before the PVC fix was applied.

When the strain from this load cell during the experiment is examined, it appears to increase in appropriate intervals based on the established linear load-strain relationship. This suggests that the gauge was functioning properly after the fix was applied. In order to be able to attain usable loading information for this portion of the house, the zeroing will be done in the same manner as for all the other zeros; using only the final zeroing data and disregarding the first two zeros as inaccurate.

Thermal Adjustment of Strain Zero Readings to Acquire Experimental Zeros

Due to the insignificance of the difference in zero strain readings between all three zeroing times after an adjustment for thermal strain has been performed, the zeros from 14h40 will be used as the actual zeros for the experiment. These zeros are being used because 14h40 is when the maximum exterior temperature is reached. After this point, the temperature inside the laboratory building did not cool down. Therefore, these are the most accurate zeros to use for the experiment. Figure A10 shows the forecast change in normalized strain (average across all channels) based on the hourly temperatures and associated thermal strain in the load cells. The forecast normalized strain shown is following the outside temperature. As previously noted, the indoor temperature trend did not follow the outdoor temperature trend after the maximum temperature was reached, so following the forecast normalized strain would end up reducing the strain and load readings too much and give lower than actual loads.

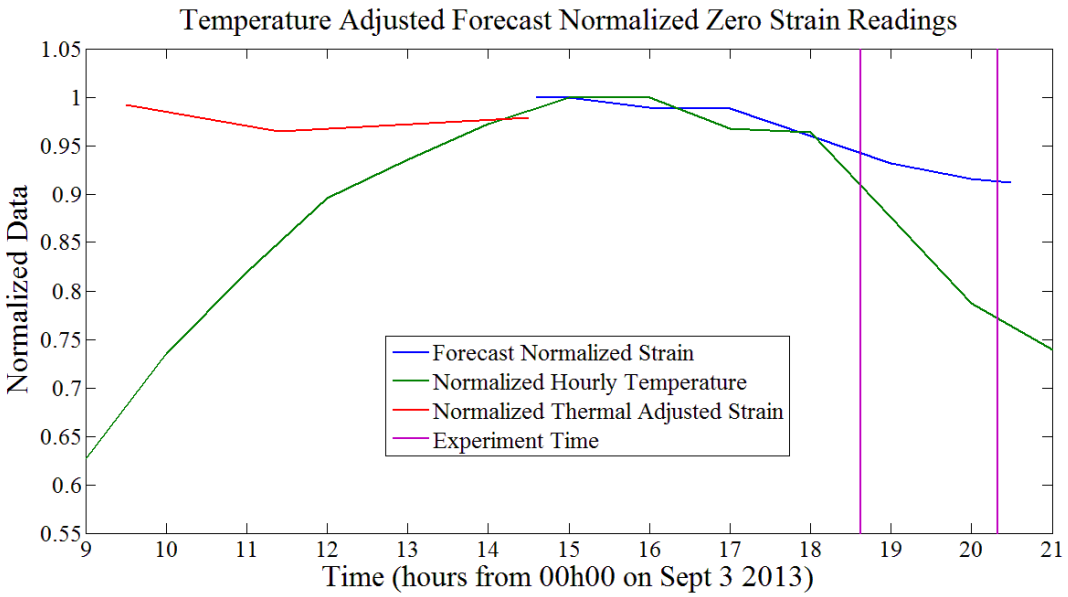

Figure A10- Temperature Adjusted Normalized Strain

The average normalized zero strain readings around the experiment time are shown in table A2. There is a change in the normalized zero strain reading over the course of the experiment. To account for this and maintain the accuracy of the strain readings used, the strain data will be zeroed using linear functions (equation A3). This allows for the most accurate calculation of the loads throughout the experiment. The final zeroing time will be used as the 1.0 normalized values, and values will be calculated off of that. The equation shown uses expected changes a linear interpolation between each hour of the actual expected change in strain reading (voltage). This is because the change in strain will be the same across all load cells, so the equation will be applicable to all.

$$18h30 \rightarrow 19h00 \quad 0 < x \leq 1800 \quad V_o^* = V_o - \frac{(0.000603 - 0.000478)}{1800} * x - 0.000478 \qquad (A3-a)$$

$$19h00 \rightarrow 20h00 \quad 1800 < x \leq 5400 \quad V_o^* = V_o - \frac{(0.000743 - 0.000603)}{3600} * x - 0.000603 \quad (A3-b)$$

$$20h00 \rightarrow 20h30 \quad 5400 < x \leq 7200 \quad V_o^* = V_o - \frac{(0.000777 - 0.000743)}{1800} * x - 0.000743 \quad (A3-c)$$

Table A2 - Average normalized zero strain due to thermal effects.

Time	Normalized Strain
18h00	0.960
19h00	0.932
20h00	0.916
20h30	0.912

Displacement Transducers

Most displacement transducers were mounted off of the galvanized reaction frame, which has a high coefficient of thermal expansion. Due to the setup of the laboratory building, fairly large temperature differentials were experienced over the course of the day on which the experiment was run. Thus, it was expected that there would be differential expansion of the reaction frame because it is not fully symmetrical. Figure A11, shows that almost all of the displacement transducers have a drift of less than 2mm. With the scale of the experimental deflections, this amount of drift is acceptable. Some displacement transducers have significantly larger drift and must be addressed. These transducers are: West North 9, East North 8, North East 5 and East North 4.

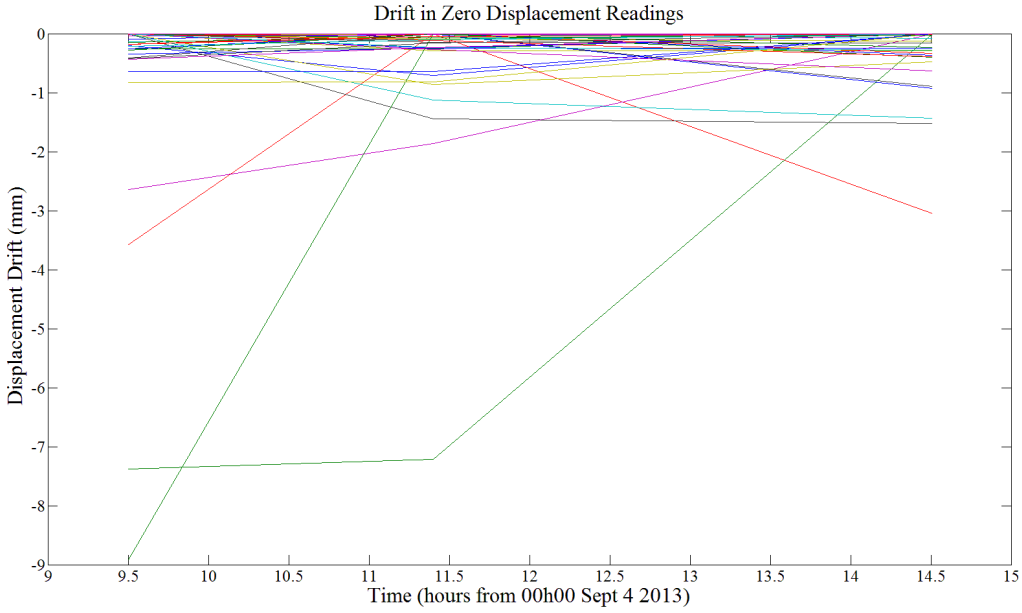

Figure A11 - Drift in displacement transducers in mm

West North 9

Located at the bottom of the West side of the house, at the North end, this displacement transducer records movements of the foundation; it is shown in Figure A12. Its zero data is shown in table A3.

Figure A12 - Displacement Transducer WN9

The final two readings are very consistent, but the first reading is not. It is expected that the displacement transducer or stand was adjusted slightly during the final walk around/displacement transducer check, which was performed at 10h20 – between the first and second zero readings. To account for this, the first zero reading will not be used for this displacement transducer. This is acceptable because of the steadiness of the readings of the other displacement transducers which worked for all three zeros. Using only two zero points (which are consistent) is not expected to have a significant effect on the experimental results.

Table A3- Zero displacement data for WN9

Time	WN9 Reading (mm)
09h30	10.534
11h40	19.455
14h30	19.223

North East 5

This displacement transducer was located at the East end of the North side of the base of the house. Figure A13 shows the transducer and its connection to the base of the house. As shown in table A4, the displacement readings at 09h30 and 14h30 are consistent with each other. However, the reading from 11h40 is significantly different. It is suspected that the angle of the displacement transducer (DT) may have been adjusted slightly. As can be seen in Figure A13, the DT was on a slight downwards angle, just below an amount of hardened wood glue (close up shown in Figure A14). One explanation for the reading change is that the transducer was adjusted to be level during the final walk around at 10h30, which then would have it contacting the hardened glue, but it slipped off sometime between 11h40 and 14h30.

Table A4 - Zero readings from North East 5

Time	NE5 Reading (mm)
09h30	3.170
11h40	6.750
14h30	3.699

For this displacement transducer, the final zero point will be used as the zero value. It is important to note that because of this DT's location, its main function is to ensure that there was not movement of the foundation of the house. As the value of read by the displacement

Figure A13 - Displacement Transducer North East 5

Figure A14- Close up of the DT connection to the metal plate at the base of the house

transducer remained constant throughout the experiment and the evidence suggests no drift of the displacement transducer readings over time, the final zeroing value is acceptable to use as a zero for this transducer.

East North 8

Pictured in Figure A15, the displacement transducer East North 8 was mounted on 2x4" wood members dropping down from the reaction frame. It was located on the East wall of the master bedroom, midway between the corner with the South wall and where the interior wall for the ensuite bathroom connected to the exterior wall. The readings from this DT are shown in table A5. The first two displacement readings are very consistent, however the final reading is not. There is no noted (or observed in photographs) pictures showing changes in the setup or orientation of this displacement transducer. As well, while the react frame is expected to have undergone some thermal expansion and contraction throughout the experiment/experiment day, the first two readings are insignificantly different. There was enough change in temperature between the first two zeroing times that if thermal expansion was affecting the DT readings, it would be noticable. As well, no other DT's appeared to be singficantly effected by thermal expansion/contraction of the reaction frame, so this is likely not the cause of the change in zero reading.

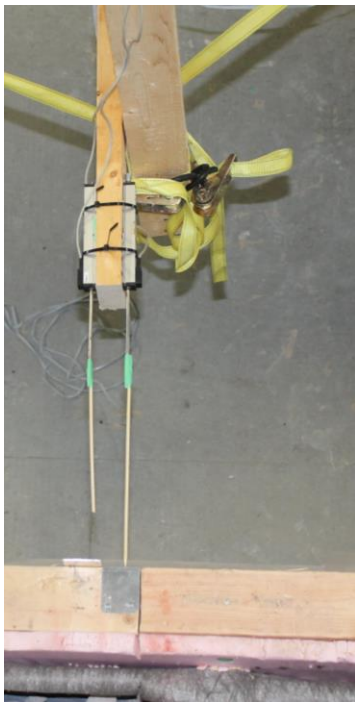

Figure A15 - Displacement Transducers EN8 (right) and EN9 (left) before the test.

East North 4

The drift in East North 4 was quite small (~3mm), but still big enough to warrant a more detailed examination. There were no noted adjustments to this LVDT (seen in Figure A16), so that is not the reason for the change in displacement reading. However, with a drift as small as it was, this is unlikely to be the reason for this drift. One possible explanation for the change in displacement reading is slippage of the skewer attached to the LVDT. The angle of the skewer may have slightly slipped/moved, which would cause a small change in displacement reading. Another explanation is differential expansion of the reaction frame, this is examined in more detail later.

Table A5 - Zero readings for displacement transducer EN8.

Time	EN8 Reading (mm)
09h30	4.497
11h40	4.655
14h30	11.875

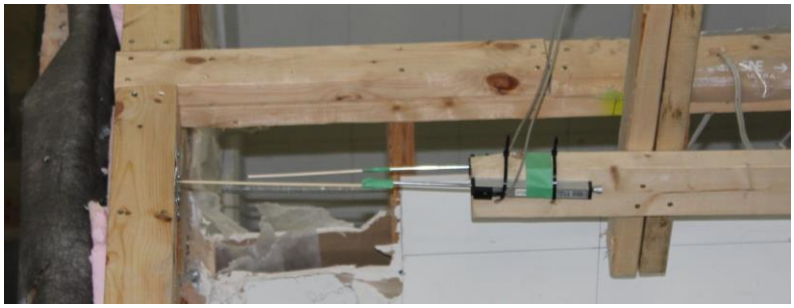

Figure A16 - LVDTs EN4 (closest) and EN5 (farthest away).

Appendix I: Justifying Data Accuracy for the Wall Test with No Brick Veneer

Strain Gauges

The load cells used were the same as used in the full wall test of the house. The same argument is used to justify the accuracy of the load data for this experiment as the full experiment. Figure I1 shows the normalized zero strain readings and normalized hourly temperature readings throughout the day before and morning of the experiment. The results show the trend which is expected based off of the previous experiment, the zero strain readings are correlated with the ambient temperature. The data acquisition system was left on from before the first zeroing until after the experiment concluded, in order to prevent electronic components from less predictable thermal strain and resulting drift.

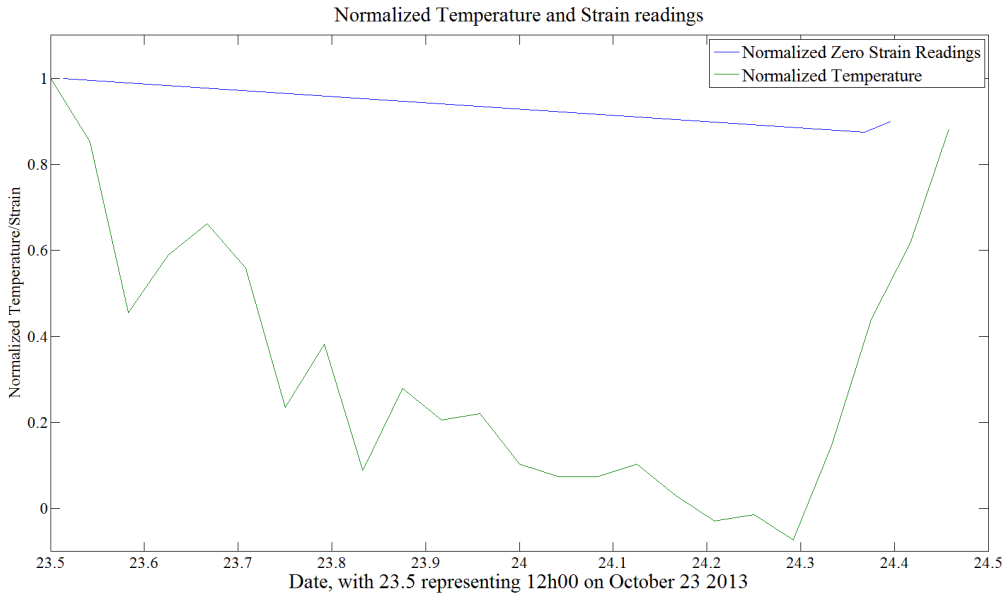

Figure I1 - Normalized Temperature and Normalized Zero Strain readings before the wall test with no brick veneer.

Zeroes were collected at 5 different points before the experiment was run, 11h00, 12h20 and 14h30 on October 23; and 08h50 and 09h30 on October 24th, with the experiment taking place between 09h30 and 11h00 on the 24th. The outside temperatures and expected change in voltage reading are shown in table I1.

Table I1 - Thermal Strain and Voltage change due to outside temperature.

Time	Temperature (°C)	Ɛ	Vo
11h00	5.3	0.0000	0.0000
12h20	6.5	0.0042	0.0137
14h30	3.6	-0.0059	-0.0059
08h50	2.7	-0.0091	-0.0360
09h30	3.6	-0.0059	-0.0557

When the thermal changes are removed from the voltage readings, the trend of the zero data still has more drift than is desireable. However, when the average normalized zero strain readings before and after the thermal adjustments are compared (Figure I2) in this Figure, the adjusted readings still follow the same general shape as the adjusted readings with less extreme peaks. This means that removal of the temperature effects has had the effect of creating more consistent zero readings.

An explanation for the adjusted zero readings following the same general trend as the unadjusted is the actual temperature differences. The temperatures used for thermal strain were calculated using outside temperatures at the time of zeroing. For the wall test with no brick veneer, the large hanger door to the building was left shut the whole time, due to the cold outside temperatures. Both the 23rd and 24th of October were sunny days, the sun on the outside of the

steel laboratory building causes a larger increase in the temperature inside than out, as well as retaining heat as the temperature cools down outside. The sun radiation causing a larger temperature increase can explain why the adjusted readings go up even after the outside temperature induced increase in strain is accounted for.

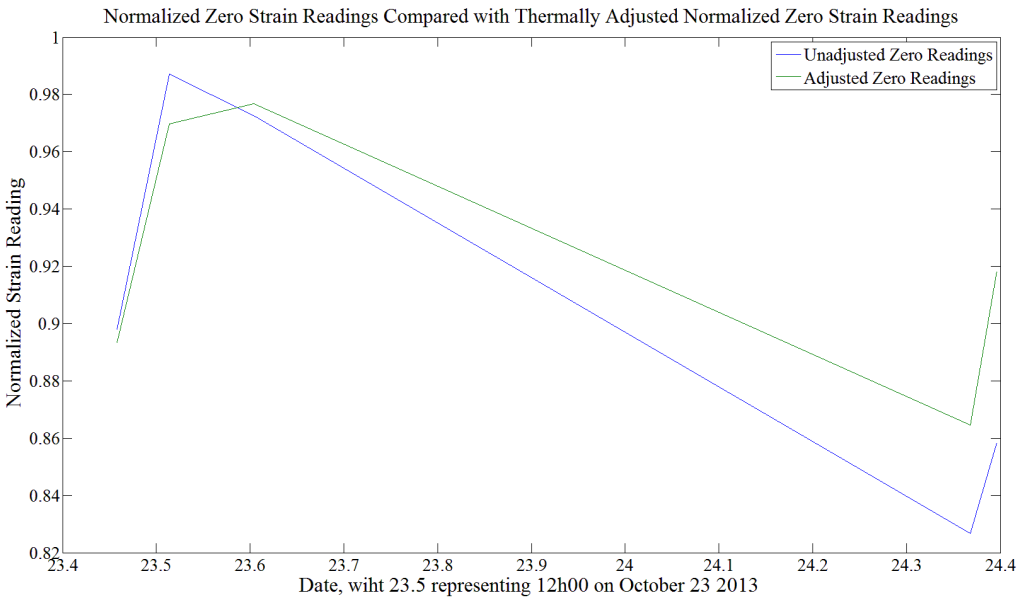

Figure I2 - Zero strain readings from before and after thermal strain adjustment.

Because similar trends in the zero strain readings and trends are seen as were seen in the full house experiment, it can be assumed that the final zeroes, which took place directly before the experiment started, can be used as the actual zeroes.

Displacement Transducers

A wood frame was built dropping down from the North West corner of the react frame in order to capture and curvature of the wall as well as the maximum displacement before failure. Figure I3 shows the displacement drift in mm for each of the displacement transducers. All but three of the LVDTs appear to have a very small amount of drift, these LVDTs are N3, W5 and W6; these LVDTs will be examined in detail later.

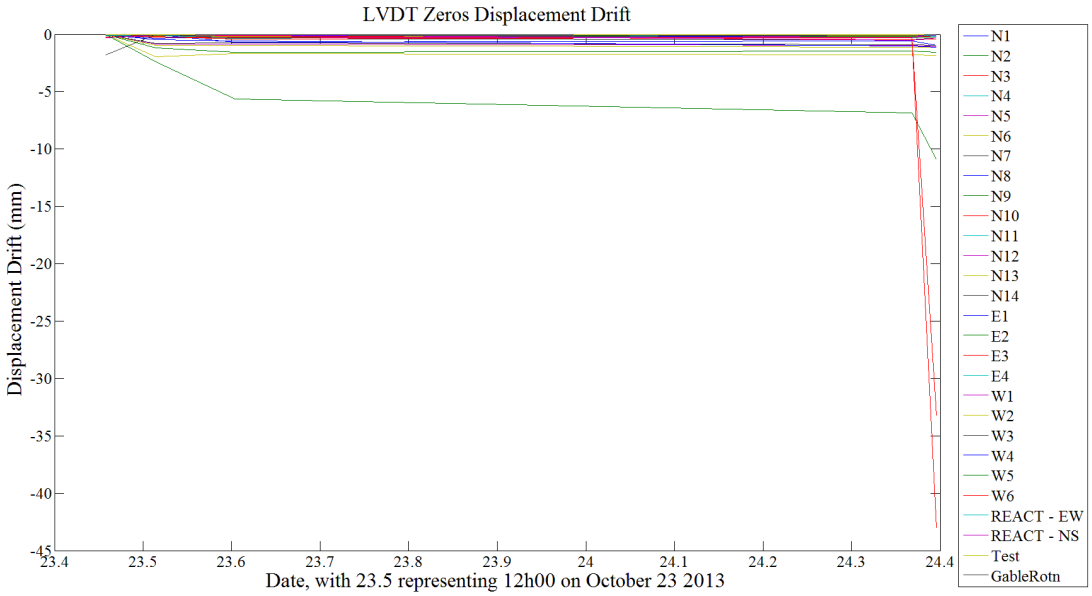

Figure I3 - Displacement drift for all LVDTs

Figure I4 shows the displacement drift when the three problem LVDTs are not shown. This plot shows small drift in the displacement (max of under 2mm) of all the LVDTs. As well, after the first zeroing, the displacement drift appears very small. This is shown in Figure B5, where the displacement drift is shown when it excludes the first zeroing time.

When the first zeroing time is not considered, the drift is very small; with an average absolute maximum drift of 0.27mm. This number is insignificantly small compared to the scale of the experiment being less than 0.0027%[i] of the maximum displacements expected to be read

by the LVDTs during the experiment. For this reason, the final zero reading will be used as the zero readings for the experiment.

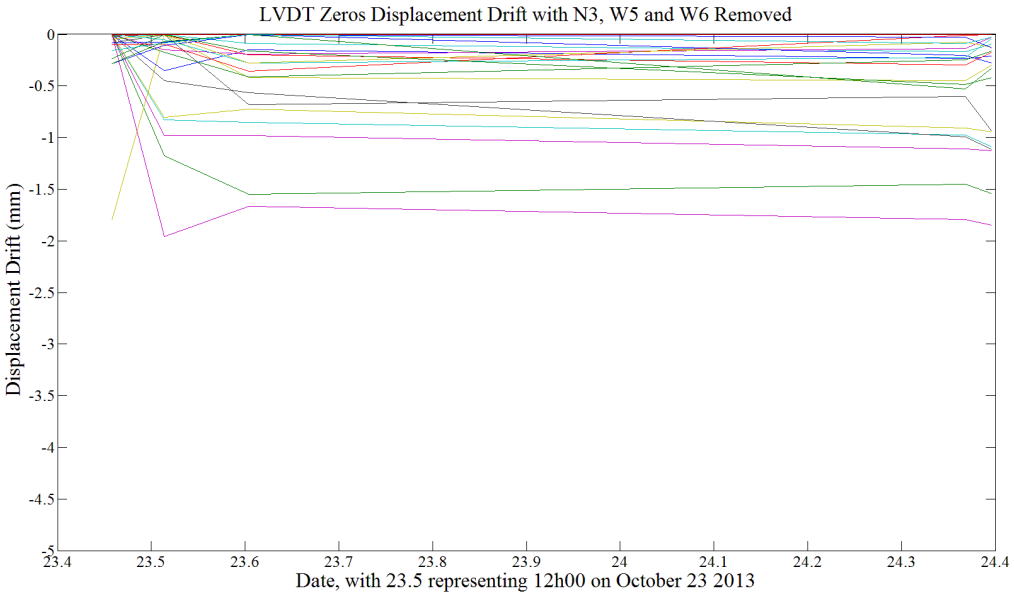

Figure I4 - Displacement drift with problem LVDTs removed

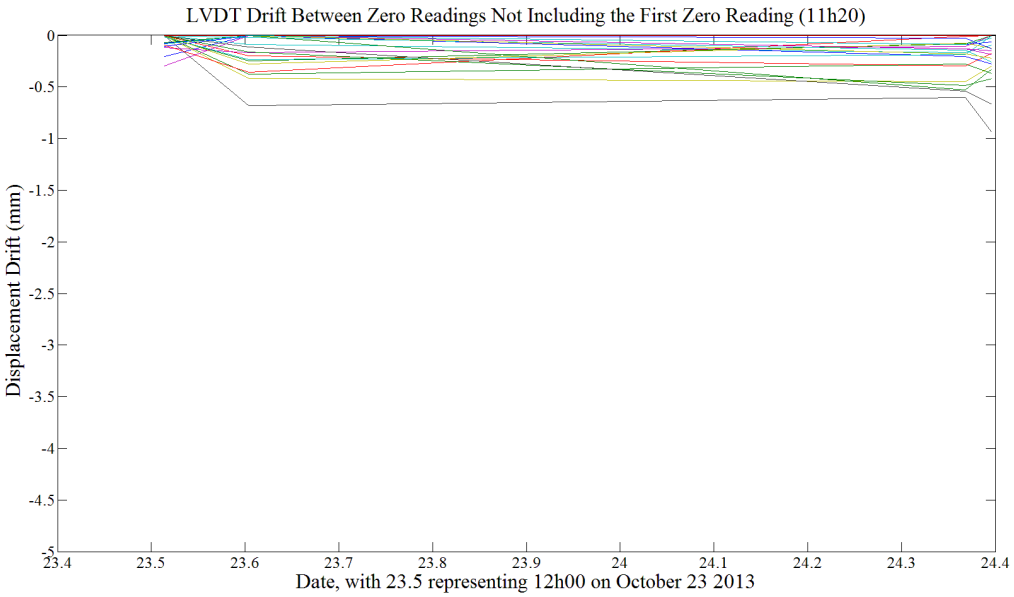

Figure I5 - Displacement drift with problem DTs removed and the first zero reading not included

LVDT N3

It was noted in the experimental log that LVDT N3 was sticking and not fluidly moving back and forth when tested. It is very likely that the LVDT was not giving an accurate reading for the first zeroes, before the final zero was taken all the LVDTs were checked to ensure they were reading. This would have caused the large change between the all the regular and the last zero displacement readings for this LVDT.

LVDT W5

LVDT W5 saw zero displacement readings which decreased every zeroing. The decreases totalled just less than 11mm. This LVDT had a skewer attached to span the distance between the wood beam and the top plate. This displacement transducer was set up to read outward movements of the wall (to lengthen); a result of this is there is a very slight spring force acting outwards on the wall. This force is insignificant in terms of loads on the house, but may have caused enough shear force in the taped connection between the skewer and the LVDT to cause some gradual slippage. This would result in the changes in zero displacement readings observed.

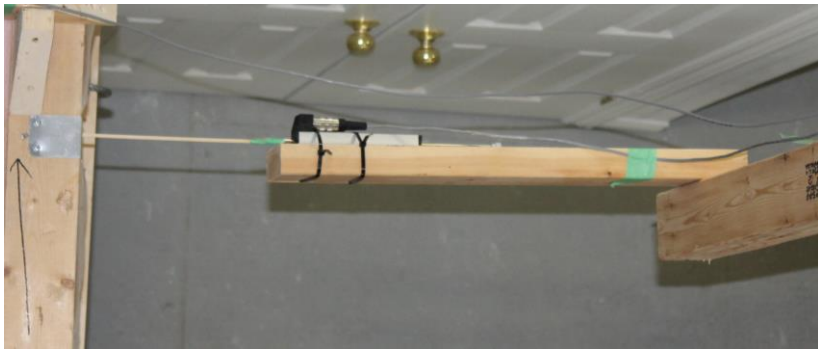

Figure I6 - LVDT W5 in place.

LVDT W6

There was a 42.7mm change in the displacement reading for this LVDT when the final zero reading was taken. No adjustment in the position of the LVDT was noted, however, it is most likely that this is what was done. A movement of the entire house or wood frame can be ruled out because of the consistency of readings of other LVDTs in the area. There is also no

significant change in the displacement readings for all of the other zero readings for W6, so it is not the electronics drifting. This supports the theory that this LVDT was simply adjusted before the final zeroing, which is also likely because all the LVDTs were touched/tested between the second last and final zero readings.

Conclusions

As with the full house test data, the final set of zeroes were be used as the zeroes for this experiment. This is because there was no significant drift in the equipment when thermal strain and outliers were addressed and there was not a large temperature change between the start and end times of the experiment.

Based off of maximum LVDT draw length, with the experiment providing more displacement than the maximum LVDT draw.

Appendix J: Net Loading Effects on Top Plate Movements

Almost all of the load-deflection curves around the house show similar behaviour: namely, a section when the load increases are monotonically increasing, but then a drop in load accompanied by increases in displacement. This saw-tooth pattern repeats multiple times as the overall load applied to the walls is increased. An example of this can be seen in the red circle in

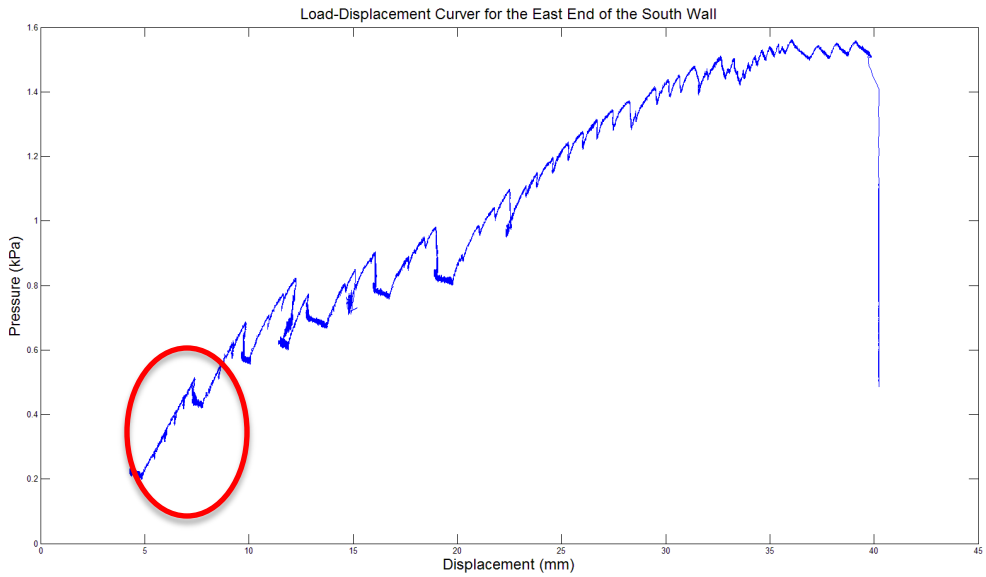

Figure J1 - A raw load deflection curve in the Master bedroom.

Figure J1, which shows the load-deflection curve for a transducer (#SE1 located in square I10 in Figure 3.4) measuring displacements of the top-plate at the South end of the East wall. There are two factors which cause this behaviour: (i) overshoots and relaxing in the load application, likely due to the ratcheting of the come-alongs, and (ii) the load application pattern, which was sequential around the house as described in section 3.3.4. These two aspects are discussed in detail below.

Figure J2(a) shows the load time history for the southern half of the east wall, as measured by one of the load cells at that position. Figure J2(b) shows portion of the time history

pertaining to the red circle in Figure J1, the load shows a clear short duration overshoot during the loading sequence, followed by a point where the load settles to a constant magnitude (until the next time it is increased in the sequence). Small overshoots and settlements can be seen during the increase in load as well ("A", "B" and "C" in Figure I2(b)), these overshoots show the tightening of the cables and minor peaks as each individual ratchet is applied to the come along. At the largest loads, the saw-tooth pattern remains, but the magnitude of the variation is only about 3% of the total load, so is inconsequential to the final loads.

After the drop in load following the overshoot, the discontinuity continues with a slightly increasing displacement corresponding to no local increase in load. This change in readings is caused by net movement of the house when adjacent portion of the wall is loaded in sequence. Because the house is all one system, loading in one part of the house affects other parts of the house. Specifically, when the East end of the South wall (F10-J10) is loaded, causing an increase in deflection, the West end of the South wall (A10-E10) and the South end of the East wall (J6-J10) will also see an increase in deflection. The increase in deflection observed by each wall section decreases moving further away from the area where the local load increase is applied.

This phenomenon is explained in Figure I3, which shows two plan views of the house, the first with arrows indicating the location and direction of load application (left hand side). The right hand side shows a plan view with displacements that would be expected if all the exterior walls were long beams pinned at each end. Load is applied (6) and the North wall is pulled outwards (1). This forces a rotation at the North East corner (2), causing the East wall to want to bend inwards (3) - in the same direction as its loading. The inward bending of the East wall causes a rotation in the South East corner (4), which in turn leads to outwards movement of the South wall (5).

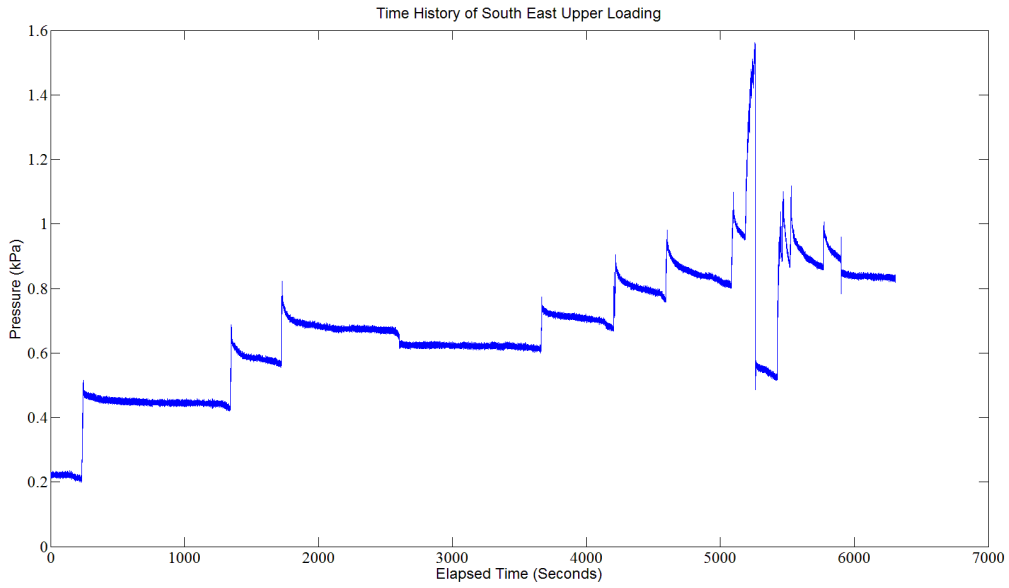

Figure J2(a) - Time history of the South wall East side loading.

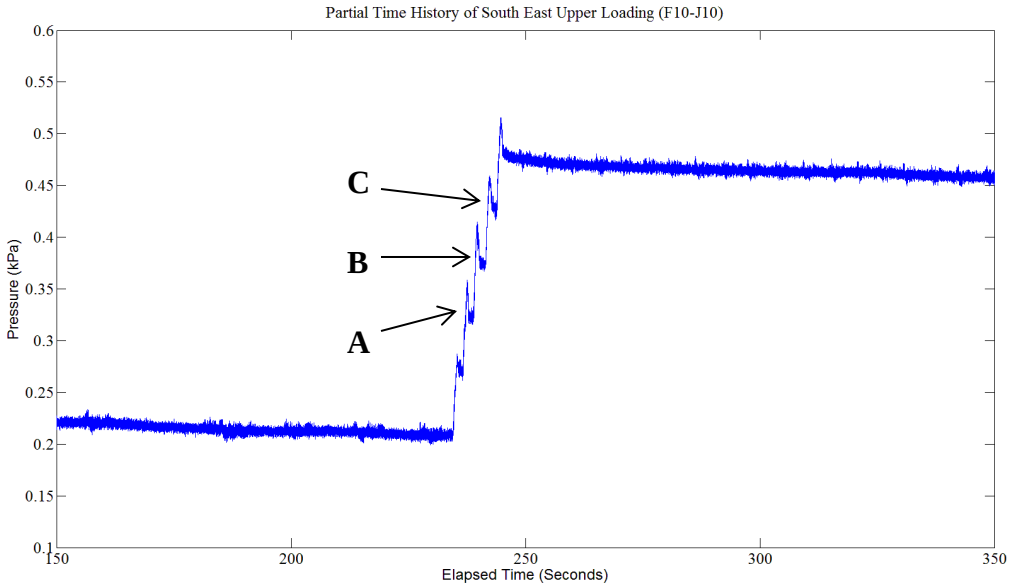

Figure J2(b) - Time history of the South wall East side loading, showing only the initial portion of the loading.

.

.

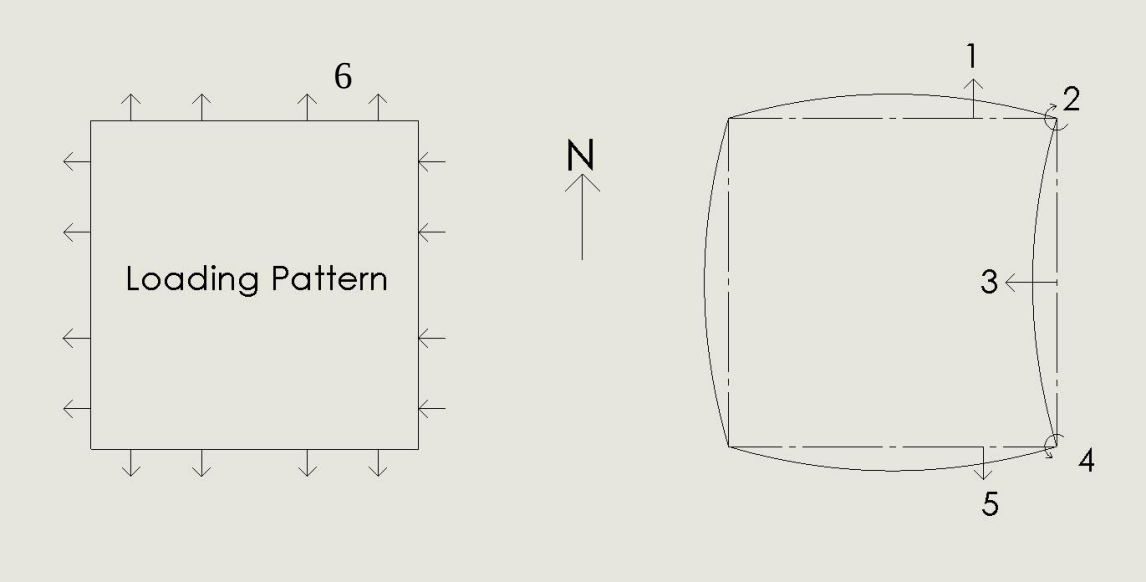

Figure J3 - A sketch illustrating how the load is transferred from one side of the house to another

Appendix K: Deflected Shape of A1-E1 Bedroom Wall

A line of six displacement transducers was installed to measure top plate movements in the North West bedroom during the test with no brick veneer. The intent behind the placement of this line of transducers was to capture the deformed shape of the wall under load. It was hypothesised that the closeness of the two interior walls at the East end of the room would act as a fixed connection and the corner would act more like a pinned connection. This hypothesis was based on observations made in the full house test with the brick installed. The displacement transducers were placed at intervals shown in Figure K1. Displacement transducer N2 did not function properly and could not be used for data analysis.

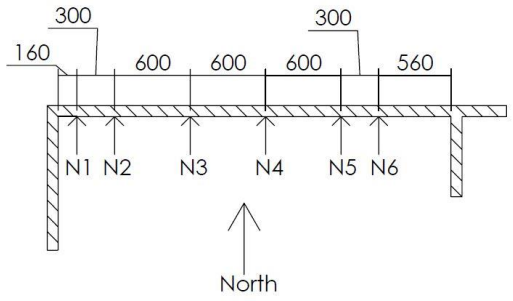

Figure K1 - North Wall LVDT arrangement for the wall test with no brick veneer

The data is presented in two, ways, first with the actual deflections at each load level[7]. This shows the progression of outwards deflection of the wall as the load increased, shown in Figure K3. The second way has the deflections of the wall normalized by the maximum deflection at that load level (Figure K4). This allows a more direct analysis of the deflected shape of the wall as loading is applied. The deflected shape of the wall at the top three load levels (3.5kN, 3.8kN and 4.5kN) are not shown because displacement transducers

Figure K2 - North wall looking from the West during the test with no brick veneer

[7] Load levels chosen using time history of loads applied to that wall.

N3 and N4 and N5 ran out of travel, so there is no longer enough data to accurately show the shape of the wall at these loads. The end points (the north west corner and where the interior wall connects) were set to zero values for clarity of the curve. It was acceptable to set the end values to zero based off of photographic evidence from the experiment as well as observations. The corners as well as interior walls prevented displacement of the exterior walls at the points of intersection. This can be seen in Figure K2, which shows the A1-J1 wall during the test with no brick veneer. The wall can be seen to be clearly bowing out wards but is held back at the corner and where the two interior walls connect near the top of the picture. The array of displacement transducers can also be seen.

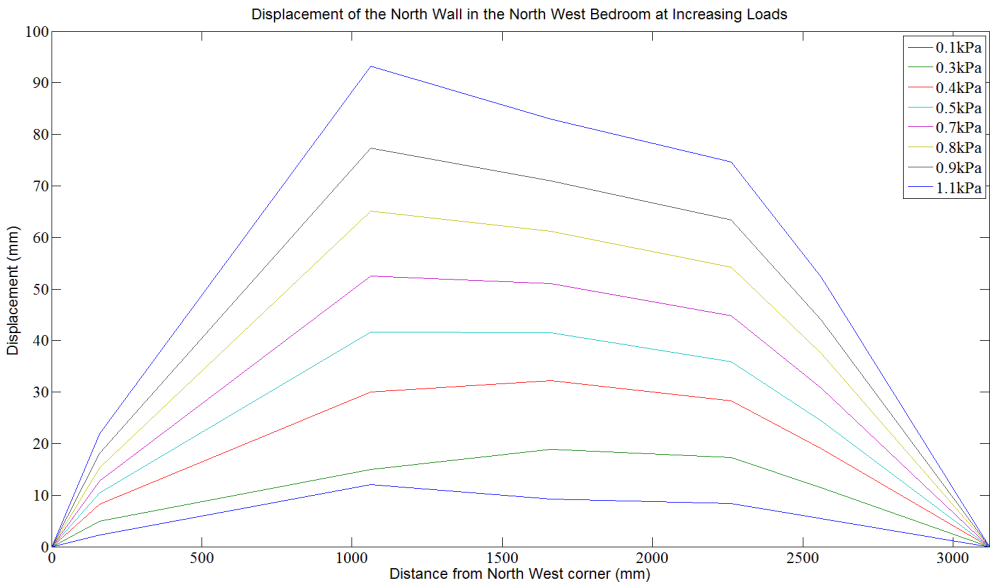

Figure K3- Displacement values across the North wall as the load was increased.

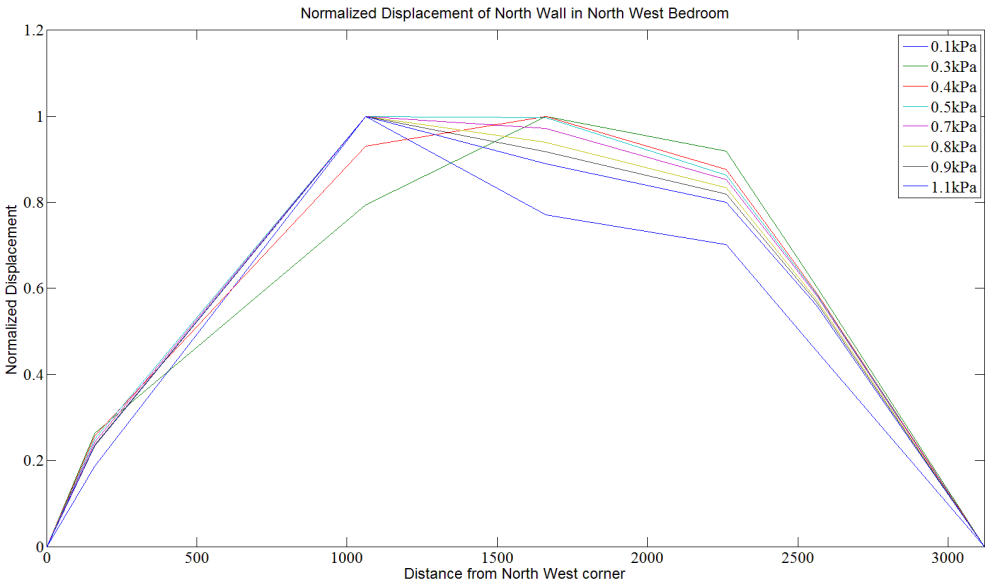

Figure K4 - Normalized Displacement values across the North wall

In this Figure, there are two behaviours which can be seen. The first is visible at the lower loads, specifically 0.1kPa -0.4kPa; at these loads, the displacement curve shows a maximum much closer to the middle of the span. As the load increases, the maximum load moves towards the point above N3, the displacement reading closest to the point of failure. The significance of this is that there was a weakness in the wall at this point, which is why the wall displaced the most here, even though it was not the center of the span, where the maximum displacement would be expected.

The normalized displacement curves show a remarkable amount of consistency. Generally, the normalized maximum recorded displacement occurred at N3, with N4 having a similar value. The dark blue line showing the normalized displacement at 1.1kPa is an exception, with N4 being ¾ of the N3 displacement. This likely occurred because the wall was approaching the failure load and the point where the failure occurred was where N3 was on the wall, so the most stress and displacement was located there at failure.

To determine the effect of the corner and interior wall connections on the displacement, the average of the normalized displacement values was taken - to create one general curve for the reaction of the wall. The closeness of the wall curves at different loads allowed this to be performed. This curve was then compared to the known displacement curves for different beam types; the different curve types considered are shown in table K1.

Table K1 - Connection and loading scenarios considered for displacement curves.

Connection Type		Load Type
Corner	Interior Wall	
Pin	Pin	Uniformly Distrubuted
Pin	Pin	Point Loads
Pin	Fixed	Uniformly Distrubuted
Pin	Fixed	Point Loads

The point loading cases use the location of application of the two point loads located at the locations where the cables pulling on the load pads were. This is based on the assumption that the load from the load pad is applied evenly to the two wall studs on each side of the cable. The load then travels up to the top plate where the displacement was measured.

Figure K5 shows the results from the average of the normalized actual data as well as the four different beam types considered. From the data, it can be observed that the North West corner of the house acted very close to a pinned connection. The same can be said for the other end of the wall, where the interior wall meets the exterior wall. This is a different result than was expected.

The behavior of the connection of the interior and exterior walls as a pin can be partly explained by the location of the top plate joints. At the connection, the top plate from the interior wall extends on top of the lower level of the top plate on the exterior. The lower level of the exterior wall top plate does not extend very far beyond this connection

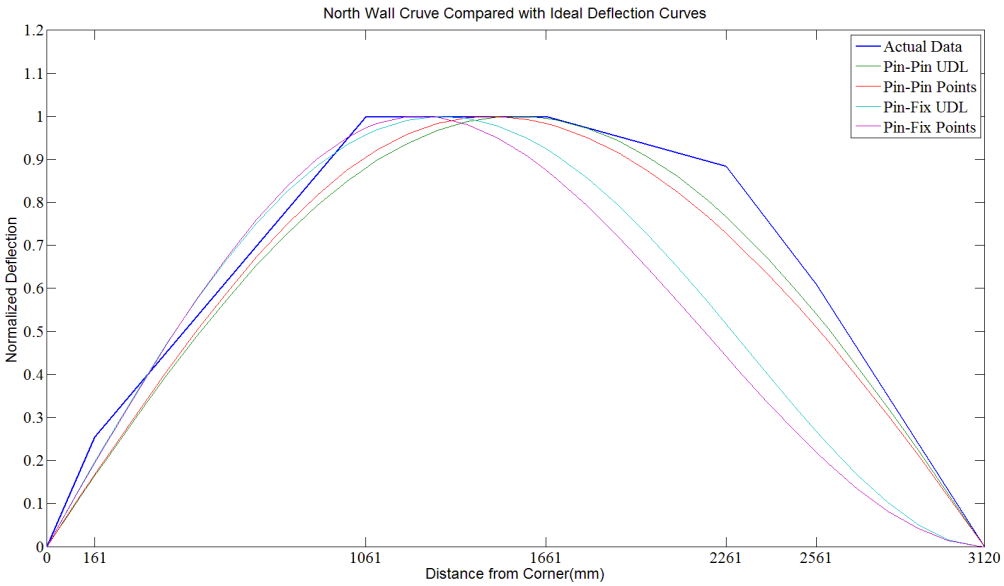

Figure K5- A comparison of the actual displacement curve and theoretical displacement curves for different beam

(towards the left in Figure K6). This means that only two nails are preventing rotation of the top plate; instead of it acting as more of a continuous member as it would if the lower top plate member continued further beyond the joint and had additional nails to prevent rotation. Rotation of the lower member of the top plate relative to the upper member of the top plate is easily visible in Figure K6, just to the left of where the interior wall enters from the top of the image.

Figure K6 - Interior-Exterior wall connection on North Wall, North is down.

Appendix L: Experiment Day Log – Sept 4 2013

09h30: arrival at site, setting of DAQ, zero reading recorded to determine instrument drift from the night before.

09h45: LVDT check with Nicole moving around moving LVDTs while I watched the DAQ

10h20: LVDT check complete

10h24: Walk around underway by others, a few small geometric problems fixed

11h30: Briefing and time to start running the experiment

11h42: Start, quick stop and restart

12h11: pause to fix and check SWU and NWU which are giving funny strain readings

13h20: during a fix, power to DAQ accidentally shut off. DAQ re-started to new data file WallTestTWO. PVC pipe cover is being installed on top of a couple questionable strain gages. +ve wall at 0.8kN, all others at 0.4kN.

14h00: preparing for the restart

14h22: go back to slack in cables, to re-acquire zeros. Lengthening of ENU come-along required/underway

14h40: re-restart. Bracket pulley loop/swag slipped into a different position, created more slack in the system.

15h36: up to 0.8kN all around, SWU and NWU giving odd strain readings, I suspect a zeroing problem. Lengthening of come-alongs is taking time, but going along. SWU is heavily loaded ~5mm of displacement.

16h16: working around, swages/loops on top bracket need adjustment

18h37: re-adjusted all loops and come-alongs, starting DAQ file FOUR

Loading Progression:

0.4, 0.8, 1.2, 1.5, 1.8, 1.8 (re-tension after come-along adjustment, hence repeat), 2.1, 2.4, 2.7 (kN).

Positive wall 1.5kN – Bricks fell off above window. Creaks in the NW side

1.8kN

- NE wall moving with pulls @1.8kN

- SW corner moving (top)

- WN dropped bricks off the top

- visible bowing to E and S walls, they appear to be acting as one beam.

- loud creaking from house in most situations now

- come-along pulls are visible corresponding to DT changes now

2.1kN

- dropdowns are twisting

- cracking in NW top plate

20h20 – South wall fails

20h24 – DAQ stopped, failure achieved

Vitae

Name	Derek A Stedman
Post-Secondary Education and Degrees	Department of Civil and Environmental Engineering The University of Western Ontario London, Ontario, Canada 2008-2012, BESc Department of Civil and Environmental Engineering The University of Western Ontario London, Ontario, Canada 2012-2014, MESc
Honours and Awards	Dean's Honour List 2008-2012 NSERC USRA Scholarship Summer 2010, 2011 Graduated with Distinction 2012
Related Work Experience	Teaching Assistant Department of Civil and Environmental Engineering The University of Western Ontario 2012-2014 Sr Analyst – Model Development Risk Management Solutions Inc Newark, California Feb 2014 - present